UNIVERSIDADE FEDERAL DE SANTA CATARINA
PROGRAMA DE PÓS GRADUAÇÃO EM CIÊNCIA E ENGENHARIA DE MATERIAIS

Mylena Mayara Matias Carrijo

SYNTHESIS AND PROCESSING OF Ti_3SiC_2-BASED INKS VIA INK-JET AND SCREEN PRINTING TECHNOLOGY FOR ELECTRONIC APPLICATIONS

Florianópolis
2018

UNIVERSIDADE FEDERAL DE SANTA CATARINA
PROGRAMA DE PÓS GRADUAÇÃO EM CIÊNCIA E ENGENHARIA DE MATERIAIS

Mylena Mayara Matias Carrijo

SYNTHESIS AND PROCESSING OF Ti_3SiC_2-BASED INKS VIA INK-JET AND SCREEN PRINTING TECHNOLOGY FOR ELECTRONIC APPLICATIONS

Thesis submitted to the Graduate Program in Materials Science and Engineering at Federal University of Santa Catarina for obtaining the Doctor's Degree in Materials Science and Engineering.

Supervisor: Prof. Dr. Carlos R. Rambo

Co-Supervisor: Prof. Dr. Nahum Travitzky

Florianópolis
2018

Mylena Mayara Matias Carrijo

SYNTHESIS AND PROCESSING OF Ti_3SiC_2-BASED INKS VIA INK-JET AND SCREEN PRINTING TECHNOLOGY FOR ELECTRONIC APPLICATIONS

This thesis was deemed sufficient to obtain the title of "Doctor in Materials Science and Engineering", and approved in the final form by the Graduate Program in Materials Science and Engineering (PGMAT).

Florianopolis, 23th February 2018.

_____

Prof. Dr. Guilherme M. O. Barra
PGMAT Coordinator

_____	_____
Supervisor: Prof. Dr. Carlos R. Rambo Universidade Federal de Santa Catarina	Co-Supervisor: Prof. Dr. Nahum Travitzy University of Erlangen-Nuremberg (Erlangen - Germany)

Examining Committee:

_____

Prof. Dr. Antonio Pedro Novaes de Oliveira
Universidade Federal de Santa Catarina

_____	_____
Prof. Dr. Guilherme M. O. Barra Universidade Federal de Santa Catarina	Dr. Marcela Guiotoku Empresa Brasileira de Pesquisa Agropecuária - Embrapa (Embrapa Florestas - Colombo, PR)

I dedicate this work to my family and husband.

AKNOLEDGMENTS

I would like to gratefully thank my supervisor in Brazil, Prof. Dr. Carlos R. Rambo, who offered me the chance to do what I love most. For the support in my academic and personal life, all knowledge shared and friendship.

I would like to thank my supervisor in Germany, Prof. Dr. Nahum Travitzky, who accepted me in his Additive Manufacturing research group in the Department of Materials Science – Glass and Ceramic (WW3) at the University of Erlangen-Nuremberg to develop an essential part of my master's and doctoral work. Thank you very much for providing me a wonderful experience, for all the support in my academic and personal life, for the patience and for all the given teachings.

I would like to express my gratitude to Prof. Dr. Guilherme Mariz de Oliveira Barra, who always helped me independent of the situation. For the knowledge shared during doctoral qualification exam and support during my academic life. To Prof. Dr. Dachamir Hotza for the contributions during doctoral qualification exam and for giving me the opportunity to study and work abroad, that changed my life forever. Thank you very much.

I would like to thank my husband, Hannes Lorenz, who helped me every day with my experiments and research. Thanks for the support, patience and most of all, thanks for always believing in me and encouraging me to be the best of me.

I would like to thank my colleagues from Federal University of Santa Catarina: Bruna Rosa, Daliana Muller, Patricia Vargas, Scheyla Kuester, Aline Manteiga, Leticia Scarabelot, Vieve Pinheiros and Luciana Vargas. My colleagues from WW3: Jonas Biggemann, Philipp Geiger, Maria Rita Cicconi, Karin Bichler, Alexander Bonet, Franziska Eichhorn, Ruth Hammerbacher, Alfons Stiegelschmitt, Sabine Fiedler, Andreas Thomsen, Thimotheus Nunes, Heiko Huber, Corinna Böhm and Eva Springer. For the great work environment, relaxation moments and help.

To Ph.D Joseph Harris, who corrected the English grammar of this work and all scientific assistance.

To Dr. Francielly Cesconeto, who was always by my side regardless the situation. Thanks for all the help, support and friendship.

To M.Sc. Rogério Antônio Campos, secretary of the Graduate Program in Materials Science and Engineering, for all help and great work environment.

To all my friends in Brazil and Germany, who helped me directly or indirectly during this journey.

Finally I would like to thank the Federal University of Santa Catarina, the Graduate Program in Materials Science and Engineering, Friedrich-Alexander-Universität Erlangen-Nürnberg and the National Council for Scientific and Technological Development (CNPq) for the infrastructure and financial support.

Nothing in life is to be feared, it is only to be understood.

(Marie Curie)

RESUMO

Neste trabalho, é apresentada composições de tintas de Ti_3SiC_2 para o processamento via serigrafia e impressão à jato de tinta, para uso em dispositivos eletrônicos. Para o processo de serigrafia, foi investigada a influência de diferentes quantidades de cargas de enchimento (Ti_3SiC_2) (20 a 40 vol%) e ligante (EC - etilcelulose) (0 a 5 vol%) nas propriedades das pastas (reologia, rugosidade e microestrutura), bem como na qualidade de impressão. Como substrato de impressão, foram utilizados laminados de Al_2O_3 produzidos através do técninca de produção de papéis pre-cerâmicos. Os filmes impressos foram sinterizados durante 1 h a 1600 °C em argônio. As pastas de Ti_3SiC_2 com maior viscosidade, como as pastas contendo 30 vol% e 40 vol% de Ti_3SiC_2, produziram filmes com superfícies mais regular e a melhor qualidade de impressão independentemente da quantidade de EC. Análises de DRX e MEV mostraram que apenas as pastas com 30 vol% de Ti_3SiC_2 na sua composição inicial apresentaram TiC como fase primária e Ti_3SiC_2 como fase secundária após a sinterização, sugerindo a decomposição parcial do Ti_3SiC_2. Para as demais pastas ocorreu a decomposição total do Ti_3SiC_2. A condutividade elétrica dos filmes impressos com 30 vol% de Ti_3SiC_2 na sua composição inicial e diferentes quantidades de EC variou de 1.25×10^5 $S.m^{-1}$ a 2.84×10^5 $S.m^{-1}$ em uma faixa de temperatura de 25 °C a 400 °C. A síntese *in situ* do Ti_3SiC_2 via serigrafia a partir dos pós elementares de Ti, TiC, Si e graphite também foi realizada com sucesso. Após a sinterização durante 5 h a 1400 °C em argônio, pastas com TiC e excesso de Si na sua composição incial apresentaram uma alta qualidade de impressão com Ti_3SiC como fase primária e $Ti_5Si_3C_x$ como fase secundária. A condutividade elétrica dessas amostras variou de 4.63×10^4 $S.m^{-1}$ a 2.57×10^4 $S.m^{-1}$ em uma faixa de temperatura de 25 °C a 400 °C. Para o processo de impressão à jato de tinta, foi feita a formulação de uma suspensão aquosa de Ti_3SiC_2 para utilização como tinta. Para obter o padrão de tinta requerido pela impressora utilizada, foram realizados processo de moagem de alta energia, análises reológicas e de potencial zeta. Polietilenimina (PEI) foi utilizado como dispersante e a faixa de printabilidade (Z) foi calculada. Foi obtida uma suspensão aquosa contendo 0.05 vol% de Ti_3SiC_2, 2% em massa de PEI e 40% em massa de glicerol, pH 4.3 e o valor de Z igual a 11. Como superfície de impressão, foram utilizados vidro, KOH e ITO (Óxido de índio-estanho).

Palavras-chave: carbeto de silício titânio, serigrafia, impressão à jato de tinta, aplicações eletrônicas.

RESUMOS EXPANDIDO

Introdução

O carbeto de silício titânio (Ti_3SiC_2) pertence à classe dos carbonetos e nitretos ternários com estrutura lamelada conhecida como fases MAX. Este material é conhecido por sua combinação singular das propriedades mecânicas, elétricas e térmicas dos materiais metálicos e cerâmicos. Mais especificamente, possui excelente resistência ao choque térmico, alta condutividade elétrica e térmica, resistência à oxidação, alta rigidez e alto módulo de elasticidade. O processo de serigrafia pertence às técnicas de impressão que hoje são usadas para a fabricação de linhas e filmes condutores. Esta técnica está lentamente substituindo os métodos convencionais para a produção de dispositivos eletrônicos, como por exemplo, os processos de litografia. É uma técnica de alta performance, com alta velocidade de processamento, baixo custo, alta confiabilidade e oferece a capacidade de impressão em diferentes substratos. A tecnologia de impressão à jato de tinta é um processo bem conhecido para produzir peças sólidas sem a necessidade de máscaras, moldes ou interferências humanas. Esta tecnologia é baseada na deposição direta, controlada por computador, do material desejado gota por gota sobre o substrato. Até o momento, não há relatos de estudo envolvendo serigrafia e pastas à base de Ti_3SiC_2 ou tintas de Ti_3SiC_2 utilizadas para impressão direta à jato de tinta. Assim, devido às excepcionais propriedades do Ti_3SiC_2, este trabalho propõe o processamento deste material através de processamento diferentes: (i) serigrafia e (ii) impressão direta à jato de tinta, para aplicações em dispositivos eletrônicos. Além disso, também é proposta a síntese *in situ* do Ti_3SiC_2 a partir do pós elementares de Ti/TiC/Si e grafite através da serigrafia.

Objetivos

Produção de pastas de Ti_3SiC_2 para serigrafia, formulação de tintas de Ti_3SiC_2 para impressão direta à jato de tinta e avaliação de propriedades microestruturais e elétricas das estruturas impressas via serigrafia e à jato de tinta para aplicações eletrônicas.

Metodologia

Como substratos de impressão para o processo de serigrafia, foram fabricados laminados retangulares de óxido de alumínio (Al_2O_3) produzidos através da técnica de produção de papeis pré-cerâmicos. A conversão do papel pré-cerâmico em material cerâmico foi obtida por meio da sinterização a 1600 °C durante 4 h em ar. Para a produção das

pastas de Ti_3SiC_2 para o processo de serigrafia, foi utilizado o pó comercial de Ti_3SiC_2 com 2 % em massa de TiC/Ti_5Si_3. Etilcelulose (EC) e terpineol foram usados como ligante e solventes, respectivamente. Doze composições de pastas foram produzidas variando as quantidades de ligante e Ti_3SiC_2. Para a síntese *in situ* do Ti_3SiC_2 através do processo de serigrafia, as pastas foram produzidas usando seus pós elementares, tais como Ti, TiC, Si e grafite. Foram utilizadas duas misturas de pó: (i) Ti/Si/C e (ii) Ti/TiC/Si/C. Para cada mistura, foram preparadas duas estequiometrias diferentes somando um total de quatro composições. O processo de serigrafia, para as pastas de Ti_3SiC_2 e pastes de sínteses, foi realizado a uma velocidade de impressão de 150 mm/s, com uma abertura da tela de 333 μm, e pressão de rodo de 100 N. Os filmes impressos de Ti_3SiC_2 foram sinterizados a 1600 ° C durante 1 h em atmosfera de argônio e os filmes produzidos a partir das pastas de síntese foram sinterizados a 1400 °C durante 1, 3 e 5 h também em atmosfera de argônio. Técnicas de caracterização, tais como reologia, termogravimetria, topografia, difração de raio X (DRX), microscopia eletrônica de varredura (MEV) e condutividade elétrica foram utilizadas para caracterizar tanto os filmes à base de Ti_3SiC_2 quanto os filmes produzidos a partir das pastas de síntese. Para o processo de impressão à jato de tinta, foi primeiramente necessário adaptar as propriedades da suspensão de Ti_3SiC_2 aos parâmetros requeridos pela a impressora utilizada. Assim, foi necessário atingir o tamanho de partícula exigido para o pó comercial de Ti_3SiC_2 e os valores ideais de pH e viscosidade da suspensão. Para as suspensões cerâmicas, utilizou-se o pó de Ti_3SiC_2 do processo de moagem com $D_{50} \leq 0{,}2$ μm. Água deionizada e polietilenimina (PEI) foram utilizados como solvente e dispersante, respectivamente. O pH foi ajustado através da adição de soluções de NH_4OH 0,1 M e HNO_3 0,1 M. Glicerol foi utilizado para ajustar a viscosidade das suspensões. A impressão foi realizada usando uma impressora à jato de tinta com 16 bocais de impressão piezoelétrico. Foram utilizados como substrato de impressão superficies de vidro, KOH e ITO (Óxido de índio-estanho). Cada bico foi excitado independentemente com 24 V e uma frequência de 2 kHz. O pó de Ti_3SiC_2, e a suspensão de Ti_3SiC_2 foram caracterizados utilizando análises de tamanho de partícula, DRX, MEV, espectroscopia Raman, reologia e tensão superficial. A faixa de printabilidade (Z) foi calculada utilizando o inverso do número Ohnesorge.

Resultados e Discussão

De acordo com os resultados apresentados pela análise reológica, para o processo de serigrafia, tanto o ligante quanto o conteúdo cerâmico mostraram ter influência no comportamento reológico das pastas de Ti_3SiC_2. Todas as pastas foram impressas com sucesso, exceto as pastas com 40 vol% de Ti_3SiC_2 e 4 vol% e 5 vol% de EC, que apresentaram as viscosidades mais altas dentre todas as amostras. Os filmes impressos com as pastas contendo 30 vol% de Ti_3SiC_2, independentemente da quantidade de EC, apresentaram a melhor qualidade de impressão, superfície mais regular e maior quantidade de Ti_3SiC_2 após sinterização durante 1 h a 1600 ° C. Em filmes compostos de pastas contendo 20 vol% e 40 vol% de Ti_3SiC_2 em sua composição inicial ocorreu a decomposição do Ti_3SiC_2 em TiC e $Si_{(g)}$ durante a sinterização durante 1 h a 1600 ° C em argônio. Os filmes resultantes continham Ti_3SiC_2 como fase secundária. Através desses resultados é sugerido a existência de limiar, em que o conteúdo das partículas EC e Ti_3SiC_2 seja ideais para o processo de serigrafia. Todos os filmes impressos via serigrafia mostraram a ausência de rachaduras após a sinterização e as pastas sem a adição de EC aparentaram ter a maior porosidade, além dos maiores tamanhos de poros. A condutividade elétrica dos filmes à base de Ti_3SiC_2 depositados via serigrafia variou de 1.25×10^5 $S.m^{-1}$ a 2.84×10^5 $S.m^{-1}$ numa faixa de temperatura de 25 °C a 400 °C. Para a síntese *in situ* do Ti_3SiC_2 via serigrafia, foram preparadas pastas contendo Ti/Si/C e Ti/TiC/Si/C, onde observou-se, que ao contrário das pastas de Ti_3SiC_2, nas pastas de síntese o conteúdo da EC teve maior influência na viscosidade. Todos os filmes impressos a verde apresentaram uma boa qualidade de impressão. Após a sinterização dos filmes impressos durante 1, 3 e 5 h a 1400 ° C em argônio, Ti_3SiC_2 foi obtido como fase primária e TiO_2, Ti_5SiC_x, $TiSi_X$ e Al_2O_3 como fases secundárias. Isso sugere a ocorrência de dois fenômenos simultâneos: (i) a síntese do Ti_3SiC_2 e (ii) reação química entre Al_2O_3 e pó elementar de Ti. As pastas que continham Ti/TiC/Si/C em sua composição inicial apresentaram menor rugosidade superficial, microestrutura mais densa e maior adesão filme/substrato em comparação com os filmes sem adição de TiC na sua composição inicial. As pastas contendo Ti/TiC/Si/C e excesso de Si na sua composição inicial obtiveram Ti_3SiC_2 como fase primária e Ti_5SiC_x como fase secundária. A condutividade elétrica dos filmes à base de Ti_3SiC_2 sintetizados *in situ* via serigrafia variou de 4.63×10^4 $S.m^{-1}$ a 2.57×10^5 $S.m^{-1}$ numa faixa de temperatura de 25 °C a 400 °C. Para o processo impressão à jato de tinta, uma suspensão de Ti_3SiC_2 foi formulada e caracterizada. Parâmetros como tamanho de partícula, densidade, tensão superficial e viscosidade

foram otimizados com o objetivo de obter estruturas impressas de alta qualidade. A dispersão em suspensão foi melhorada pela adição do dispersante catiônico PEI. Através das análises reológicas e de potencial zeta, foi encontrada uma quantidade ideal igual a 2 % em massa de PEI para a formulação da suspensão de Ti_3SiC_2. A viscosidade da suspensão foi aumentada com o aumento do teor de glicerol. Mais especificamente, a tinta contendo 40% em massa de glicerol mostrou as melhores propriedades para o processo de impressão. A impressão exibiu uma boa formação de gota, o que mostra que a taxa de secagem da tinta foi baixa o suficiente para evitar a secagem antes da ejeção da gota. A deposição de gotas nas superfícies de vidro, KOH e ITO mostrou gotas com diâmetros médios de 53 μm, 50 μm e 37 μm, respectivamente.

Considerações Finais

O processamento de pastas Ti_3SiC_2 através da serigrafia e o processamento de pastas para a síntese *in situ* de Ti_3SiC_2 via serigrafia para posterior utilização em dispositivos eletrônicos foi alcançado. Os resultados apresentados são úteis para a produção de suspensões aquosas de Ti_3SiC_2 adequadas para impressão direta à jato de tinta de materiais cerâmicos. Os filmes a base de Ti_3SiC_2 impressos via serigrafia oferecem uma possível aplicação no campo de materiais condutores de alta temperatura, tornando o processo de serigrafia um método alternativo para o fabrico de tais componentes. No entanto, é importante mencionar que, apesar de ambos os processos permitirem a fabricação de estruturas à base de Ti_3SiC_2, somente usando o processo de serigráfica foi possível produzir estruturas com significativa condutividade elétrica.

Palavras-chave: carbeto de silício titânio, serigrafia, impressão à jato de tinta, aplicações eletrônicas.

ABSTRACT

In this work, the formulation of a novel Ti_3SiC_2 ink for screen printing and ink-jet printing, for subsequent use in electronic devices is presented. For the screen printing process, the influence of different amounts of Ti_3SiC_2 filler (20 to 40 vol%) and binder (EC - ethyl cellulose) (0 to 5 vol%) on the pastes properties, such as rheology, roughness and microstructure as well as the printing quality were investigated. The pastes were screen printed onto paper-derived Al_2O_3 substrates and sintered for 1 h under an argon atmosphere at 1600 °C. Samples with higher viscosity, such as pastes containing 30 vol% and 40 vol% Ti_3SiC_2 gave the smoothest surfaces and highest printing quality regardless of binder. XRD measurements and SEM analysis showed that only pastes with an initial 30 vol% Ti_3SiC_2 yielded TiC as a primary phase and Ti_3SiC_2 as a secondary phase after sintering, suggesting partial decomposition of Ti_3SiC_2. For the others samples the total decomposition of Ti_3SiC_2 occurred. The electrical conductivity of pastes with an initial 30 vol% Ti_3SiC_2 and different amounts of EC ranged from 1.25×10^5 $S.m^{-1}$ to 1.25×10^5 $S.m^{-1}$ in a temperature range from 25 °C to 400 °C. The *in situ* synthesis of Ti_3SiC_2 from elementary powders Ti, TiC, Si and C via screen printing was also successfully performed. After 5 hours sintering at 1400 °C, pastes with TiC and excess Si gave a high printing quality with Ti_3SiC_2 as the primary phase and $Ti_5Si_3C_x$ as a secondary phase. The electrical conductivity of these samples was found to range from 4.63×10^4 $S.m^{-1}$ and 2.57×10^4 $S.m^{-1}$ in a temperature range of 25 °C to 400 °C. For the formulation of an aqueous Ti_3SiC_2 suspension for use as an ink for direct ceramic ink-jet printing, a preliminary study was performed in order to determine the required grain size of Ti_3SiC_2 powder and the fluid properties of the suspension for the chosen printer. A high energy milling process, zeta potential and rheological analysis were carried out to achieve the ink pattern required. Polyethylenimine (PEI) was used as a dispersant and the range of printability was calculated from the inverse of the Ohnesorge number (Z). An aqueous suspension containing 0.05 vol% Ti_3SiC_2, 2 wt% PEI and 40 wt% glycerol, at pH 4.3 and Z-value of 11 was obtained. As a printing surface, glass, KOH and ITO (indium tin oxide) were used.

Key-words: Titanium silicon carbide, screen printing, ink-jet printing, electronic applications.

LIST OF FIGURES

LIST OF TABLES

LIST OF ABBREVIATIONS

Al: Aluminium
C: Graphite
CMOS: Complementary metal-oxide-semiconductor
D_{50}: Particle size distribution
DCIJP: Direct ceramic ink-jet printing
E: Young's modulus
EC: Ethyl cellulose
EDS: Energy-dispersive spectroscopy
G': Storage modulus
G": Loss modulus
IC: Integrated circuits
IEP: Isoelectric point
ITO: Indium tin oxide
KD-1: Hypermer KD-1
KOH: Potassium hydroxide
LVER: Linear viscoelastic region
MEMS: Microelectromechanical system
Oh: Ohnesorge number
OLEDs: Organic light-emitting devices
PCB's: Printed circuits boards
PEI: Polyethylenimine
R_a: Average surface roughness
R_q: Root mean square deviation
SEM: Scanning electron microscopy
Si: Silicon
SOFC: Solid oxide fuel cells
TGA: Thermogravimetric analysis
Ti: Titanium
TiC: Titanium carbide
Vol%: Volume percent
Wt%: Weight percent
XRD: X-ray diffraction
Z: Range of printability
ζ: Zeta
ρ: Electrical resistivity
ρ_m: Measured electrical resistivity
σ: Flexural strength

SUMMARY

1. INTRODUCTION

The importance of materials science to the development of engineering, technology and society is undeniable. Materials science is the key to the development of technological materials for a wide variety of applications, ranging from civil, mechanical and nuclear engineering to consumer items, such as smart phones and decoration articles.

In recent decades, science has become increasingly more interdisciplinary which has allowed for the development of suitable materials for specific applications and needs. Even for specific area such as electrical and electronic engineering, the range of utilities is quite enormous. For example, robotics, computer and mechanical engineering, information technology, biotechnology and medical sciences, instrumentation and consumer items (GUPTA, GUPTA, 2015a).

In the field of ceramics, an example of a remarkable and versatile material, which has been gaining attention over the past years, is the titanium silicon carbide (Ti_3SiC_2). This material is a good example of an versatile material, because it combines the characteristic properties of both ceramic and metals (BARSOUM M.W, 1996; EL-RAGHY, BARSOUM, 1998b; GAO et al., 2002). As it provides the high eletrical and thermal conductivity of metals and the mechanical and chemical stability over a wide range of temperature of ceramics, (GUPTA, GUPTA, 2015a) making it a material with great potential for a wide field of application in various areas including eletrical and electronics.

Furthermore, Ti_3SiC_2 belongs to the class of ternary carbides and nitrides with a laminated structure well known as MAX phases (BARSOUM M.W, 1996). This material is noted for its unique combination of mechanical, electrical and thermal properties of both metal and ceramic materials. It exhibits excellent thermal shock resistance, high electrical and thermal conductivity, oxidation resistance, thermal and chemical resistance, high rigidity, easy machinability, high hardness and high Young's modulus (BARSOUM M.W, 1996; EL-RAGHY, BARSOUM, 1998b; GAO et al., 2002). Its electrical conductivity ranges from $4.5 \times 10^6\ \Omega^{-1}\ m^{-1}$ to $9.6 \times 10^6\ \Omega^{-1}\ m^{-1}$, which is considerably high for ceramics (BARSOUM M.W, 1996; SUN, ZHOU, 1999; CARRIJO et al., 2017), and renders it's potential uses in electrical contacts, high-power electronics, corrosion protective coatings and heat exchanges (EMMERLICH et al., 2007) among others.

The synthesis and processing of Ti_3SiC_2 has been achieved by different technologies, for instance indirect ink-jet printing, preceramic

paper fabrication, HIP-SHS techniques, DC magnetron sputtering and mechanical alloying, among others (CARRIJO et al., 2017; EMMERLICH et al., 2007; LORENZ et al., 2017; LORENZ et al., 2017; DCOSTA et al., 2002; LI, ZHAI, 2005; SCHULTHEIß et al., 2015; CARRIJO et al., 2016; LORENZ et al., 2017). In the electrical and electronic field ink-jet printing and screen printing have gained attention due to their simplicity, low cost and speed velocity.

The screen printing process belongs to the printing techniques which are nowadays used for the fabrication of conductive lines and films. This technique is slowly replacing the conventional methods for production of electronic devices, such as lithography processes. It is a high performance and high-processing speed technique which is low cost, has high reliability, is environmentally friendly and offers the ability to print on different substrates (FADDOUL, REVERDY-BRUAS, BLAYO, 2012). The performance of this process and the quality of the screen printed ceramic films are directly related to the composition and rheological properties of the paste and to the screen-printing parameters, with the main emphasis on the complex relation between paste composition and its rheological behavior (PHAIR, LUNDBERG, KAISER, 2009).

The screen printing process results in the fabrication of thick films due to the deposition of the ceramic paste through a screen mesh and under a determined pressure applied by a squeegee. The printing geometry is drawn onto the screen mesh and thus, it uses only the sufficient quantity of the pastes thereby reducing waste (FADDOUL, REVERDY-BRUAS, BLAYO, 2012; LIN et al., 2008). This process has been used successfully for the fabrication of semiconductors, printed circuits board (PCB), oxide layers in solid oxide fuel cells (SOFC), chemical-sensors arrays and hybrid pH sensors among others (FADDOUL, REVERDY-BRUAS, BLAYO, 2012; GOLDBERG et al., 1994; PHAIR, 2008).

On the other hand, the ink-jet printing technology is a well-known process to produce solid free form parts without the need of masks, die tooling or human interference (TRAVITZKY et al., 2014; MATSUO et al., 2006; SONG, EDIRISINGHE, EVANS, 1999). This technology is based on a computer controlled direct deposition of an ink droplet by droplet through a nozzle onto a substrate. The drop deposition is precise and the amount of the printed ink is well adjusted, which minimizes the material wasting and energy consumption leading to a low cost and time saving process (KUSCHER et al., 2012).

In the ink-jet printing, the success of the printing process is directly related to the optimization of the ink and substrate properties and the printer parameters. Therefore, identification of the particle size and the

fluid properties of the required suspension are critical. The physical parameters of the ink, such as density, viscosity and surface tension are strongly linked with the quality of the jetting process characterized by drop formation, drop diameter and spreading of the droplet on the substrates (KUSCHER et al., 2012). The Direct Ceramic Ink-jet Printing (DCIJP) allows fabrication of microscale ceramic parts, such as microelectromechanical system (MEMS), micro components for fuel cells, sensors and integrated circuits (IC). Currently, microfabrication of ceramic parts is an expensive and time consuming process. For example, the fabrication of ICs and MEMS via lithography requires a specific infrastructure, expensive process conditions and several processing steps, which may last few weeks to obtain the final chip. An alternative option to replace this long process is the freeform fabrication of ceramic parts using ceramic inks through DCIJP (RAMAKRISHNAN et al., 2005).

As of yet there have been no reports of the screen printing of Ti_3SiC_2-based pastes via screen printing or Ti_3SiC_2 inks via direct ink-jet printing. Thus, due to the properties of Ti_3SiC_2 this work proposes the processing of this material via two different processing approaches, (i) screen-printing and (ii) direct ink-jet printing, for electronic materials applications. Beyond that, the *in situ* synthesis of Ti_3SiC_2 from its elemental powder via screen printing is also proposed. The rheological, structural and electrical properties were investigated after each processing technique.

For the screen printing process the formulation of Ti_3SiC_2 pastes with different Ti_3SiC_2 contents, using terpineol as solvent and EC as a binder were proposed. Furthermore, the influence of the pastes composition on its viscoelastic properties and the quality of the printed films onto paper-derived Al_2O_3 substrates were investigated. The same procedures were adopted for the *in situ* synthesis of Ti_3SiC_2. However, for the fabrication of synthesis pastes, commercial Ti, TiC, SiC and graphite powders were used in order to produce pure Ti_3SiC_2 without secondary phases.

For the fabrication of a novel Ti_3SiC_2 ink for DCIJP, it was first necessary to optimize the particle size of the commercial Ti_3SiC_2 by high energy milling and stabilization of the Ti_3SiC_2 suspension. The rheological properties of the pastes and the influence of these on the printing process were investigated.

2. FUNDAMENTALS

2.1. TITANIUM SILICON CARBIDE

2.1.1. General overview

Titanium silicon carbide (Ti_3SiC_2) belongs to the class of ternary carbides and nitrides with a nanolaminated structure well known as MAX phases (EL-RAGHY, BARSOUM, 1998a). This class of materials has the general chemical formula $M_{n+1}AX_n$, where M corresponds to a transition metal; A represents an element of the non-metallic group of the periodic table, more precisely columns 13 to 16 and X refers to carbon or nitrogen and the subscribed index can assume either 1, 2 or 3. (EL-RAGHY, BARSOUM, 1998a; BARSOUM, 2000; DAHLQVIST, ALLING, ROSÉN, 2010; BARSOUM, RADOVIC, 2011; SUN, 2011; RADOVIC, BARSOUM, 2013). Ti_3SiC_2 is so far the most studied MAX phase, it possesses a hexagonal layered crystal structure with two TiC octahedral separated by a planar Si layer (Fig. 1) (EL-RAGHY et al., 1997; RILEY et al., 2002).

Figure 1 – Unit cell of Ti_3SiC_2.

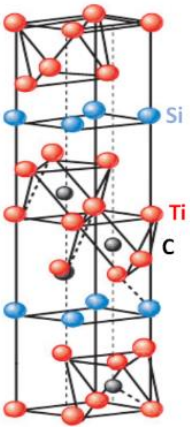

Source: adapted from (BARSOUM, RADOVIC, 2011).

Due to its combination of metallic, covalent and ionic bonds, this material is known as a metal-ceramic system (ARUNAJATESAN,

CARIM, 1995; RADOVIC, BARSOUM, 2013; ABU, MOHAMED, AHMAD, 2014) it also combines the mechanical, electrical and thermal properties of both metals and ceramics. Its metallic character gives Ti_3SiC_2 high electrical and thermal conductivity, low hardness, thermal shock resistance, damage tolerance and ductility. Whereas its ceramic properties bestow it with high Young's modulus, high temperature oxidation and corrosion resistance and render easily machinable without the need for cooling and lubrication (BARSOUM, EL-RAGHY, 1996; EL-RAGHY, BARSOUM, 1998a; EL-RAGHY, BARSOUM, 1999; ZHOU, SUN, 2000; GAO et al., 2002; SUN, 2011; ABU, MOHAMED, AHMAD, 2014).

2.1.2. Synthesis

More than 50 years ago, Jeitschko and Nowotny were the first to synthesize Ti_3SiC_2 via the solid state chemical reaction of TiH_2, Si, and graphite at 2000 °C (JEITSCHO, NOWOTNY, 1967). Subsequent scientific interest has focused on the synthesis of Ti_3SiC_2 by other methods. The pure single-phase Ti_3SiC_2 has been synthesized by chemical vapor deposition (CVD), reactive hot pressing of Ti, graphite and SiC powders at 40 MPa and 1600 °C (BARSOUM, EL-RAGHY, 1996; EL-RAGHY et al., 1997; GAO, MIYAMOTO, ZHANG, 1999) and via CVD of $SiCl_4$, $TiCl_4$, CCl_4 and H_2 as source gases (BARSOUM, EL-RAGHY, 1996; EL-RAGHY et al., 1997; GAO, MIYAMOTO, ZHANG, 1999);(NICKI, SCHWEITZER, LUXENBERG, 1972; GOTO, HIRAI, 1987). Furthermore, techniques such as combustion synthesis, reactive sintering, hot isostatic pressing, arc-melting and consecutive annealing, thermal explosion and spark plasma sintering from elemental powders has also been effectively used for the synthesis of this material (LIS et al., 1995; TONG et al., 1995; BARSOUM, EL-RAGHY, 1996; GAO et al., 2002; SUN et al., 2002; RADOVIC, BARSOUM, 2013; ABU, MOHAMED, AHMAD, 2014).

This research has demonstrated that the main challenge in synthesis of Ti_3SiC_2 is formation of a single-phase product free from unwanted secondary phases. This can be achieved within the strait stable region of Ti_3SiC_2 in the ternary phase diagram of the Ti-Si-C system (Fig. 2) (WAKELKAMP, LOO, METSELAAR, 1991; SAMBASIVAN, PETUSKEY, 1992; ARUNAJATESAN, CARIM, 1995; GAO et al., 2002). Former studies have shown the presence of secondary phases such as TiC, SiC or titanium silicide formed in the synthesis of bulk Ti_3SiC_2

(EL-RAGHY *et al.*, 1997). More specifically, El-Raghy and Barsoum (1996) fabricated samples with less than 2 vol% of SiC and TiC secondary phases via reactive hot pressing from 3Ti/SiC/C at 1600 °C for 4 h (BARSOUM, EL-RAGHY, 1996; GAO, MIYAMOTO, ZHANG, 1999; GAO et al., 2002). A two-step process has also been used to make polycrystalline Ti_3SiC_2 samples in which either titanium, silicon and a carbon powder or TiC, silicon and carbon mixture were first reacted together to form a powder compact that was subsequently pulverized and then hot pressed to give the desired product. These procedures however led to mixtures of Ti_3SiC_2, TiC_x, and $TiSi_2$ and sometimes $Ti_5Si_3C_x$, and/or SiC (EL-RAGHY, BARSOUM, 1999).

Figure 2 - Ternary phase diagram of Ti-Si-C system at 1200 °C (a) under 0.1 MPa (1 atm pressure) and (b) under 240 MPa.

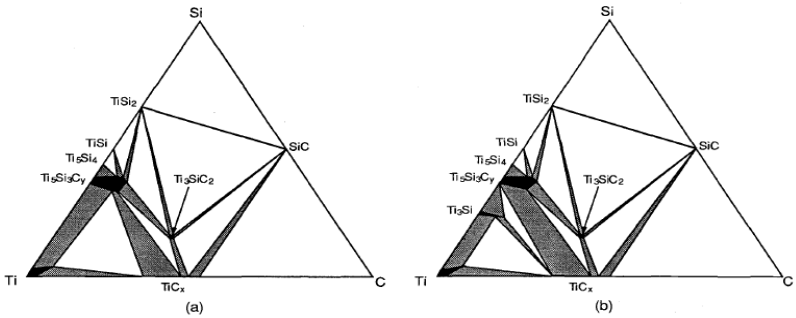

Source: (SAMBASIVAN, PETUSKEY, 1992; ARUNAJATESAN, CARIM, 1995).

The chosen synthesis route for Ti_3SiC_2 directly influences the produced phases and yield. Lis and co-wokers (1995) synthesized samples with 80 vol% to 90 vol% Ti_3SiC_2 and with TiC as a secondary phase via combustion synthesis followed by hot isostatic pressing (PAMPUCH et al., 1989; LIS et al., 1995; MORGIEL, LIS, PAMPUCH, 1996). Zhang and co-workers (2006) used an *in situ* HP solid-liquid synthesis of dense Ti_3SiC_2, resulting in ~ 92 wt% Ti_3SiC_2 (ZHANG et al., 2006) . Riley et al. (2002) used self-propagating high temperatures to synthesize a Ti_3SiC_2-based material with TiC as secondary and minority phase (RILEY et al., 2002). Recently, Lorenz *et al.* (2017) have successfully synthesized pure Ti_3SiC_2 via preceramic paper fabrication process using different elementary powder stoichiometries. In their work,

they optimized the stoichiometry to 3Ti/3TiC/3Si/C and after one hour sintering at 1600°C in argon were able to obtain Ti_3SiC_2 without any other detectable phase (LORENZ et al., 2017).

2.1.3. Properties

Due to formation of multiple phases in the synthesis of Ti_3SiC_2, the properties of the resulting such systems are limited by the chemical interactions and the formation of reaction products (ARUNAJATESAN, CARIM, 1995). For instance, reaction of Ti_3SiC_2 with carbon to form TiC surface layers significantly enhances hardness of the composite. Reaction with silicon, on the other hand, enhances the oxidation resistance and the surface hardness (EL-RAGHY, BARSOUM, 1998a; EL-RAGHY, BARSOUM, 1999).

Temperature also has an influence on the properties of Ti_3SiC_2. At room temperature it is brittle. At temperatures between 1000 °C and 1200°C it has plastic behavior with yield points of 300 MPa and 100 MPa in compression and flexure strength, respectively, and it undergoes a brittle-to-plastic transition (BPT). Whereas at higher pressure Ti_3SiC_2 is plastic even in tension (EL-RAGHY, BARSOUM, 1999; RADOVIC, BARSOUM, 2013).

The multiple properties of Ti_3SiC_2 make it a potential material in fields ranging from civil engineering to military applications. Furthermore it has been considered as a promising material for high-temperature applications, such as sputtering targets for electrical contact deposition, turbine blades (Impact Coatings, Sweden) (RADOVIC, BARSOUM, 2013), wear and corrosion protection, heat exchangers, components where rotating parts are used and low friction applications based on basal plane lubricity (SUN, 2011) (EMMERLICH et al., 2007).

2.1.4. Electronic applications

In the field of electrical and electronic materials Ti_3SiC_2 has gained special attention. Zhou and Sun (2000) performed a study to understand the charge density distribution in different Ti_3SiC_2 planes (ZHOU, SUN, 2000). They concluded that the nature of the Ti_3SiC_2 chemical bonds are anisotropic and metallic-covalent-ionic with a significant contribution from the covalent metal bonds where two adjacent chains of Ti-C-Ti-C-Ti share an Si atom forming a pair of chains of similar length to the cell dimension in the c-direction. The long parallel chains of Ti_3SiC_2 are joined by nonhomogeneous metal bonds. In the atomic layers, especially

in the layers of the Ti atom, which are parallel to the basal planes, there is the strong contribution of the metallic bonds. Due to this special crystal chain structure and the metallic-covalent-ionic nature of bonding, unusual properties are expected for this phase, such as a high melting point (3000 °C) and high electrical conductivity (SUN, ZHOU, 1999; ZHOU, SUN, 2000). Barsoum and El-Raghy (1996) determined the electrical conductivity at room temperature of Ti_3SiC_2 is 4.5 x 10^6 Ω^{-1} m^{-1}. Later, Sun and Zhou (1999) found values of 9.6 x 10^6 Ω^{-1} m^{-1}, (BARSOUM, EL-RAGHY, 1996; SUN, ZHOU, 1999), which is almost two times higher than pure Ti and three times higher that TiC (SHI, ZHANG, LI, 2008).

As already mentioned, the electrical conductivity in this material is attributed to its metal bonds parallel to the basal plane in its structure (SUN, ZHOU, 1999; ZHOU, SUN, 2000). It has characteristics of a mixed conductor where the same concentrations and mobilities of free electrons and holes over an extended temperature range are observed (BARSOUM et al., 2000). Moreover, it has a negligible thermopower in the range of 300K to 800K, which makes it a potential alternative for measurement of the thermopower of other substances and high temperature thermocells (YOO, BARSOUM, EL-RAGHY, 2000).

More potential electrical and electronic applications for Ti_3SiC_2 encompass: ohmic contact formation of silicon Schottky diodes produced via screen printing (RATAKONDA et al., 1998) electrical contacts (EMMERLICH et al., 2004), electromagnetic interference shielding (SHI, ZHANG, LI, 2008), electrodes in electrochemical cells, conducting films on dielectric and semiconductors devices (RILEY et al., 2002), among others.

2.2. PRECERAMIC PAPERS

Preceramic paper is a lightweight structure made up of organic fibers (pulp fibers) and ceramic fillers. The difference between preceramic papers and ordinary writing paper is the amount of filler content and the type of filler. Writing paper consists of 20-30 wt% of inorganic fillers, for instance, kaolin, titanium and alumina. Preceramic papers have an amount of ceramic filler up to 95 wt%. The papermaking process itself offers cost-efficiency, shapeability and production output and when used for the fabrication of preceramic papers has the added advantage of allowing fabrication of complex structures (SCHLORDT et al., 2014).

The paper formation process consists of three main steps: (i) preparation of an aqueous feedstock suspension containing pulp fiber and ceramic filler, (ii) retention process due to coagulation and flocculation of the fibers and filler using polymeric additives and (iii) paper formation by dewatering of the feedstock suspension, and subsequent wet pressing and drying. A schematic representation of the preceramic paper sheet fabrication is shown in Fig. 3 (TRAVITZKY et al., 2008; SCHLORDT et al., 2014).

Figure 3 – Illustration of preceramic paper sheet manufacturing.

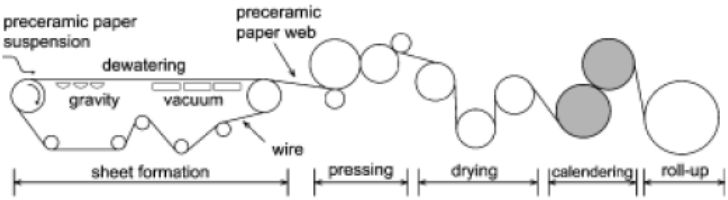

Source: (TRAVITZKY et al., 2008)

The success of paper formation is directly linked to the composition of the feedstock suspension, which contains fibers, fillers, retention aid and binder. If it has a low solid content (0.5 – 5 wt%) filler and fiber retention may attain a weight ratio of 5:1 to 10:1 in the dry state of the sheet formation, which is considered a high value. Therefore, the interaction of filler-to-filler and filler-to-fiber is essential to achieve a high filler loading of preceramic paper that can present flexibility and strength required for paper-based shaping and machining procedures (TRAVITZKY et al., 2008). Besides that, the properties of the green paper such as, porosity, smoothness, dimensional stability, strength, stiffness and pore size distribution will depend on chemical interactions between the fibers, filler content and particle size of the filler (TRAVITZKY et al., 2008; SCHLORDT et al., 2014).

Pulp fibers are well known in the papermaking process and are derived from different wood plants, such as eucalyptus, pine and many others (LORENZ et al., 2015). The most used fibers in papermaking are the lignocellulosic fibers, which are composed of cellulose, hemicelluloses and lignin. Cellulose ($C_6H_{10}O_5$) is the load-bearing components present in fibers. It holds six hydroxyl groups, which provide the fibers a high

stiffness and tensile strength due to intermolecular and intermolecular hydrogen bonding (TRAVITZKY et al., 2008; SILVA et al., 2009).

For a high retention filler a particle size smaller than the fiber diameter is required. Thus, the retention process for papermaking is a filtration process or mechanical entrapment, e.g. a ceramic-fiber web is formed on the wire due to the obstruction of the filler particles on the fiber matrix. The denser the fiber network, the greater the filler entrapment. Furthermore, flocculation and coagulation process are used in chemical assisted retention when high-speed paper machines are needed. In these cases, colloidal aggregation plays a significant role, once the residence time is reduced, causing a low contribution of mechanical entrapment (TRAVITZKY et al., 2008).

Coagulation is the process of neutralization of the surface charges in the aqueous feedstock suspension. The coagulating agent prevents electrostatic repulsion due to neutralization of the charge surface and thus induces agglomeration of the particles. The negative surface charges resulting from carboxyl and sulfonic acids groups is neutralized by an effective cationic coagulant, which reduces the distance between particles so that the flocculants can "link" them. Flocculation is the step in which a high-molecular-weight (HMW) polymer is used to bridge the neutralized particles and form agglomerates (TRAVITZKY et al., 2008).

After fabrication and the intended conformation processing (shaping, cutting, compression, calendering, Laminated Object Manufacturing (LOM) among others) of the preceramic papers conversion into a ceramic product can be undertaken. This step consists in of the burn out of the pulp fibers and consolidation of the ceramic content (TRAVITZKY et al., 2008). The high amount of ceramic present in this material guarantees the conversion of the green preceramic paper into a dense particle-packing structure (SCHLORDT et al., 2014). Depending on the type of ceramic filler used (oxide, carbide or nonoxide ceramics), the ceramic products may present different properties. However, the thermal decomposition of the cellulose-based fibers must be controlled (TRAVITZKY et al., 2008).

After sintering the paper derived-ceramic yields a porous structure (TRAVITZKY et al., 2008) (LORENZ et al., 2015), which can be used for a wide range of applications, like heating insulation structures, kiln furniture, porous burner substrates, fire protection structures and catalyst support (JUNKES et al., 2013; LORENZ et al., 2017).

Al_2O_3 has gained attention due to its outstanding mechanical properties at both room and high temperature. It is resistant to erosion, has a high melting point and is widely used as an insulator in electronics (SHI, ZHANG, LI, 2008). For instance, Al_2O_3 is extensively used for

ceramic packages due to its good insulating properties, thermal and mechanical characteristics and chemical inertia (LU et al., 1995). Paper-derived Al_2O_3 combines both, the outstanding properties of the material and the cost-effective production of preceramic paper formation methods.

2.3. SCREEN PRINTING

Despites the number of studies involving the synthesis of Ti_3SiC_2 and the *in situ* synthesis of thin films via different processes (PALMQUIST et al., 2002; EMMERLICH et al., 2004; HÖGBERG et al., 2005; LANGE, BARSOUM, SCHAAF, 2007), there are no studies involving the synthesis and processing of thick films from this material via screen printing technology.

This technique is an age-old printing process originated by the Chinese and Japanese in which a semi-liquid pigment was pressed using a squeegee through a fine-mesh "silk" screen to form the given design onto any desired surface (ALKEMA, 1990). Nowadays, it is a well-known technique used for the deposition of thick films (PAN, TONKAY, QUINTERO, 1999). The process consists of deposition of a paste onto a substrate with the aid of a squeegee under a certain pressure through the screen mesh. The paste has the composition of the required material. The screen mesh possesses the required printing geometry and thus, it uses only the sufficient paste quantity avoiding waste (LIN et al., 2008; FADDOUL, REVERDY-BRUAS, BLAYO, 2012). Fig. 4 illustrates the screen printing process.

Figure 4 – Illustration of screen printing process and screen mesh.

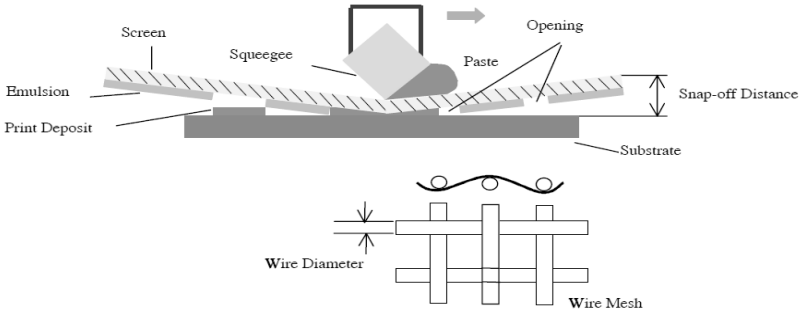

Source: Adapted from (PAN, TONKAY, QUINTERO, 1999)

The performance of this process and the quality of the screen printed films of ceramics depends on the composition and rheological properties of the paste, manufacturing steps and screen-printing parameters with the main emphasis on the complex relation between paste composition and its rheological behavior (PHAIR, KAISER, 2009).

The pastes properties directly influence the quality of the screen printed layer but also the performance of the screen printing process. Adjustment of the rheological properties of the pastes is required to optimize the screen printing process itself. Fig. 5 presents the viscosity and the shear rate requisite in the four main steps during the screen printing process (PHAIR, KAISER, 2009). During screen printing the pastes will be submitted to different shear rates through the various step processes. 100 s^{-1} is the maximum value of shear rate that an ordinary printing screen can reach during ink penetration through the screen mesh (LIN et al., 2008).

Figure 5 - Viscosity and shear rate requisite during screen printing process steps. I: Rest, II: Squeegee, III: Mesh and IV: Recovery.

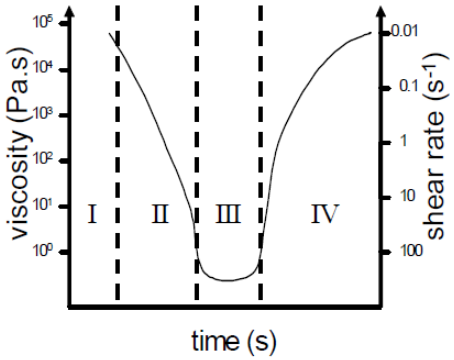

Source: (PHAIR, KAISER, 2009)

Screen printing pastes are normally composed of vehicles (solvent and additives) and inorganic powders (ceramic and glass powders). While paste preparation depends on the required properties of the printed films (LIN et al., 2008), the printing quality will be affected by the dispersion and stability of the ceramic content and rheological behavior (liquidity, thixotropy and viscoelasticity) (LEE et al., 2006; LIN et al., 2008;

MURAKAMI et al., 2014). As shown above, during the screen printing process the pastes are submitted to different shear rate which explains why the rheological characteristics of pastes at high shear rate values muss be taken into account (LIN et al., 2008).

The dispersion and stability of screen printing pastes includes the choice of the optimal vehicle (solvent and binder) which will allow the fabrication of high loaded ceramic pastes. The binder plays an important role in the manufacturing of screen printing pastes. Even low contents of the paste will affect the viscoelastic properties of the paste due to its capacity. It also allows printing of high-density pastes without defects. However, the excess addition of binder can induce clogging of the screen printer stencil, poor fluency and absence of ink during the screen printing process. The binder also influences the thickness and the levelling of screen printed films. The levelling of the screen printing pastes is important because it will determine the smoothness, which influences the mechanical and electrochemical performance of the film (PHAIR, KAISER, 2009). Furthermore, the binder also provides strength, density, adhesion, retardation of sedimentation and inner structure to the green films (LEE et al., 2006; MURAKAMI et al., 2014; PHAIR, KAISER, 2009)

Ethyl cellulose (EC) is widely used in paste fabrication as a binder due to its ability to tailor rheological properties (thixotropic and shear thinning behavior) for screen printing. This arises from the ability of EC to form hydrogen bonds and its surface affinity. EC is a polymer comprised of glucose as monomers. It can be produced by replacement of ethoxyl groups (-OC_2H_5) by hydroxyl groups (-OH) in the cellulose structure (Fig. 6) (LEE et al., 2006; INUKAI et al., 2015) The control of the rheological properties will assure that the screen printed films will be successfully produced without any defects or pinholes (MURAKAMI et al., 2014).

Figure 6 - Chemical structure of ethyl cellulose.

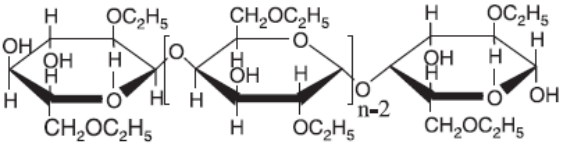

Source: (LEE et al., 2006)

It is not just the composition of the paste which influences the properties of the screen printed films, a number of process parameters also influence the final quality of the screen printed films (PAN, TONKAY, QUINTERO, 1999). Fig 7 shows the different factors which have an influence on the screen printing quality.

Figure 7 - Summary of the different factors that influence the screen printing quality.

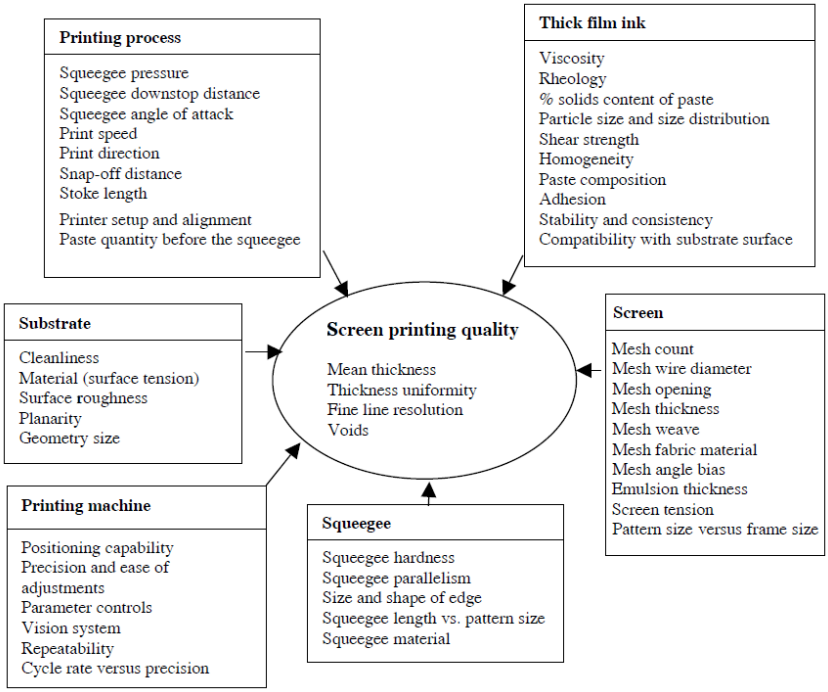

Source: (PAN, TONKAY, QUINTERO, 1999)

The screen printing process has been used for many years for a number of different applications, ranging from production of clean energy, such as oxide layers in Solid Oxide Fuel Cells (SOFC) and oxygen separation membranes (PHAIR, KAISER, 2009) to manufacturing of chemical-sensors arrays, hybrid pH sensors (GOLDBERG et al., 1994; LIN et al., 2008; PHAIR, 2008) and organic light-emitting devices (OLEDs) (JABBOUR, RADSPINNER,

PERYGHAMBARIAN, 2001). Goldberg and co-workers (1994) used the screen printing process to deposit silver epoxy contacts on an aluminum sensor pad and polymeric membrane in various sites of a multisensory chip to fabricate 3 different types of chemical sensor chips with different complexities of design more than 10 years ago (GOLDBERG et al., 1994). More recently, Jabbour and co-wokers (2001) used screen printing for the deposition of ultrathin layers of organic materials with less than 15 nm for OLEDs production (JABBOUR, RADSPINNER, PERYGHAMBARIAN, 2001).

Moreover, the screen printing process belongs to the range of printing process techniques used nowadays for fabrication of conductive lines and films. Conventional techniques to produce electronic devices involve silicone micromachining and manufacturing using lithographic methods. However, lithography is an expensive, time consuming and limited process, which consists of several steps, including chemical treatments, silicone oxide growth, spin coating, photo-exposure, banking and negative development. Therefore, screen printing has emerged as a potential alternative as it offers high performance, low cost, a high processing speed, reliability, tailoring to different substrates and environmentally friendly. (FADDOUL, REVERDY-BRUAS, BLAYO, 2012). Additionally, it promotes a division of the processing steps, which is no longer possible using complementary metal–oxide–semiconductor processing (CMOS), (GOLDBERG et al., 1994).

It is widely used in the electronics industry for preparation of solder pastes, printed circuits boards (PCB's) (PHAIR, KAISER, 2009), fabrication of conducting lines on to ceramic substrates for microelectronic interconnection and multilayered interconnection arrays, including successive printing of conductor and insulator layers (SAVAGE, 1969; GUPTA, GUPTA, 2015b). For instance, DuPont Electronic & Communication Technologies reported in 2004 the use of screen printing for the fabrication of thick film materials for circuits (GUPTA, GUPTA, 2015b).

2.4. INK-JET PRINING

Ink-jet printing technology is a well-known process to produce free form parts without the need for masks, die tooling or human interference (SONG, EDIRISINGHE, EVANS, 1999; MATSUO et al., 2006; TRAVITZKY et al., 2014). This technology encompasses two approaches: direct and indirect ink-jet printing (TAY, EVANS, EDIRISINGHE, 2013; TRAVITZKY et al., 2014).

The indirect ink-jet printing approach, known as Drop on Powder or Drop on Bed deposition, consists of an ink composed of a binder solution that is printed directly onto a powder layer, bonding one layer to another until the body is completely formed (SLADE, EVANS, 1998; DIMITROV, SCHREVE, BEER, 2006; TRAVITZKY et al., 2014). In this approach, the three-dimensional printer possesses a spray head with a cartridge - which is responsible for depositing the binder solution - and two bays, one for powder feeding and another for a building, where the part is created. After receiving a command from CAD-program the spray head starts to deposit the binder solution onto the first powder layer. Once that the spray head moved across the two bays, it rolls over a new layer of powder from the feed bay to the build bay, and then the spray head deposits the binder solution onto the new layer (Fig. 8) This process is repeated until the final part is obtained (SUN et al., 2002).

Figure 8 – Illustration of indirect ink-jet printing for 3D structures.

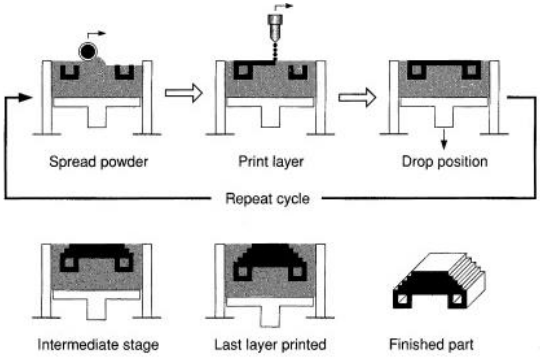

Source: (JEE, SACHS, 2000)

The direct ink-jet printing method, also called Drop on Drop deposition, consists of an ink composed of the desired material, which is printed onto a printing substrate (Fig. 9) (SLADE, EVANS, 1998; SONG, EDIRISINGHE, EVANS, 1999; DIMITROV, SCHREVE, BEER, 2006). In the field of ceramics, ceramic suspensions are used as an ink as they can be printed and then dried due to the evaporation of the volatile solvent leaving a printed ceramic (RAMAKRISHNAN et al., 2005; TRAVITZKY et al., 2014). Bonding between the ceramic suspension and the substrate is achieved by printing onto an absorbent substrate. As ink-jet printing produces dense ceramic parts, it is the only technique in

additive processing that does not require post-processing treatments (TSENG, LIN, WANG, 2006; TRAVITZKY et al., 2014).

Figure 9 – Illustration of direct ink-jet printing process.

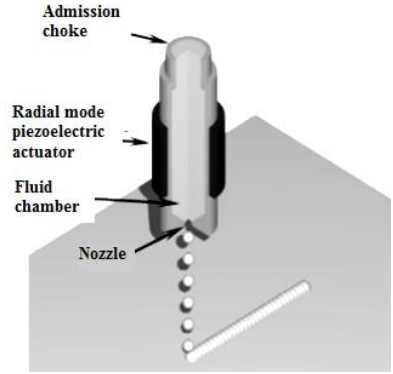

Source: adapted from (LEWIS et al., 2006)

In the specific case of ceramic suspensions used as inks for piezoelectric ink-jet printing, the term direct ceramic ink-jet printing (DCIJP) is commonly used (SONG, EDIRISINGHE, EVANS, 1999; RAMAKRISHNAN et al., 2005; PRASAD et al., 2006). In this specific approach, the optimization of the ink and substrate properties and the printer parameters are important factors for the quality and success of the printing process (KUSCHER et al., 2012). Therefore, it is essential to identify the particle size and the fluid properties of the suspension. The diameter of the printer nozzle usually ranges from 20 to 75 µm. Consequently, an ideal particle size will prevent the clogging of the nozzle during the jetting process (RAMAKRISHNAN et al., 2005) and avoid pressure fluctuation, which may switch off the control system. Suitable formulation and stabilization of a colloidal ink are key factors in the DCIJP process. On the one hand, unsuitable formulation of the ink may lead to the formation of agglomerates, and thus, the nozzle of the printer can be clogged. On the other hand, unstable suspensions may sediment in the pipelines and valves of the printer (SONG, EDIRISINGHE, EVANS, 1999).

An ink formulation with high ceramic content is usually desired owing as it increases the rate of deposition. Increasing ceramic content is, however, a limiting factor because the ink needs to flow through the

micron size nozzles (RAMAKRISHNAN et al., 2005). The physical properties of the ink such as density, viscosity and surface tension are strongly linked with the quality of the jetting process characterized by drop formation, drop diameter and spreading of the droplet on the substrates (KUSCHER et al., 2012). From these properties the range of printability (Z) of the ink can be measured using the inverse of the Ohnesorge number (*Oh*) prior to undertaking the printing process (FROMM, 1984; JANG, KIM, MOON, 2009).

The advantages of DCIJP include the ability to tailor the ink through blending and diluting the ceramic suspension. This gives access to graded composition quality, good surface properties, high density of printed bodies (MOTT, EVANS, 1999; TRAVITZKY et al., 2014), low cost, time saving and no material wasting. Moreover, correct ink composition allows the process to be computer controlled so that direct deposition of the ink droplet by droplet through a nozzle onto the substrate can be achieved giving precise high fidelity deposition (KUSCHER et al., 2012). This allows microscale fabrication of ceramic parts, such as microelectromechanical system (MEMS), micro components for fuel cells, sensors and integrated circuits (IC). Currently, microfabrication of ceramic parts is an expensive and time consuming process. For example, the fabrication of integrated circuits (ICs) and MEMS via lithography requires a specific infrastructure, expensive process conditions and, consequently, it takes few weeks to obtain the final chip. An alternative option to replace this long process is the freeform fabrication of ceramic parts using ceramic inks through ink-jet printing (DCIJP) (RAMAKRISHNAN et al., 2005). However, in direct ink-jet printing the variety of materials is limited (DIMITROV, SCHREVE and DE BEER, 2006).

Different ceramic inks have been formulated from nanopowders of TiO_2, ZrO_2, Al_2O_3, CeO_2 and $BaTiO_3$ nanopowder (RAMAKRISHNAN et al., 2005; DING et al., 2004; MATSUO et al., 2006; PRASAD et al., 2006; TSENG, LIN, WANG, 2006; EBERT et al., 2009; KUSCHER et al., 2012; TRAVITZKY et al., 2014). Whilst, Ti_3SiC_2 has already been processed via indirect ink-jet printing (CARRIJO et al., 2016; SUN et al., 2002) it has not yet been used as a feedstock material for the DCIJP process.

In this work, ink-jet and screen printing were chosen as the printing processes for the fabrication of Ti_3SiC_2 structures for potential electronic applications. As of yet there have been no reports of the screen printing of Ti_3SiC_2-based pastes via screen printing or Ti_3SiC_2 inks via direct ink-

jet printing. Beyond that, the *in situ* synthesis of Ti_3SiC_2 from its elemental powder via screen printing is also proposed.

3. OBJECTIVES

3.1. GENERAL

- Production of Ti_3SiC_2 pastes for screen printing;
- Formulation of Ti_3SiC_2 ink for direct ink-jet printing;
- Evaluation of microstructural and electrical properties of ink-jet and screen printed structures for electronic applications.

3.2. SPECIFIC

- Production of pastes for the screen printing process varying the concentrations of Ti_3SiC_2 and binder as well as pastes based on Ti, TiC, Si, and graphite for *in situ* synthesis of Ti_3SiC_2 via screen printing;
- Evaluation of the influence of the pastes on the screen printing process and on the properties of the Ti_3SiC_2-based screen printed structures onto paper-derived Al_2O_3 substrates before and after sintering;
- Evaluation of the influence of the Ti_3SiC_2 inks on the direct ink-jet printing process and on the properties of the Ti_3SiC_2-based ink-jet printed structures;
- Evaluation of the feasibility of the screen and direct ink-jet printing in the production of the Ti_3SiC_2-based structures for electronic applications.

4. EXPERIMENTAL PROCEDURE

4.1. PAPER-DERIVED Al_2O_3 SUBSTRATES

4.1.1. Preceramic paper formation

Paper-derived Al_2O_3 was used as a substrate for the screen printing of Ti_3SiC_2 and synthesized pastes. The preceramic paper sheets loaded with 75 vol% Al_2O_3 (CT 3000 SG, Almatis GmbH, Frankfurt, Germany) with particle size of 0.5 µm and pulp fibers were fabricated using a handsheet former (Dynamic hand-sheet former D7, Sumet Systems GmbH, Denklingen, Germany). The flow rate was 5.45 mL/min and the wire speed was set to 1000 rpm. For the pulp fiber content a mixture containing 40 wt% non-refined thermomechanical softwood pulp (Orion ECF, Zellstoff Pöls AG, Pöls, Austria) and 60 wt% non-refined hardwood pulp (Celbi PP, Celulose Beira Industrial (Celbi) S.A., Figueira da Foz, Portugal) was prepared. The softwood pulp had an average diameter and length of 22 µm and 1665 µm, respectively, and the hardwood pulp had an average diameter and length of 15 µm and 657 µm, respectively. The organic additives consisted of anionic (Fibraffin A5, Südstärke, Germany) and cationic starch ester (Fibraffin K72, Südstärke, Germany). Latex and polyacrylamides were used as retention aid (Percol, BASF Paper Chemical, Germany). The addition of these components aided in the flocculation process of the feedstock suspension and thus allowed sheet formation due to its solid retention. After processing, the paper sheets were dried in a paper dryer machine for 15 min at 110 °C.

4.1.2. Laminates fabrication

Laminates of Al_2O_3 preceramic papers were fabricated with the aim to improve the mechanical properties of the substrates. They consisted of four layers of the Al_2O_3 preceramic papers with a rectangular geometry. The layers were stacked together using glue based on 58.1 wt% thermoplastic adhesive (Planatol AD95, Planatol Holding, Thansau, Germany), 27.4 wt% Al_2O_3 powder, 13.0 wt% distilled water and 1.5 wt% dispersant (Darvan CV, Vanderbilt Minerals, Norwalk/CT, USA). The deposition of the glue on the three bottom layers was made by coating manually with a spiral doctor blade. The coated layers were first dried at

60 °C for 10 min and afterwards the 4 layers were pressed together with 10 MPa at 80 °C for 5 min.

4.1.3. Sintering

The conversion of preceramic paper into paper-derived Al_2O_3 was achieved by sintering at 1600 °C for 4 h in air. Before the sintering process the laminated structures were submitted to burn out of the organic contents in air. A dwell time of 1 h at 350 °C and 800 °C was chosen according to dilatometry analysis. Fig. 10 exhibits the burn out and sintering profile applied.

Figure 10 - Burn out and sintering profile used for the laminate Al_2O_3 preceramic papers.

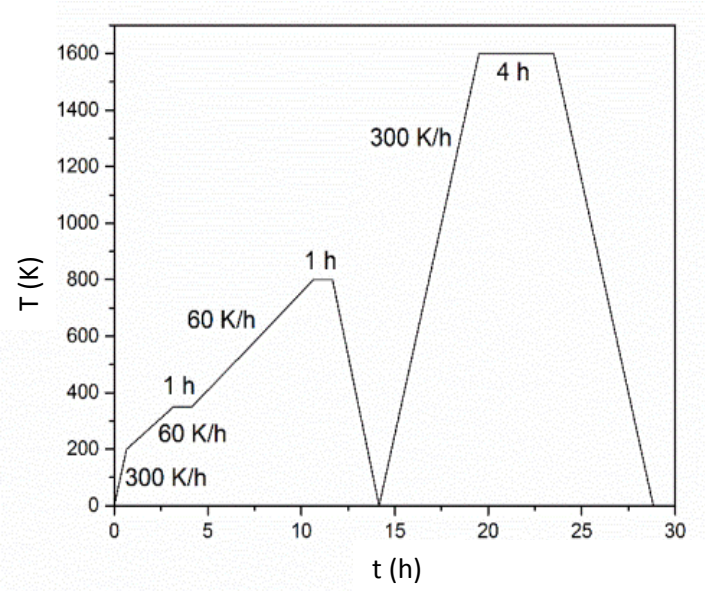

4.1.4. Characterization

For the characterization of the laminates of paper derived-Al_2O_3 an average of ten samples were used for each analysis.

4.1.4.1. Density

The apparent density for the sintered samples was determined using the Archimedes method (DIN EN 623-2, 1993). Distilled water was used in all the measurements and the values are given by equation (1).

$$\rho = \frac{M1}{M1-M2} \times \rho H_2O \quad (1)$$

Where,
M_1 = dry mass of the sample;
M_2 = mass of the sample immersed in water;
ρH_2O = 0.9978 g/cm^3 (at 22 °C)

4.1.4.2. Dimensional changes

The dimensional changes after sintering were calculated using equation (2), according to changes in the length (Δy), width (Δx), height (Δz) and volume (ΔV).

$$\Delta x = \frac{X\,initial - X\,final}{X initial} \times 100 \quad (2)$$

For the dimensional measurement a tapered micrometer gauge was used to measure at least five points of each sample.

4.1.4.3. Mechanical properties

The effective Young's Modulus of sintered laminates was measured with an ultrasonic measuring device (Krautkrämer GmbH, Hürth, Germany), according to EN 843-2 (DIN EN 843-2, 2007). The propagation time of a longitudinal wave in the sample was defined and the resonance peaks in the horizontal and vertical directions of the samples were measured as showed in equation (3).

$$E = \varphi \cdot \left(\frac{l}{t}\right)^2 \cdot \frac{(1+\nu).(1-2\nu)}{1-\nu} \quad (3)$$

Where,
E = Young's Modulus (GPa);

l = length of sample (mm);
t = resonance time (μs);
ν = Poisson ratio for Al_2O_3 (0.21);
φ = real density (g/cm^3).

A ring-on-ring setup (DIN 51105, 2010) was required to obtain the flexural strength by using a universal testing machine (model 4204, Instron Deutschland GmbH, Pfungstadt, Germany). A top ring with 3 mm radius and bottom ring with 8 mm radius were used. From equation (4) it was possible to calculate the flexural strength.

$$\sigma_E = \frac{3P\left[\frac{(1-\nu)\left(a^2-r_0^2\right)}{2b^2}+(1+\nu)\cdot\ln\left(\frac{a}{r_0}\right)\right]}{2\pi d^2} \quad (4)$$

Where,

d = thickness of the sample (mm);
ν = Poisson's ratio for Al_2O_3 (0.21);
a = supporter ring's radius (mm);
r_0 = load ring's radius (mm);
b = $b' \cdot \frac{(1+\sqrt{2})}{4}$ (mm); where b' = edge length of the samples
P = breaking load (N).

4.2. SCREEN PRINTING

4.2.1. Production of Ti_3SiC_2 pastes

Ti_3SiC_2 powder (Beijing Jinhezhi, Material Co, Ltd, Bejing, China) with 2 wt% of TiC/Ti_5Si_3 and particle size of 1.5 μm (D_{50}) was used as ceramic filler for paste production. Ethyl cellulose (EC) and terpineol (Fluka Chemie GmbH, Buchs, Switzerland) were used as a binder and solvent, respectively. The binder was first dissolved in terpineol using mechanical stirring at ~ 80 °C and afterwards Ti_3SiC_2 powder was added using a three-roll mill (Exakt Advanced Technologies GmbH, Norderstedt, Germany). A fixed amount of 2 vol% of dispersant (Hypermer KD-1, Uniqema, Everberg, Belgium) was used in the preparation process. Table 1 presents the composition of the Ti_3SiC_2 pastes.

Table 1 – Composition of Ti_3SiC_2 pastes.

Pastes	Terpineol		EC		KD-1		Ti_3SiC_2	
	vol%	wt%	vol%	wt%	vol%	wt%	vol%	wt%
P (0-20)	79.6	45.0	0.0	0.0	0.4	0.27	20.0	54.7
P (0-30)	69.4	32.2	0.0	0.0	0.6	0.33	30.0	67.4
P (0-40)	59.2	23.3	0.0	0.0	0.8	0.37	40.0	76.3
P (3-20)	76.6	43.1	3.0	2.1	0.4	0.27	20.0	54.5
P (3-30)	66.4	30.7	3.0	1.7	0.6	0.33	30.0	67.2
P (3-40)	56.2	22.1	3.0	1.4	0.8	0.37	40.0	76.1
P (4-20)	75.6	42.5	4.0	2.7	0.4	0.27	20.0	54.4
P (4-30)	65.4	30.2	4.0	2.3	0.6	0.33	30.0	67.2
P (4-40)	55.2	21.7	4.0	1.9	0.8	0.37	40.0	76.0
P (5-20)	74.6	41.9	5.0	3.4	0.4	0.27	20.0	51.4
P (5-30)	64.4	29.8	5.0	2.8	0.6	0.33	30.0	67.1
P (5-40)	54.2	21.3	5.0	2.4	0.8	0.37	40.0	76.0

The first numerical index in the pastes composition corresponds to the amount of binder (vol %) and the second numerical index represents the amount of ceramic content (vol %) present in the pastes.

4.2.2. Production of synthesis pastes

For the *in situ* synthesis of Ti_3SiC_2 via the screen printing process, pastes were produced using its elementary powders, such as Ti, TiC, Si, and graphite (Table 2).

Table 2 - Particle size (D_{50}) and raw materials suppliers.

	D_{50}	Supplier
Ti	25 µm	ABCR GmbH & Co. KG, Karslruhe, Germany
TiC	2.5 µm	H.C.Starck, Laufenberg, Germany
Si	3 µm	Siligrain, Kristiansand, Norway
C	4 µm	Lehmann und Voss Co. KG, Hamburg, Germany

Two different powder mixtures were used: (i) Ti/Si/C and (ii) Ti/TiC/Si/C. For each mixture, two different stoichiometries (Table 3) were prepared. The organic additives, such as EC and terpineol, were used as binder and solvent. The amount of carbon provided from these additives was also taken into account.

Table 3 - Composition of synthesis pastes.

	$P_{1.1}$ (7-27)		**$P_{1.2}$ (5-28)**		**$P_{2.1}$ (3-36)**		**$P_{2.2}$ (3-35)**	
	vol%	wt %	vol%	wt%	vol %	wt%	vol %	wt %
Terpineol	65.5	41.6	67.3	42.1	61.1	33.1	61.6	34.5
EC	7.2	19.8	4.5	12.1	3.4	7.8	2.9	7.0
Ti	10.5	26.2	13.0	32.0	9.6	20.6	8.4	18.5
Si	7.9	10.2	9.7	12.5	10.8	12.0	14.1	16.1
Graphite	8.9	2.2	5.5	1.3	4.1	0.9	3.5	0.8
TiC	----	----	----	----	11.0	25.7	9.5	23.1
Stoich.	3Ti/2Si/2C		3Ti/2Si/C		3Ti/3TiC/3Si/C		3Ti/3TiC/4.5Si/C	
Mixture	Ti/Si/C				Ti/TiC/Si/C			

The subscribed index indicates the composition and stoichiometry of the pastes. The first subscribed index corresponds to the composition (powder mixture) and the second subscribed index indicates the stoichiometry. For instance, $P_{1.1}$ corresponds to the paste with Ti/Si/C and stoichiometry of 3Ti/2Si/2C, whereas $P_{1.2}$ corresponds to the paste with Ti/Si/C but with stoichiometry of 3Ti/2Si/1C.

4.2.3. Screen printing and sintering process

A screen printer (ELA, DEK - ASM Assembly Systems GmbH, Munich, Germany) was used to deposit the Ti_3SiC_2 and synthesis pastes onto the paper-derived Al_2O_3 substrates. The screen printing process was undertaken at a print speed 150 mm/s, with a screen mesh of 333 µm, snap-off distance of 2 mm and a squeegee pressure of 100 N. The screen used was made of polyester (Koenen GmbH, Riemerling, Germany).

Table 4 contains the detailed parameters of the printing process and the screen. A single print was made onto the substrate, followed by drying for 24 h at room temperature (~ 20 °C) and further drying for 24 h at 80 °C.

Table 4 - Screen printing process parameters.

	Parameters	Characteristics
Screen	Mesh opening	333 µm
	Mesh thickness	250 µm
	Open screen surface	49 %
	Thread diameter	140 µm
	Mesh count	21 cm^{-1}
Print process	Snap off	2 mm
	Squeegee Pressure	100 N
	Print speed	150 mm/s

After drying, the green screen printed samples of Ti_3SiC_2 pates were sintered at 1600 °C for 1 h in a flowing argon atmosphere with a heating and cooling rate of 180 K/h. The synthesis pastes were sintered at 1400 °C for 1, 3 and 5 h in a flowing argon atmosphere with a heating and cooling rate of 180 K/h.

The print design is presented in Fig. 11. In order to obtain more accurate measurements the print design was classified in two parts: (1) corresponding to the thinner line and superior part of the design and (2) to the larger and lower part.

Figure 11 - Print design.

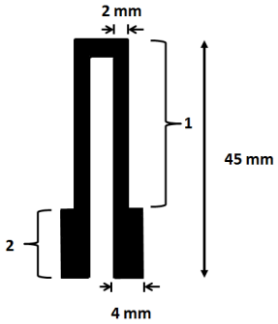

Source: the author

4.2.4. Characterization

4.2.4.1. Pastes

Before the screen printing process the Ti_3SiC_2 and synthesis pastes were submitted to rheological and thermal analysis. For the rheological characterization, averages of five runs for each sample were performed.

4.2.4.1.1. Rheological analysis

Measurements of the rheological behavior of the pastes were carried out at 20 °C using a modular compact rheometer (MCR 302, Anton Paar GmbH, Graz, Austria). For high viscosity samples the parallel-plate geometry with diameter of 50 mm and gap of 1mm was used and for low viscosity samples a cone and plate set up with diameter of 17 mm and gap of 1 mm was used. The flow behavior measurements were carried out with shear rates in the range from 1 s^{-1} to 100 s^{-1}. All pastes presented a shear thinning behavior and therefore, measurements at higher shear rates were not conducted.

For the dynamic viscoelastic test the storage modulus (G') and loss modulus (G") were measured using a sweep measurement for shear stresses ranging from 0.01 to 1000 Pa at a frequency of 1.0 Hz.

The 3-step recovery test was used to simulate the screen printing process. In the first and third step an oscillatory shear stress of 1 Pa at 1.0 Hz was applied for 600 s. In the second step a high rotational shear rate of 100 s^{-1} was applied for 180 s. In order not to interfere with the pastes network, the pastes were left to rest for 300 s in the apparatus prior to analysis, thus, the samples had time to recover. The recovery ratio (%) was calculated from the measurement on the first and third step using equation (5) (INUKAI et al., 2015).

$$\text{Recovery ratio} = \frac{\text{G'at 1680 s in third step}}{\text{G' at 900 s in the first step}} \text{ x } 100 \qquad (5)$$

4.2.4.1.2. Thermal analysis

Thermogravimetric analysis (TGA) (STA 449F3 Jupiter, Netzsch Instruments GmbH, Selb, Germany) was performed on pastes containing

3 vol% EC. The measurement was performed under an argon atmosphere from 20 °C up to 1500 °C with a heating rate of 5 K/min.

The same analysis was performed for the organic additives present in the pastes up to 600 °C. The aim of this analysis was to determine the amount of residual carbon for the calculation of the synthesis pastes.

4.2.4.2. Screen printed layers

After the screen printing process of the Ti_3SiC_2 and synthesis pastes, the green and sintered structures were characterized using the analysis below.

4.2.4.2.1. Surface analysis

A confocal microscope (NanoFocus AG, Oberhausen, Germany) was used in order to evaluate the surface properties of the green and sintered screen printed layers. For the line profile, topography images and measurement of thickness and roughness values, a scan image surface ≈ 1.0 mm x 3.0 mm) of part 1 of the print design (Fig. 11) was used. For evaluation of the data, WinSam 2.6.08 software (Department of Manufacturing Technology - LFT, University of Erlangen Nuremberg), was used. The software anables a three-dimensional surface area scan of the sample. The quality of the images was optimized using a leveling method called line to line. The line to line leveling method comprises the adjustment of an image profile line with a polynomial equation which is then subtracted from that image line. The average height of each line is set equal to the previous corrected line (MÉNDEZ-VILAS, DÍAZ, 2007).

The calculation of surface roughness parameters such as R_a (average surface roughness) and R_q (root mean square deviation) was performed by drawing ten section lines (~2 mm) over each screen printed layer. For the calculation along a measured line (Z(x)), equation (6) and (7) (DIN EN ISO 4287, 2010) were required.

$$R_a = \frac{1}{l} \int_0^l \left| Z(x) \right| dx \tag{6}$$

$$R_q = \sqrt{\frac{1}{l} \int_0^l Z^2(x) dx} \tag{7}$$

4.2.4.2.2. Phase composition

For X-ray diffraction analysis (D8 Advance, Bruker Corporation, Billerica, USA), solid area films were prepared in order to avoid interference from the substrates during analysis. The solid area films of all pastes compositions were prepared manually and sintered with the same sintering profile as the screen printed samples. For the analysis, samples were exposed to monochromatic Cu-Kα radiation with a scanning rate of 0.01 °/s over a 2θ-range from 25 ° to 95 °.

4.2.4.2.3. Microstructure

The microstructure of the sintered samples were analyzed using scanning electron microscopy (SEM, Quanta 200, FEI, Prague, Czech Republic) coupled with energy-dispersive X-ray spectroscopy (EDX, INCA x-sight TVA3, Oxford Instruments, Oxford, UK) for compositional analysis. Both the surface of printed pastes and polished cross-section were analyzed.

4.2.4.2.4. Electrical properties

For electrical measurements of the sintered screen printed layers part 2 of the print design was used. A heating apparatus (PE95/T95 System Controller, Linkam Scientific Instrument, Tadworth, UK) was required in order to do the analyses in a temperature range between 25 °C and 400 °C. The electrical resistivity was measured using a DC four-point probe method (Keithley 2450 source Metter, Tektronix Inc., Beaverton, USA) and its values were obtained using equations (8) and (9).

$$\rho_m = 2\pi s R \tag{8}$$

$$\rho = 0.73\left\lfloor\frac{th}{s}\right\rfloor \rho_m \tag{9}$$

Where,
ρ_m = measured resistivity (Ω.m);
ρ = resistivity (Ω.m);
R = resistance (Ω)
th = thickness (m);
s = probe distance (m).

When a conductive film is deposited onto an insulating surface, a correction factor (0.73) is necessary once the ratio between sample thickness and distance of probes (th/s) is smaller than 1. The samples thicknesses were measured using a confocal microscope (item 4.24.2.1) and all samples were analyzed in triplicate.

4.3. INK-JET PRINTING

4.3.1. Formulation of Ti_3SiC_2 ink

For the production of Ti_3SiC_2 inks it was first necessary to tailor the ink properties to the patterns required for the chosen piezoelectric printer (Table 5). Therefore, it was first necessary to achieve the required particle size of Ti_3SiC_2 powder and the optimal pH and viscosity values of the ink.

4.3.1.1. Milling process

The as-received Ti_3SiC_2 powder (Beijing Jinhezhi, Material Co, Ltd, Bejing, China) with 2 wt% of TiC/Ti_5Si_3 and initial D_{50} of 6 μm was used for the production of ink suspensions. To achieve a smaller particle size, the as-received Ti_3SiC_2 powder was first dry milled in a planetary ball mill (PM 100, Retsch GmbH, Haan, Germany) in a stainless steel jar at 300 rpm. The milling time ranged from 0.5 to 5 h, with a ball to powder weight ratio of 20:1 using milling balls with a diameter ranging from 1 to 5 mm.

4.3.1.2. Production of the Ti_3SiC_2 ink

For the ceramic suspensions, the Ti_3SiC_2 powder from the milling process with $D_{50} \leq 0.2$ μm was used. Deionized water and polyethylenimine (PEI) (molecular weight: 10,000.00; Sigma-Aldrich Ltda, Sao Paulo, Brazil) were used as solvent and dispersant, respectively. The pH was adjusted by addition of 0.1 M KOH and 0.1 M HNO_3 solutions. Glycerol was added to adjust the viscosity of the suspentions.

For preparation of the ink, the samples were placed for one hour in an ultrasonic bath and the agitated for 2 minutes with an ultrasounic probe (750 Watt and 20 kHz) prior to further filtration before the printing process. A filtration stage was required in order to ensure that only Ti_3SiC_2 with a particles size equal to or less than 0.2 μm were used in the suspensions. Therefore, a filter with a pore size of 0.2 μm was utilized (Chromafil ® RC-20/15, Macherey-Nagel GmbH & Co. KG, Düren, Germany).

As explained above, the pastes composition had to be tailored to the patterns of the chosen printer. Thus, the ink compositions are shown and discussed in item 5.2.

4.3.2. Preparation of the printing substrates

In order to evaluate the performance of the Ti_3SiC_2 inks, three different types of surface were used as substrate: (i) a commercial glass plate (Cat.No.7101, Bioslide, Curitiba, Brazil), (ii) a commercial glass plate coated with KOH and (iii) a glass plate coated with ITO (indium tin oxide) (Sigma-Aldrich, Co., St. Louis, USA). All substrates had dimensions of 10 mm width, 10 mm length and 1 mm thickness.

For the printing process, the commercial glass plate and glass plate coated with ITO were cleaned with an aqueous detergent solution, ethyl alcohol and acetone using the ultrasonic bath for half an hour for each solvent. To prepare the KOH surface, a commercial glass plate was first mechanically cleaned with an aqueous detergent solution and afterwards immersed manually in a 0.1 M KOH aqueous solution until a film of KOH on the glass was formed before being removed. The KOH film was left to dry at room temperature.

4.3.3. Ink- Jet printing process

The Ink-Jet Printing was performed using a drop-on-demand piezoelectric ink-jet printer (Dimatix DMP 2831, Fujifilm Dimatix Inc., Santa Clara, United States) with 16 nozzles and a nozzle diameter of 21.5 µm. Each nozzle was excited independently with 24 V and a frequency of 2 kHz. The drop speed was set to 6 m/s. The printer patterns are presented in Table 5.

Table 5 – Printer patterns for the suspension.

Particle Size (µm)	Solvent volatility (°C)	Density (g/cm^3)	Viscosity (mPa.s)	Surface Tension (mN/m)	pH
< 0,2	>100	>1	2-30	32-42	4-9

100 droplets in a 10 x 10 grid and in lines were printed on the three types of substrates. After optimizing the printing parameters, lines with 1, 2 and 3 layers were printed (Fig. 12).

Figure 12 - Lines pattern.

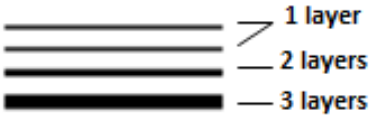

Source: the author.

4.3.4. Characterization

4.3.4.1. Ti_3SiC_2 powder

4.3.4.1.1. Particle size

The particle size distribution (D_{50}) of Ti_3SiC_2 powder was measured after the milling process in water at pH 9 using dynamic light scattering (Zetasizer zen 3600, Malvern, instrument Ltd, Malvern, United Kingdom).

4.3.4.1.2. Phase composition

In order to know the crystallographic structure and crystallite size after the milling process, the Ti_3SiC_2 powder from different milling time was analyzed by the X-ray diffraction (Kristalloflex D500, Siemens, Karlsruhe, Germany). The diffraction angle (2θ) was measured with a scanning rate of 1.2 °/min in a range of 10 ° to 70 ° with Cu-Kα radiation. The crystallite size was determined from the Debye-Scherrer formula (equation (10)).

$$0.9 \times \lambda = d \times B \times \cos\theta \qquad (10)$$

Where,

d = particle size (nm);
λ = equipment wavelength (1.54056 Å);
B = width of the line at half height of the highest intensity diffraction peak (radians);

θ = incidence angle of the X-ray beam at the most intense peak of the diffractogram.

The samples were also analyzed by Raman spectroscopy using an thermo Scientific Nicolet™ Almega Raman spectrometer coupled with a high-quality Olympus visible microscope, and a high resolution grating (2400 lines/mm) using a 532 nm laser.

4.3.4.1.3. Morphology

Scanning electron microscopy (SEM - Quanta 200, FEI, Czech Republic) was used to analyze the morphology of the Ti_3SiC_2 powder before and after milling with the D_{50} required for production of the ink. For SEM analysis, the powder was deposited on an aluminum stub and sputtered with gold.

4.3.4.2. Ti_3SiC_2 ink

4.3.4.2.1. Zeta potential

The zeta potential as a function of pH was required to investigate the stability of aqueous suspensions of Ti_3SiC_2 with D_{50} of 0.16 μm as a function of PEI content (1.2 and 3 wt%). The analysis was performed at room temperature using a ζ-potential analyzer (Zetasizer zen 3600, Malvern instrument Ltd, Malvern, United Kingdom) and a bench top pH Meter (K39-2014B, Kasvi, Sao José dos Pinhais, Brazil). For the pH adjustment, 0.1 M HNO_3 and NH_4OH solution were used. All suspensions were prepared with 0.008 vol% of Ti_3SiC_2.

4.3.4.2.2. Rheology

For the rheological analysis a rotational viscometer with concentric cylinder geometry (HAAKE VT550, Thermo Fisher Scientific GmbH, Dreieich Germany) at shear rates up to 1000 s^{-1} was used. This analysis was used for two purposes: (i) identification of the optimal amount of PEI to be used for the production of the Ti_3SiC_2 suspensions and second, to suit the viscosity of the suspensions with the viscosity required by the printer. For the first purpose, suspensions with 5 vol% Ti_3SiC_2 and different contents of PEI (1 to 3 vol%) were analyzed. For viscosity analysis, suspensions with 0.05 vol% and 0.1 vol% Ti_3SiC_2 with different glycerin contents (20 to 40 wt%) were analyzed.

4.3.4.2.3. Surface tension

Surface tension was measured with aqueous suspensions containing Ti_3SiC_2 (D_{50} = 0.16 µm), 2 wt% PEI and different contents of glycerol with 20, 30 and 40 wt%. The measurement was performed at room temperature using a pendant drop method with a contact angle measuring device (OCA 30, Dataphysics instruments GmbH, Filderstadt, Germany).

4.3.4.2.4. Printability

From the properties of the ink, the range of printability can be measured using the inverse of the Ohnesorge number (Oh), represented by Z (equation (11)) (FROMM, 1984; JANG, KIM, MOON, 2009).

$$Z = \frac{(\alpha\rho\gamma)^{\frac{1}{2}}}{\eta} \qquad (11)$$

Where,
α = nozzle diameter (21.5 µm);
ρ = ink density (g/cm^3);
γ = ink surface tension (mM/m);
η = viscosity of the ink (mPa.s).

5. RESULTS AND DISCUSSION

5.1. SCREEN PRINTING

5.1.1. Paper-derived Al_2O_3 substrate

The open porosity, dimensional changes, effective Young's Modulus (E) and flexural strength (σ) of paper-derived Al_2O_3 laminates used as substrates for screen printing are shown in Table 6.

Table 6 - Properties of paper-derived Al_2O_3 laminates sintered for 1 h at 1600 °C.

Open porosity (%)	Dimensional changes (%)				E (GPa)	σ (GPa)
	Δx	Δy	Δz	Δv		
28.6 (± 4.8)	25.6 (± 0.3)	25.1 (± 0.6)	1,4 (± 0.1)	0.9 (± 0.1)	246.5 (± 9.9)	55.6 (± 10.6)

During the conversion of preceramic paper into paper-derived ceramic, the elimination of volatile compounds, such as water, carbon dioxide, acids, carbonyl groups and alcohols occurs. The conversion of cellulose into carbon involves the elimination of water (~ 150 °C), dehydration of cellulose (150 °C to 240 °C), chain scissions (240 °C to 400 °C) and formation of graphitic layers (above 400 °C) (GREIL, 2001; TRAVITZKY et al., 2008). After the removal of the organic portion, the ceramic content is consolidated by sintering (KLUTHE et al., 2012).

Due to elimination of these organic compounds a porous structure forms (TRAVITZKY et al., 2008; JUNKES et al., 2013). Similar values for porosity were found by Junkes *et al.*, (2013) and Schlordt *et al.*, (2014) for a single layer paper-derived Al_2O_3 without post-treatment. (JUNKES et al., 2013; SCHLORDT et al., 2014). The effective Young's modulus was approximately 35 % higher than that presented by Schlordt *et al.*, (2014) with same porosity values. The values of flexural strength are in the same range as the calculated values of Rhyshkewitch (1953) (RYSHKEWITCH, 1953).

5.1.2. Ti_3SiC_2 pastes

All paste compositions were successfully produced except for paste P (5-40) which showed a high viscosity preventing production. Fig. 13 present the flow curves for pastes with 20 vol%, 30 vol% and 40 vol% Ti_3SiC_2 filler and different amounts of EC.

All pastes exhibited shear thinning behavior, which became more pronounced with increasing of Ti_3SiC_2 content. Even pastes without the addition of EC showed shear thinning behavior indicating that the amount of ceramic content in the pastes was not high enough to form clusters under the applied shear rate (LIN et al., 2008; INUKAI et al., 2015).

Viscosity was observed to increase upon addition of EC. The solid content of the pastes was also observed to influence paste viscosity. Those pastes with 20 vol% Ti_3SiC_2 showed lower viscosity in comparison with pastes of 30 vol% and 40 vol% regardless the amount of EC. Fig. 13 (a), shows that paste P (4-20) had a lower viscosity than paste P (3-20), which suggests that the addition of EC up to 4 vol% for pastes with 20 vol% Ti_3SiC_2 ensured the dispersion of Ti_3SiC_2 particles (INUKAI et al., 2015).

Figure 13 - Viscosity vs. shear rate curves for pastes with (a) 20 vol% Ti_3SiC_2, (b) 30 vol% Ti_3SiC_2 and (c) 40 vol% Ti_3SiC_2 with different amounts of EC.

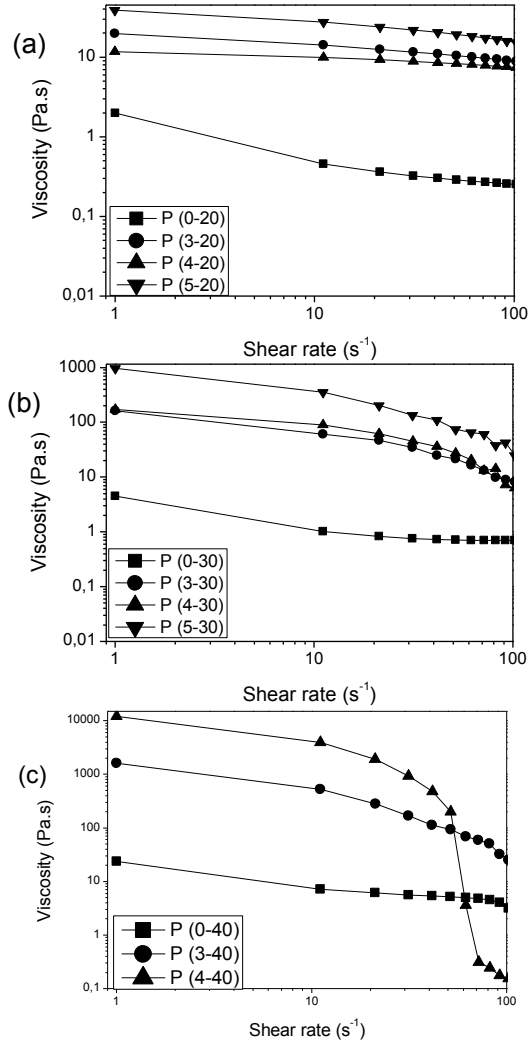

The viscoelastic properties of the Ti_3SiC_2 pastes were investigated via stress sweep analysis (Fig. 14), which presents the shear stress dependence of storage modulus (G') and loss modulus (G''). This analysis was made with the aim of examining the resistance of deformation of the pastes at a constant frequency of 1 Hz.

Figure 14 - Shear stress dependence of the storage (G') and loss (G") modulus for pastes with (a) 20 vol% Ti_3SiC_2, (b) 30 vol% Ti_3SiC_2 and (c) 40 vol% Ti_3SiC_2 with different amounts of EC.

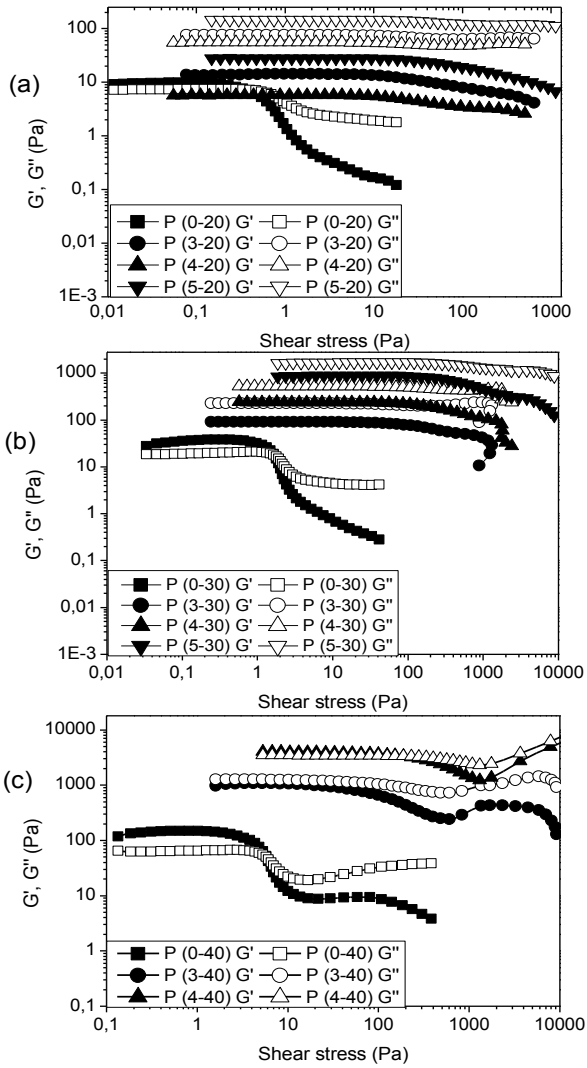

From Figs. 14 (a-c) it is possible to observe that the values of G' and G" not only increased with increasing EC content, but also with increasing particle content. This corroborates the results presented in the flow curves of Figs. 13 (a-c), which reveal not only the influence of the

binder but also the direct influence of ceramic content on paste viscosity. The influence of binder and particle content on the properties of the pastes is more evident when comparing the values of G' and G'' for pastes (0-20) and (0-40) in which, the latter paste composition consistently gave higher values. The influence of the binder is evident in the pastes without EC. Regardless of the amount of ceramic content, solid-like behavior in the a linear viscoelastic region (LVER) was observed with a cross over at approximately 7.3 Pa, 16.9 Pa and 52.2 Pa for P (0-20), P (0-30) and P (0-40), respectively. The crossover point indicates the specific stress rate where the solid- and liquid-like behaviors are equal (G' = G") (PHAIR, 2008).

Unlike the pastes formulated without binder, pastes with 20 vol% and 30 vol% Ti_3SiC_2 containing EC (Fig. 14 (a - b)) had a linear viscoelastic region (LVER) at lower stress regions (< 10 Pa). At a critical stress value, the decrease of G' for both particle content systems, with different EC contents started to occur. The same behavior was observed for the G" value for these pastes, except for pastes P (3-30) and P (4-30), where G" remained constant up until a critical stress at which increased to a maxima before decreasing again. This behavior is characteristic for a Maxwell fluid (PHAIR, 2008). In both cases (Fig. 14 (a - b)), the pastes had liquid-like behavior in the region, where the G'' value was higher than G' for the pastes with 20 vol% and 30 vol% Ti_3SiC_2 content. For pastes with 40 vol% Ti_3SiC_2 content (Fig. 14 (c)) and 3 vol% and 4 vol% EC a LVER at lower shear stress was evident, only the paste with 3 vol% EC (P (3-40)) exhibited a liquid-like state. The pastes P (0-40) and P (4-40) had a solid-like state in the lower strain region and crossover points at ~6 Pa and ~ 188 Pa, respectively.

Fig. 15 shows the 3-step recovery test for the Ti_3SiC_2 pastes. This analysis was made with the intention of simulating the screen printing process so as to identify the rheological behavior of the pastes during the screen printing process. The three step analysis simulates: (i) pre-printing, (ii) high shear flow of the paste through the mesh and (iii) the relaxation of the paste after removal of the screen mesh (DOLLEN, BARNETT, 2005). The first step consisted of measuring of the linear viscoelastic region using a low shear stress (0.1 %) in order to perturb the samples slightly. In the second step the samples were submitted to a higher shear stress of 100 s^{-1} in order to breakdown the sample's network and allow for measurement of the sample's viscosity. The third step was the same as the first step, however this step was used to identify the recovery of the G' of the samples as a function of time between first and

third step. The recovery ratio of the samples and their respective values are shown in Fig. 16 and Table 7.

Figure 15 - 3-step recovery measurement. Storage modulus (G') and viscosity as function of elapsed time for (a) 20 vol% Ti_3SiC_2, (b) 30 vol% Ti_3SiC_2 and (c) 40 vol% Ti_3SiC_2 with different amounts of EC.

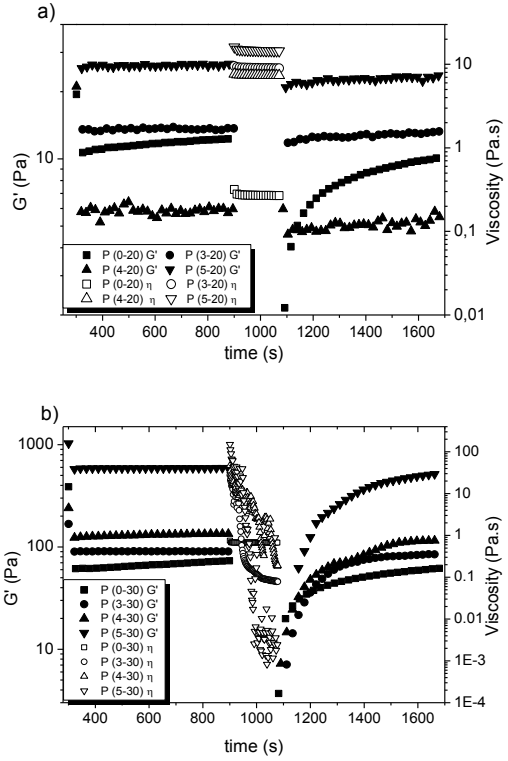

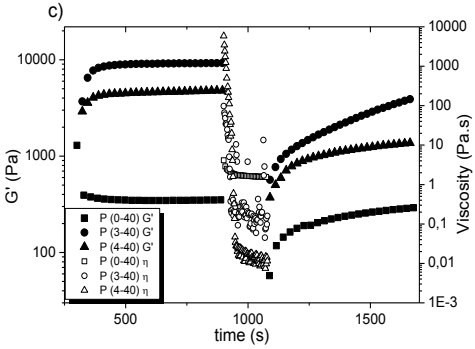

No significant change in the viscosity was observed for pastes containing 20 vol% Ti_3SiC_2 under a higher shear rate (Fig. 15 (a)), which can be attributed to the low ceramic content. The viscosity of the pastes with 30 vol% and 40 vol% Ti_3SiC_2 (Fig. 15 (b) and (c)) was time dependent. This was due to the high number of particles in the pastes, which cause a progressive breakdown of the network during shearing (INUKAI et al., 2015). However, the particle content of the samples should not be the single factor taken into account. Fig. 16 presents the recovery ratio plotted as function of EC content. For pastes prepared without EC, it is noted that regardless of the ceramic content, there was no significant difference of the G' values in the 3-step testing. This indicates that the addition of binder improved the rheological behavior. The same behavior was observed for samples with 20 vol% ceramic content regardless the amount of EC, in which the recovery ratio was in excess of 82 % (Table 7). For samples with 30 vol% Ti_3SiC_2 only the paste P (4-30) showed a significantly low recovery ratio (86.7 %). Paste P (4-30) had a higher viscosity compared to P (4-20) and its lower recovery ratio can be attributed to this factor (PHAIR, LUNDBERG, KAISER, 2009). P (3-40) and P (4-40) had the lowest recovery ratios returning values of 43.2 % and 28.6 %, respectively. The high particle content of these pastes, resulted in high viscosity values of which influenced the recovery ratio.

Figure 16 - Recovery ratio as function of EC content for the Ti_3SiC_2 pastes.

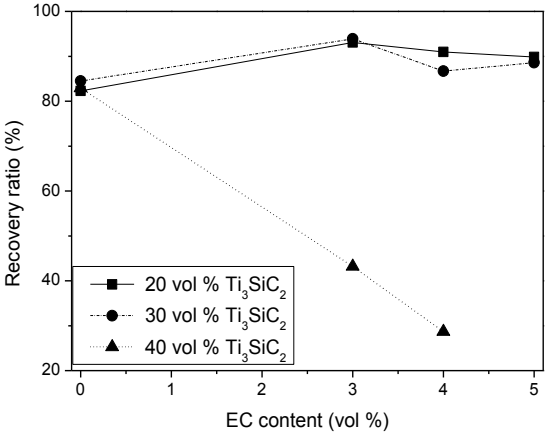

Table 7 - Recovery ratio of Ti_3SiC_2 pastes.

Ti_3SiC_2 Pastes	Recovery ratio (%)
P (0-20)	82.3
P (0-30)	84.5
P (0-40)	82.9
P (3-20)	93.1
P (3-30)	93.9
P (3-40)	43.2
P (4-20)	96.3
P (4-30)	86.7
P (4-40)	28.7
P (5-20)	89.8
P (5-30)	88.6

5.1.3. Screen printing of Ti_3SiC_2 pastes

All pastes were successfully screen printed onto paper-derived Al_2O_3 substrates, except P (4-40), which had the highest viscosity of the samples. After printing and sintering processes, pastes with lower viscosities, such as pastes without the addition of EC content and pastes containing 20 vol% Ti_3SiC_2, did not have good dimensional stability (Fig. 48 in Appendix A). Paste P (0-40) even became detached from the substrate after sintering. Fig. 17 shows the green printed structures with 30 vol% Ti_3SiC_2 and different EC contents, which had the best dimensional stability of the printed pastes. The binder content in the pastes is the main reason for the low printing quality. The amount of binder directly influenced the quality of the green and sintered films. If the strength of the green network is not high enough to maintain the printed structure, irregularities during the drying process can occur. On the other hand, if the binder content is too high it can decrease the quality or even prevent the printing process by inducing clogging of the screen printer stencil, or give poor fluency or absence of the paste (PHAIR, LUNDBERG, KAISER, 2009). Moreover, defects can occur due to the decrease in thickness as a result of binder decomposition during sintering (MURAKAMI et al., 2014). The ceramic content also plays an important role on the quality of the screen printed layers. Suspensions with high solid loading (> 80 wt%) guarantee the absence of voids and cracks during the sintering process during formation of ceramic layers (PHAIR, KAISER, 2009). However, the high amount of solid content can also alter the printing process and the quality of the screen printed structure. This could explain why it was not possible to print paste P (4-40), which had a high viscosity resulting from the high amount of binder and ceramic content. In this work, there may be a threshold value at which the content of both EC and Ti_3SiC_2 particles is optimal for screen printing. Hence, it was important to obtain an optimal paste composition to achieve high-performance of the screen printing process (PHAIR, LUNDBERG, KAISER, 2009).

Figure 17 – Representative images of pastes with 30 %Ti_3SiC_2 and different amounts of EC after screen printing.

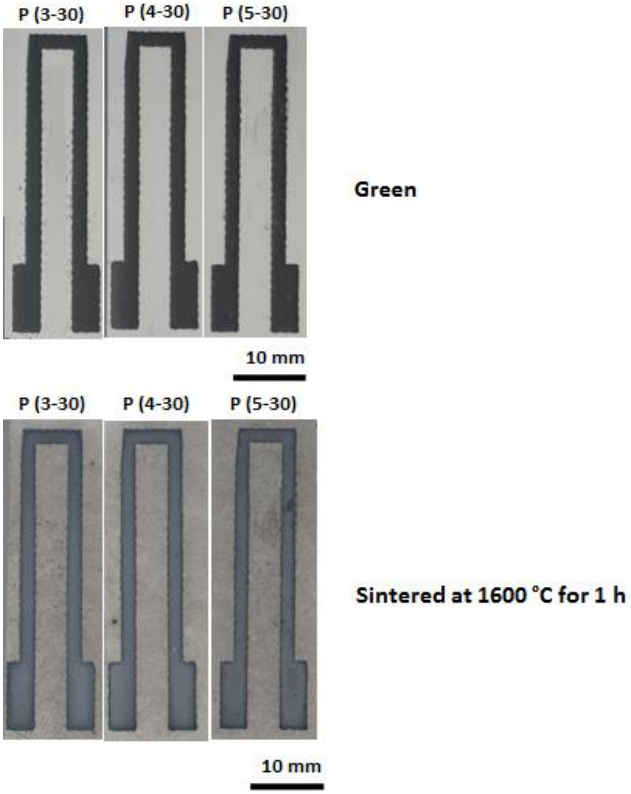

5.1.3.1. Surface analysis

Fig. 18 presents the topography of the green screen printed films. Pastes P (0-20), P (0-30) and P (3-40) were observed to have the most irregular surfaces. For P (0-20) and P (0-30), the irregular surface can be attributed to the absence of binder. However, P (0-40) did not contain EC and resulted in a film with similar surface properties to pastes with 30 vol% Ti_3SiC_2. In this case, the ceramic content is the major factor influencing the printing quality. Despite the presence of binder in pastes P (3-40), this sample had the highest viscosity among. Therefore, the well-defined depressions and humps in this sample could be attributed to the gap between the wires of the mesh, a phenomena also observed by

Phair et al. 2009 (PHAIR, LUNDBERG, KAISER, 2009). Green samples printed with pastes 30 vol% Ti_3SiC_2 exhibited the most homogeneous surfaces. This observation supports the existence of a Ti_3SiC_2 content threshold of maximum printing quality regardless of binder content.

Figure 18 - Topography images of green screen printed layers of Ti_3SiC_2 pastes.

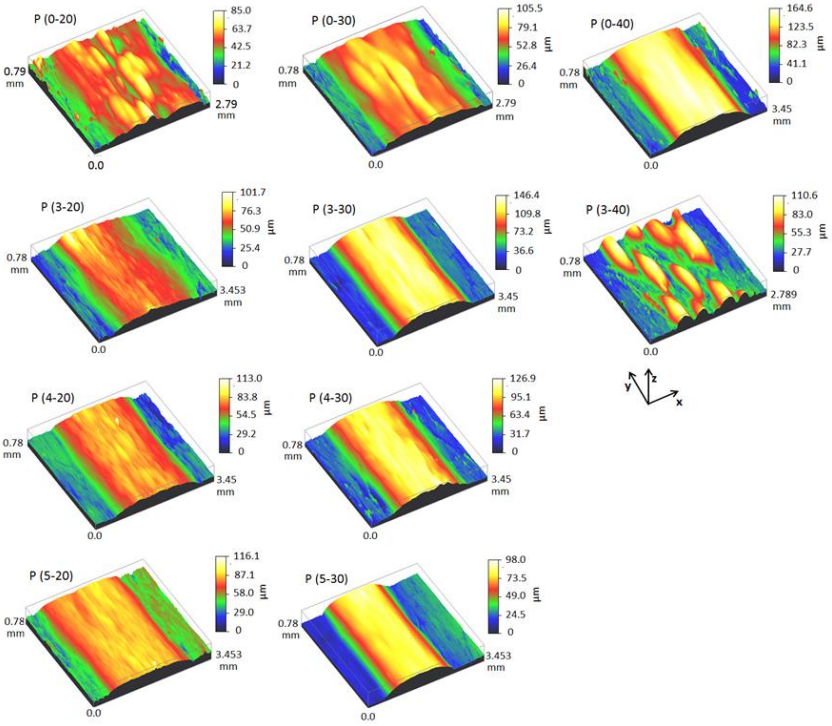

Fig. 19 shows the topography images of screen printed layers after sintering at 1600 °C for 1 h. In addition to pastes with 30 vol% Ti_3SiC_2 and different EC contents, printing of pastes with 5 vol% EC also gave films with relatively homogeneous surfaces after sintering. This result can be assigned to the amount of binder in these pastes (PHAIR, LUNDBERG, KAISER, 2009). This also correlates with the R_a and R_q values (Table 9), which were in close agreement and did not differ greatly between green and sintered samples.

Figure 19 - Topography images of sintered screen printed layers at 1600 °C for 1 h of Ti_3SiC_2 pastes.

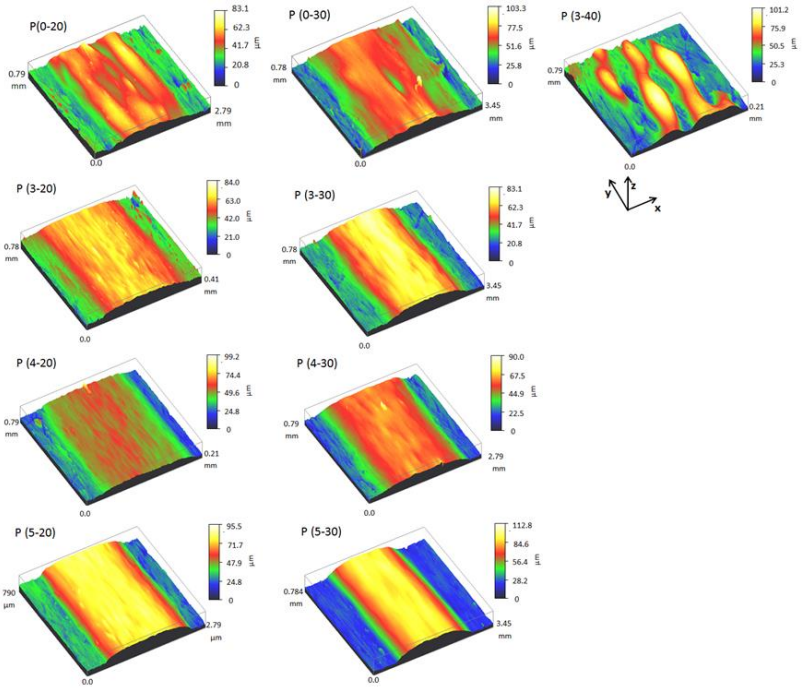

The tabulated thickness values (Table 8) give overall information about the height variation on the samples surface (SEDLAČEK, PODGORNIK, VIŽINTIN, 2009). The thickness for all samples was seen to decrease after sintering. Furthermore, the influence of both binder and solid content on the samples can be observed. After sintering, the highest sample thickness was present for films printed from pastes with higher solid content, when pastes with the same EC content were compared. Films printed from pastes with higher EC content were observed to have the highest thickness. Increased binder content in the pastes leads to an increase in the printed layer thickness (PHAIR, LUNDBERG, KAISER, 2009).

Table 8 - Thickness of screen printed films of Ti_3SiC_2 before and after sintering for 1 at 1600 °C.

Samples	Thickness (µm)	
	green	Sintered
P (0-20)	~40	~30
P (0-30)	~50	~30
P (0-40)	~80	-
P (3-20)	~40	~30
P (3-30)	~100	~40
P (3-40)	~100	~50
P (4-20)	~50	~40
P (4-30)	~75	~50
P (5-20)	~40	~40
P (5-30)	~80	~80

Line profiles of green and sintered Ti_3SiC_2 pastes were used to determine the thickness of the samples. Since samples presented an irregular surface, an approximation was made in order to know the thicknesses values. In appendix A line profiles of all samples are shown with the exception of P (0-40), which detached from the substrate after the sintering process (Fig. 49 and 50 in Appendix A).

The R_a and R_q values of green and sintered screen printed layers are presented in Table 9. P (0-20) had the highest roughness values when compared to other samples without EC content. This can be attributed to its heterogeneous surface caused by the absence of binder and lower Ti_3SiC_2 content in the paste. The highest values of roughness were observed to films printed from paste P (3-40), as was observable from the topography images (Fig. 18 and 19). This roughness occurred as a result of the high viscosity of this paste, which increase the leveling time and hence increased the surface roughness and thickness of the printed layer (PHAIR, LUNDBERG, KAISER, 2009).

Table 9 - Roughness values of screen printed layers of Ti_3SiC_2 before and after sintering for 1 h at 1600 °C.

Samples	Green		Sintered	
	R_a (µm)	R_q (µm)	R_a (µm)	R_q (µm)
P (0-20)	6.28 ± 0.77	8.04 ± 0.84	6.35 ± 0.81	7.51 ± 0.95
P (3-20)	4.48 ± 2.01	5.35 ± 0.33	2.00 ± 0.23	2.63 ± 0.33
P (4-20)	3.62 ± 0.45	4.52 ± 0.51	2.72 ± 0.33	3.38 ± 0.41
P (5-20)	3.08 ± 0.47	3.82 ± 0.54	3.30 ± 0.34	4.42 ± 0.51
P (0-30)	4.48 ± 0.75	5.81 ± 0.82	4.02 ± 0.88	5.16 ± 1.23
P (3-30)	5.71 ± 0.45	7.10 ± 0.38	3.46 ± 0.75	4.95 ± 0.95
P (4-30)	5.50 ± 0.95	6.92 ±1.20	1.99 ± 0.28	2.75 ± 0.37
P (5-30)	2.95 ± 0.47	3.64 ± 0.59	3.39 ± 0.51	4.29 ± 0.68
P (0-40)	3.92 ± 0.76	4.79 ± 0.96	----	----
P (3-40)	23.0 ± 1.74	25.83 ± 1.15	14.47 ± 2.88	14.0 ± 3.20

The sintered samples presented lower values for both R_a and R_q values than the green samples, except for films printed with pastes containing 5 vol% Ti_3SiC_2 which did not result in a significant difference in roughness between the green and sintered layers. These insignificant difference values can be attributed to the high amount of binder, which afford a higher green strength to the sample (PHAIR, LUNDBERG, KAISER, 2009). Moreover, in agreement with the topography analysis (Fig. 19) samples printed from pastes containing EC had a smoother surface than those printed from pastes without binder (P (3-40), P (0-20) and P (0-30)).

As mentioned above (Section 2.3.), the rheological properties of the paste are one of the most vital factors in ensuring structures with high printing quality are obtained. However, other factors should been taken in account, such as the contact angle and interaction between paste and substrate. Both gravitational flow and surface wetting influence the dimensional stability (for instance line broadening) of the printed layers. In the case of roughness however, only gravitational flow is acting (DOLLEN, BARNETT, 2005). Thus, the roughness of the printed layers is only influenced by the rheological properties of the paste.

5.1.3.2. Structural and microstructural analysis

Fig. 20 shows the X-ray diffraction patterns of solid area films after sintering. TiC was present in all films printed with pastes a Ti_3SiC_2 content of 20 vol%. Sintered layers printed from pastes P (3-30), P (3-40) and P (4-40) contained mainly Ti_3SiC_2. All other paste compositions resulted in sintered layers containing TiC. It is also important to note that sintered layers produced from pastes P (4-30) and P (5-30) contained less TiC peaks than the other samples. This indicates that all sintered layers produced from pastes with 30 vol% Ti_3SiC_2, regardless of the amount of EC, contained Ti_3SiC_2 after sintering. No Ti_3SiC_2 was detected in sintered layers produced from pastes with 20 vol% Ti_3SiC_2 regardless of the amount of EC after sintering.

Fig. 21 shows the microstructure of the sintered samples. Contrary to XRD analysis, SEM images showed the presence of $TiSi_x$ phases after sintering for all layers produced from pastes with 20 vol% Ti_3SiC_2 (Fig. 21 (P (0-20)), (P (3-20)), (P (4-20)) and (P (5-20))). However, TiC was also detected as a primary phase in all samples. This indicates the partial decomposition of Ti_3SiC_2 into TiC and gaseous silicon above 1300 °C (RACAULT, LANGLAIS, NASLAIN, 1994).

The Ti-Si-C diagram at 1100 °C and 1250 °C shows Ti_3SiC_2 to be in equilibrium with postulated (Ti,Si)C and TiC phases (EMMERLICH et al., 2007). Furthermore, a few attempts exist in which changes in the environment were used to influence the thermal stability of Ti_3SiC_2. Cryolite, Cu, C, Al_2O_3 and impurities such as Fe and V are examples of elements which may influence the thermal stability of Ti_3SiC_2 (RACAULT, LANGLAIS, NASLAIN, 1994; BARSOUM, 1999; WU et al., 2005; EMMERLICH et al., 2007). In general, these elements influence the thermal stability and facilitate the decomposition of this material through the evaporation of Si and formation of TiC (EMMERLICH et al., 2007). Thus in this work, it the case of the screen printed layers of pastes with 20 vol% Ti_3SiC_2 in their initial composition is suggested that absence or small amount of Ti_3SiC_2 after 1h sintering at 1600 °C is caused due to the higher amount of carbon present in these samples in comparison to the pastes with 30 and 40 vol% Ti_3SiC_2 in their initial composition.

In the Ti_3SiC_2 structure, there are Ti_3C_2 layers intercalated with atomic layers of Si. The Si atoms, are weakly bonded to the Ti atoms, whereas Ti atoms are covalently bonded to C atoms (BARSOUM, 2000; AHUJA et al., 2000; EMMERLICH et al., 2007), which can explain the out-diffusion of Si during the heat treatment.

Figure 20 - X-ray diffraction patterns of sintered pastes at 1600 °C for 1 h containing different amounts of EC and (a) 20 vol% Ti_3SiC_2, (b) 30 vol% Ti_3SiC_2 and 40 vol% Ti_3SiC_2.

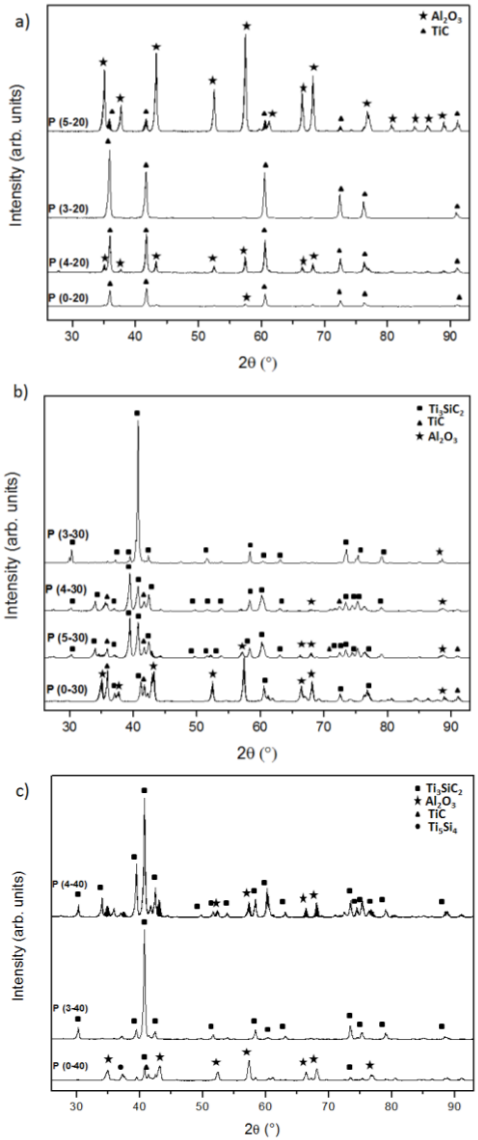

Figure 21 - Micrographs of the microstructure of the screen printed films after 1h sintering at 1600 °C. The left image corresponds to the film's surface and the right image corresponds to the sample's cross section.

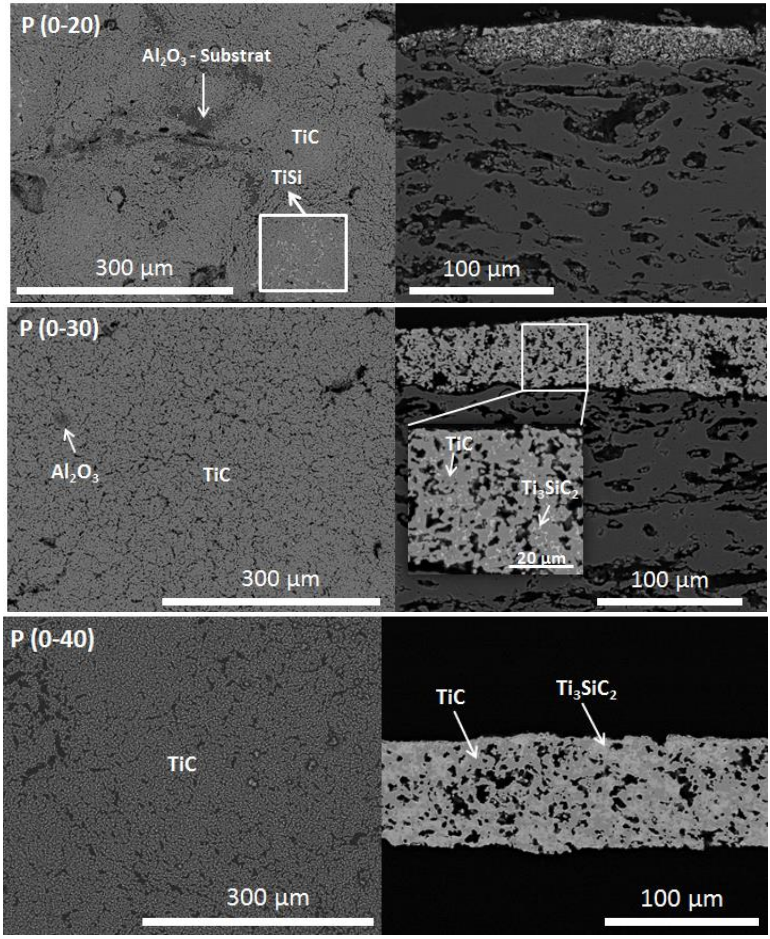

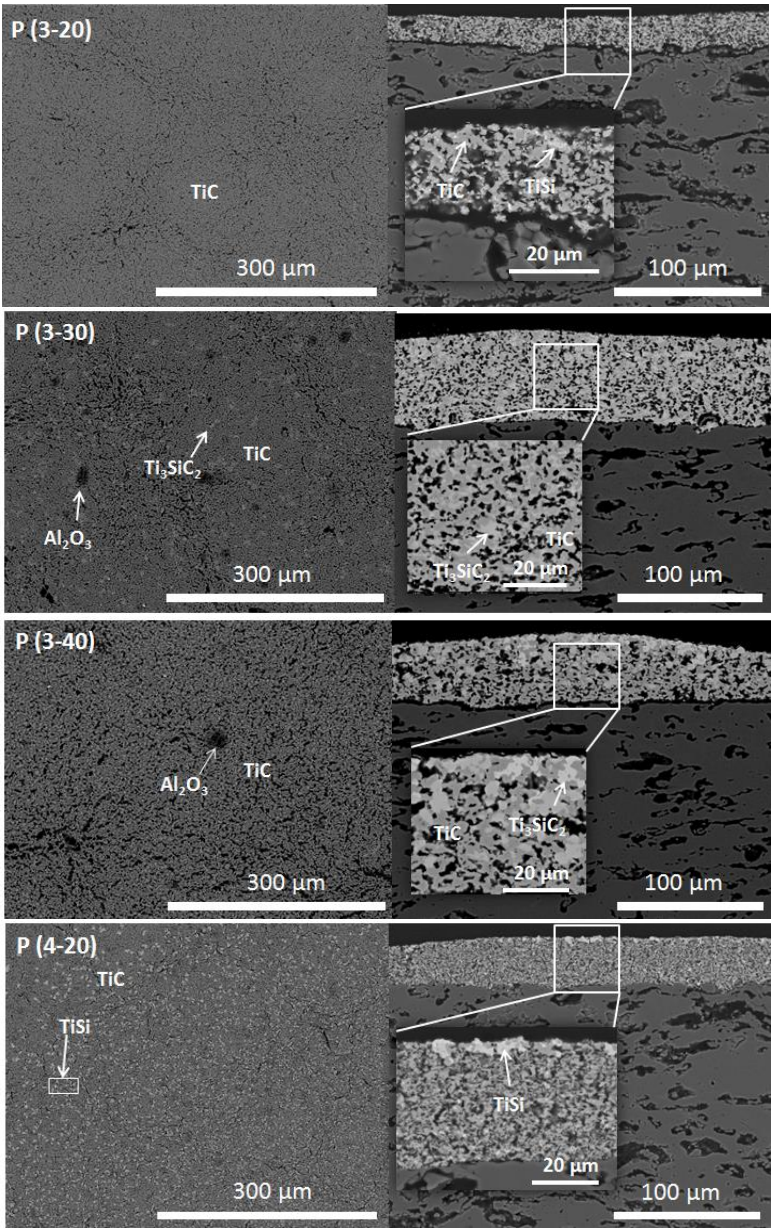
P (3-20)
TiC
300 µm
TiC
TiSi
20 µm
100 µm
P (3-30)
Ti3SiC2
TiC
Al2O3
300 µm
TiC
Ti3SiC2
20 µm
100 µm
P (3-40)
Al2O3
TiC
300 µm
TiC
Ti3SiC2
20 µm
100 µm
P (4-20)
TiC
TiSi
300 µm
TiSi
20 µm
100 µm

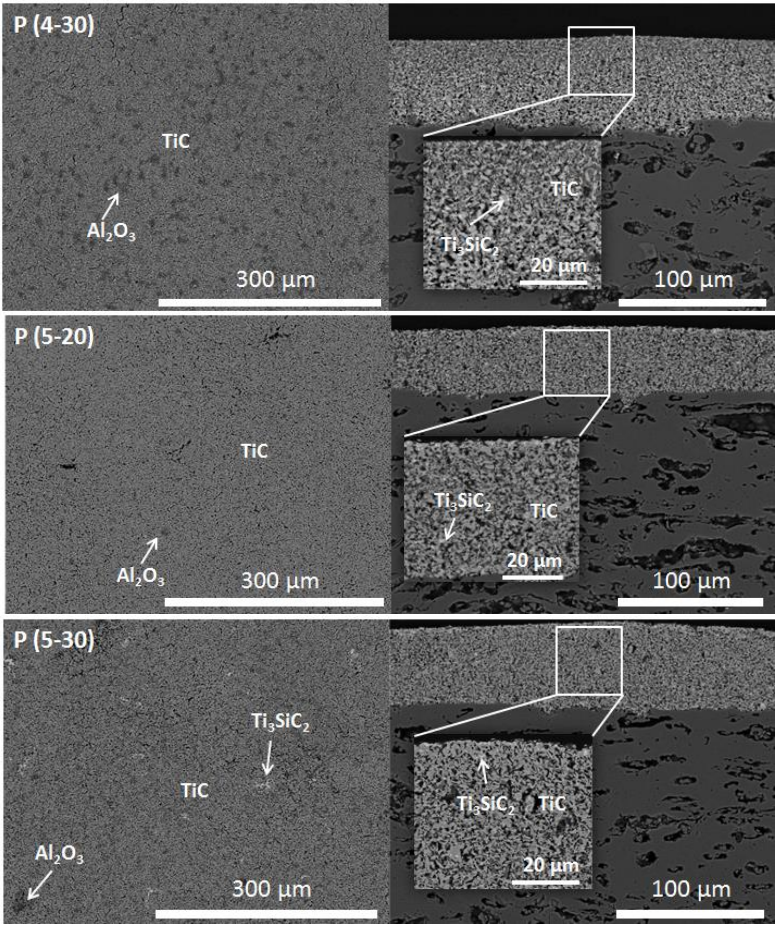

According to Racault et *al*. (EL-RAGHY, BARSOUM, 1998a) Ti_3SiC_2 is stable up to 1300 °C, and above this temperature it can decompose into TiC and gaseous silicon depending on the processing environment. In their study, Racault et al. investigated the thermal stability of a solid-state synthesis product of 95 mol% Ti_3SiC_2 and 5 mol% TiC up to 1600 °C in argon atmosphere under two different conditions. In the first case, the samples were placed in a graphite crucible. For this set of samples, it was observed that at temperatures above 1300 °C a mass loss started to occur and free Si was found in the

graphite crucible. In the second case, the samples were placed in an alumina crucible. For this second set of samples, the mass loss started above 1450 °C. Thus, graphite seems to decrease the temperature stability of Ti_3SiC_2 by 150 °C compared to alumina (RACAULT, LANGLAIS, NASLAIN, 1994). The same results were observed by El-Raghy *et al.* in the carburization of a porous Ti_3SiC_2 wafer at 1600 °C for 12 h (EL-RAGHY, BARSOUM, 1998a). In the present work, the pastes were printed onto Al_2O_3 substrates and the only extraneous source of carbon is provided from the EC and terpineol in the paste.

The presence of Al_2O_3 in paste P (0-20) can be explained by the low viscosity of the paste, which was not high enough to ensure coating of the printed area (Fig. 21 (P (0-20)). However, the presence of Al_2O_3 in the sintered samples, see Fig. 21 (P (0-30)), (P (3-30)), (P (3-40)), (P (5-20)) and (P (5-30)), can be attributed to loose Al_2O_3 powder on the surface of non-calendered paper-derived Al_2O_3. This powder was mixed with the pastes during the deposition process. This corroborate the study performed by Wu *et al.* (2007), which consisted of the fabrication of hybrid systems of Ti_3SiC_2/Al_2O_3 prepared by spark plasma sintering. After sintering at 1300 °C in vacuum atmosphere the X-ray diffraction pattern indicated that no chemical reaction between both phases and Ti_3SiC_2 and Al_2O_3 had occured (WU et al., 2007).

From Fig. 22 it is possible to observe the weight loss as function of temperature until 1500 °C for pastes with 3 vol% EC and different Ti_3SiC_2 contents. For all pastes, there are two different temperatures of decomposition. The first corresponds to the evaporation of the possible humidity content of the samples and to the decomposition of EC, which has a melting point in a range of 160 to 210 °C. Moreover, EC consists of 48 to 49.5 wt% of ethoxyl basis, which has a melting point of 1600 °C. The second decomposition can be assigned to the terpineol, which has a melting point of approximately 230 °C (DING, GU, LI, 2008). In this case, the temperature shift can be attributed to the possible adsorption of solvent on the ceramic particle surface. Above 1341 °C, 1370 °C and 1320 °C a new weight loss stage occurs for P (3-20), P (3-30) and P (3-40), respectively. This can be assigned to the evaporation of Si, which has a melting point approximately of 1410 °C (DONOVAN et al., 1983) agreeing with the decomposition of Ti_3SiC_2.

Figure 22 - TGA analysis of pastes containing 3 vol% EC and different contents of Ti_3SiC_2.

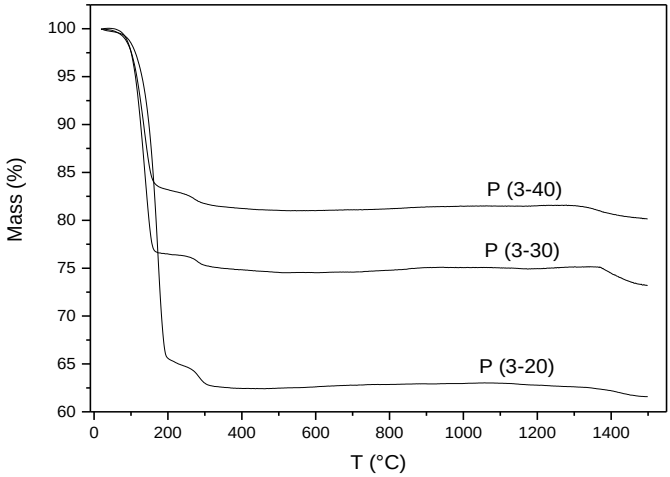

Furthermore, from Fig. 23 the absence of a reaction zone in the interface between the substrate and screen printed layers is evident, which indicates that a weak adhesion between the layer and the substrate affects the final properties of the material. For functional ceramic materials, such as integrated circuits (IC), a very strong adhesion between ceramic substrates and the metallized layer is required. Thus, some attempts showed that the deposition of a thin metallized film (for instance Ti) could be used to improve the adhesion of components (LU et al., 1995).

Figure 23 - SEM micrograph of the interface between (a) P (4-20) and (b) P (4-30) screen printed layer and paper-derived Al_2O_3 substrate after sintering for 1h at 1600 °C.

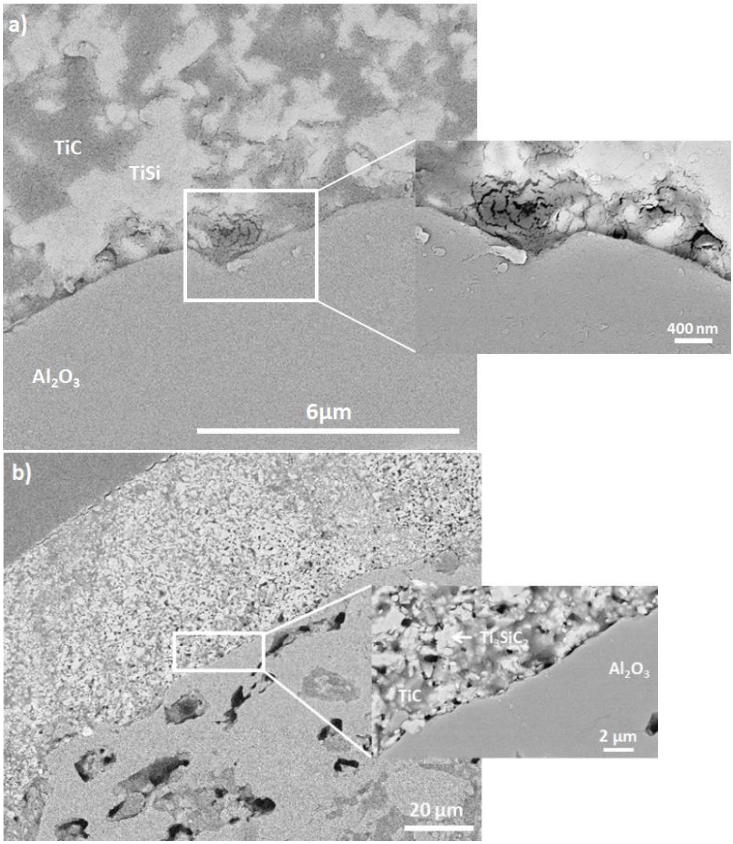

5.1.3.3. Electrical properties

As discussed above, although the decomposition of Ti_3SiC_2 occurred for all samples, XRD and SEM analysis showed that layers formed from pastes with 30 vol% and different EC contents contained Ti_3SiC_2 after sintering (Fig. 20 and 21). Additionally, a smoother surface was also evident for these samples. As roughness affects the electrical properties of films, (FADDOUL, REVERDY-BRUAS, BLAYO, 2012) further

electrical characterizations were performed for these samples. Fig. 24 presents the temperature dependence of electrical resistivity for layers produced from pastes with 30 vol% Ti_3SiC_2 and different EC contents.

Figure 24- Resistivity vs. temperature of layers printed from pastes with 30 vol% Ti_3SiC_2 and different EC content after 5 h sintering at 1400 °C.

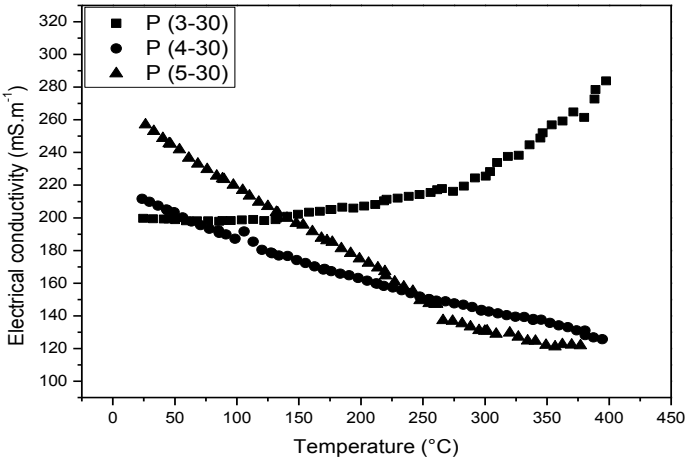

Yoo et al., (2000) and Barsoum et al., (2000) investigated the electrical properties of bulk Ti_3SiC_2 in the range from 26 °C to 576 °C. They observed a metallic-like behavior, where the electrical resistivity increased with increasing temperature (BARSOUM et al., 2000; YOO, BARSOUM, EL-RAGHY, 2000). Although the resistivity of P (4-30) and P (5-30) increased with increasing temperature, the resistivity of P (3-30) decreased with increasing temperature. However, the values of electrical conductivity at 25°C and 400°C did not vary more than one order of magnitude, as shown in Table 10.

Table 10 - Electrical conductivity of layers printed from pastes with 30 vol% Ti_3SiC_2 and different EC content at 25 °C and 400 °C.

Samples	Electrical conductivity ($S.m^{-1}$)	
	25 °C	**400 °C**
P (3-30)	2.0×10^5 ($\pm 7.90 \times 10^3$)	2.84×10^5 ($\pm 2.89 \times 10^4$)
P (4-30)	2.12×10^5 ($\pm 9.65 \times 10^3$)	1.25×10^5 ($\pm 1.20 \times 10^4$)
P (5-30)	2.49×10^5 ($\pm 8.33 \times 10^3$)	2.10×10^5 ($\pm 3.89 \times 10^4$)

The electrical conductivity of pure Ti_3SiC_2 was already reported to be in a narrow range from 4.8×10^6 $S.m^{-1}$ to 9.6×10^6 $S.m^{-1}$ at room temperature (BARSOUM, EL-RAGHY, 1996; LI, SATO, WATANABE, 1999; SUN, ZHOU, 1999; BARSOUM et al., 2000). In this work, TiC was found in all screen printed layers. It is already reported that this material has a conductivity three orders magnitudes lower than single phase Ti_3SiC_2 (SHI, ZHANG, LI, 2008). Besides that, although samples with 30 vol% Ti_3SiC_2 and different EC contents gave the smoothest surface, these samples still have an irregular surface and a mixture of phases in their composition. These factors could explain why the electrical conductivity values are one order of magnitude smaller than those reported in the literature for single phase Ti_3SiC_2.

Until the present date only Budhani *et al.* (1987) had used screen printing for synthesis of ceramic superconductor films. In their studies they observed that the surface smoothness, resistivity, crystal structure and adhesion of the films were highly sensitive to post-printing heat treatment (BUDHANI et al., 1987). Dollen and Barnett (2005) fabricated Yttria-Stabilized Zirconia layers for Solid Oxide Fuel Cells via screen printing and reported lower values for open circuit voltage (Voc) and power density compared to other processing methods, such as EVD or sputtering. This observed decrease in values ocuured due to the formation of not fully dense layers, which can cause cracks and porosity (TSAI, SCOTT, 1995; DOLLEN, BARNETT, 2005).

Furthermore, surface defects such as steps and domain boundaries greatly perturb the electron conduction through surface states. This could have altered the direct detection and quantitative measurement of the surface-state conductivity (HASEGAWA et al., 2002). Shorting risks can

be avoided by a smooth surface, which provides a continuous conductive area (FADDOUL, REVERDY-BRUAS, BLAYO, 2012)

5.1.4. Synthesis pastes

The pastes concentrations were prepared according to the results of Ti_3SiC_2 pastes. The screen printed films of pastes containing 30 vol% Ti_3SiC_2 and 3 vol% EC presented the best results before and after 1h sintering at 1600°C (as discussed in item 5.1.3.). Thus this concentration was chosen for the production of synthesis pastes.

Despite the small variation in the samples concentrations (Table 3), all pastes were successfully fabricated. Fig. 15 presents the flow curve of the synthesis pastes. All samples had shear thinning behavior. $P_{1.1}$ (7-27) presented the highest viscosity despite having the lowest solid content among all of synthesis pastes. This indicates that the EC content is the main factor that influences paste viscosity.

Figure 25 - The viscosity vs. shear rate curves of synthesis pastes.

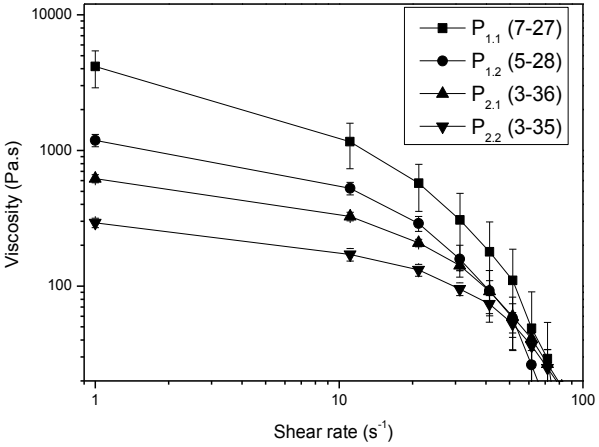

The viscoelastic properties of the synthesis pastes are presented in Fig. 26. For all samples, the G'' showed higher values compared to G' suggesting liquid-like behavior, these values increased with the increase in the viscosity. All samples presented a LVER and absence of cross over point prior to a shear stress of 100 Pa.

Figure 26 - Shear stress dependence of the storage (G') and loss (G") modulus for synthesis pastes.

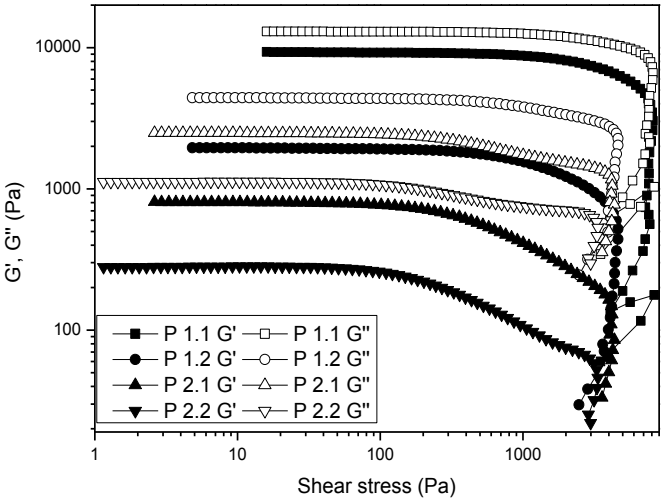

From the 3-step recovery test of the synthesis pastes (Fig. 27), it was possible to observe the time dependent viscosity of all samples. As discussed in 5.1.2., this behavior was expected due to particle content, which leads a progressive breakdown of the network during shearing (INUKAI et al., 2015).

Figure 27 - 3-step recovery measurement. Storage (G') modulus and viscosity as function of elapsed time for synthesis pastes.

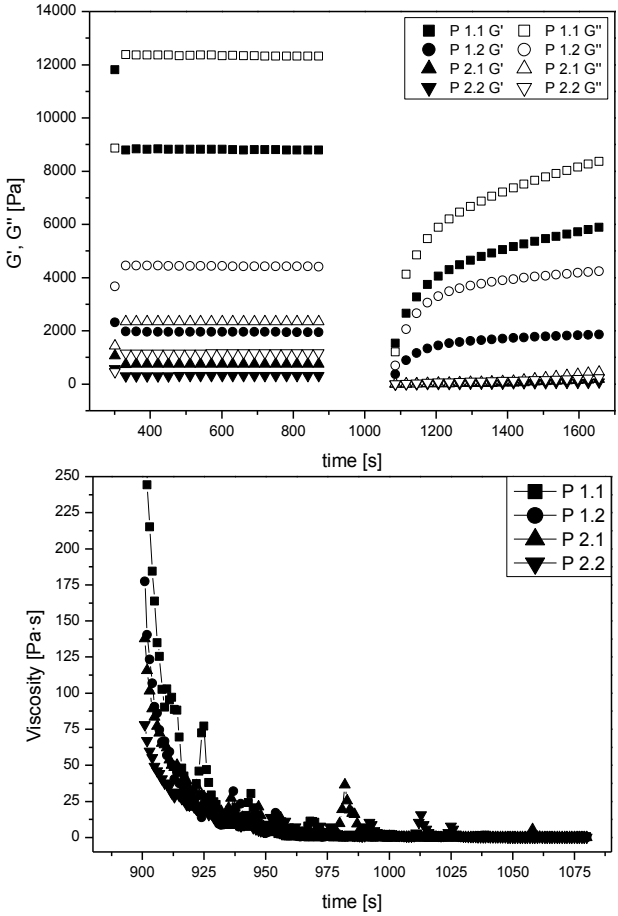

Nevertheless, the recovery ratio in the synthesis pastes was not influenced by the viscosity as shown above for the Ti_3SiC_2 pastes. In this case, the main influence was the EC content of the pastes. $P_{2.1}$ (3-36) and $P_{2.2}$ (3-35) gave the lowest viscosity values and the lowest recovery ratios. The opposite was observed for $P_{1.1}$ (7-27) and $P_{1.2}$ (5-28), which showed the highest viscosity values and the highest recovery ratios. Phair et al. (2009) observed the same behavior for screen printed zirconia films. In

their study, the amount of ethyl cellulose in the pastes directly influenced the recovery ratio of the pastes, which increased with increasing EC content (PHAIR, KAISER, 2009).

Table 11 - Recovery ratio of synthesis pastes.

Synthesis Pastes	Recovery ratio (%)
$P_{1.1}$ (7-27)	67.7 (±1.6)
$P_{1.2}$ (5-28)	95.8 (±4.7)
$P_{2.1}$ (3-36)	25.3 (±8.9)
$P_{2.2}$ (3-35)	26.0 (±8.9)

5.1.5. Screen printing of synthesis pastes

It was possible to screen print all compositions of synthesis pastes. Fig. 28 and Fig. 29 present the green and sintered screen printed structures, respectively. Due to the EC content, the green samples presented good dimensional stability and due to the solid content the sintered structures presented no defects, such as voids and cracks.

Figure 28- Images of green screen printed structures.

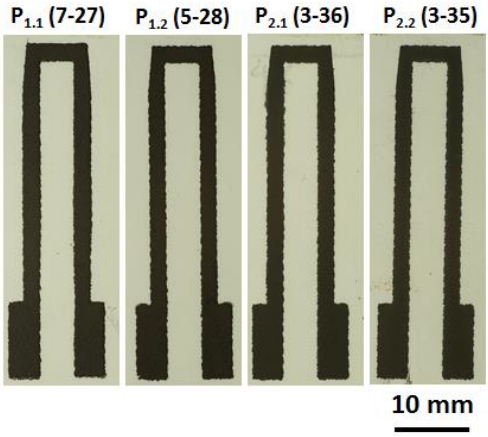

Figure 29 - Images of screen printed structures pastes after 1, 2 and 3 h sintering at 1400 °C.

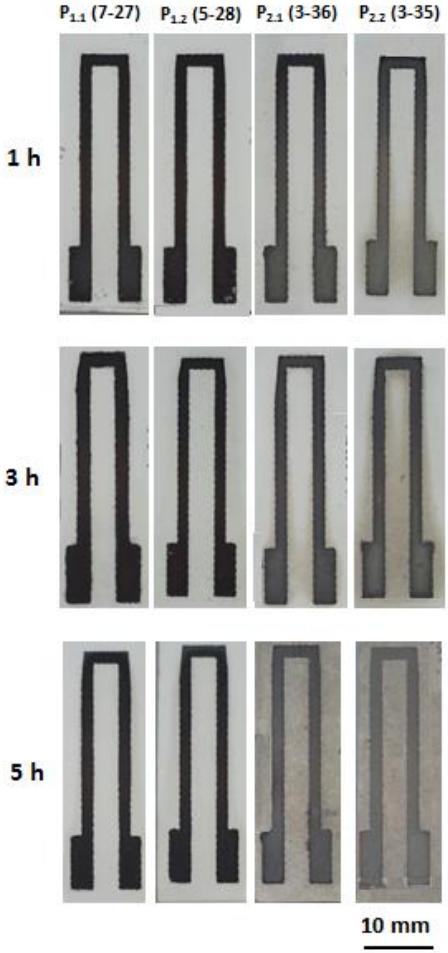

However, pastes without TiC in its composition, such as $P_{1.1}$ (7-27) and $P_{1.2}$ (5-28), exhibited lower adhesion in comparison to $P_{2.1}$ (3-36) and $P_{2.2}$ (3-35). This is evident in Fig 29 for $P_{1.2}$ (5-28), after 1 h sintering lower adhesion is seen in the lower part of the print design. Furthermore, the poor adhesion was also observed during sample handling, as the sample was unstable and was easily damaged.

5.1.5.1. Surface analysis

Fig 30 presents the topography images for green screen printed samples and Table 12 their R_a and R_q values. All pastes showed values in the same range. Nevertheless, in the synthesis phase it is possible to observe the influence of the powder composition on the roughness properties.

Figure 30 - Topography of green screen printed layers of synthesis pastes.

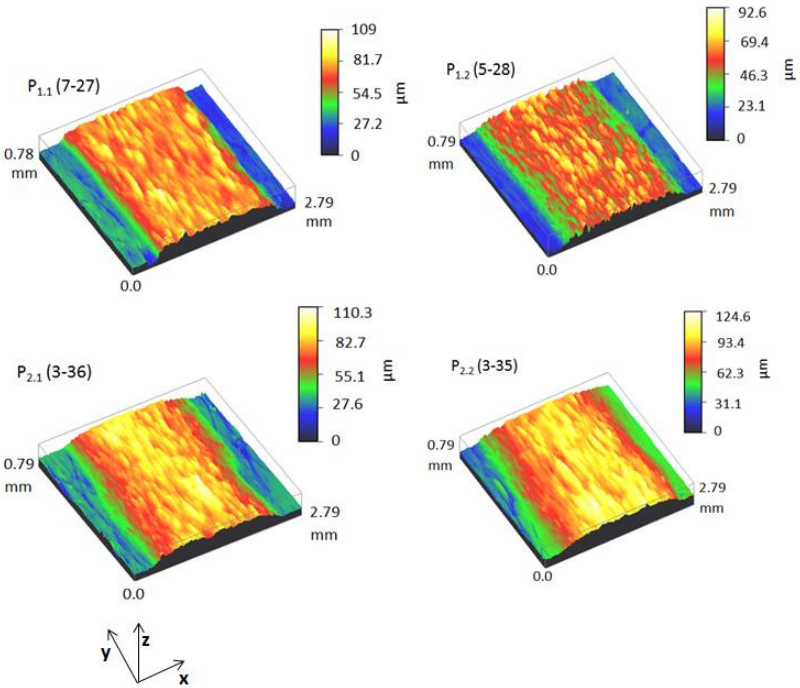

Table 12 - Roughness value, R_a and R_q for green samples of synthesis pastes.

Pastes	R_a (µm)	R_q (µm)
$P_{1.1}$ (7-27)	5.66 ± 1.07	6.91 ± 1.15
$P_{1.2}$ (5-28)	5.75 ± 0.63	7.17 ± 0.73
$P_{2.1}$ (3-36)	6.54 ± 0.53	7.99 ± 0.68
$P_{2.2}$ (3-35)	4.74 ± 0.66	6.02 ± 0.92

After sintering, films formed from pastes $P_{2.1}$ (3-36) and $P_{2.2}$ (3-30) had lower R_a and R_q values and were smoother than those formed from pastes $P_{1.1}$ (7-27) and $P_{1.2}$ (5-28) regardless of the sintering time (Fig. 31 and Table 13). The topography images of $P_{1.1}$ (7-27) and $P_{1.2}$ (5-28) after sintering are shown in Appendix A (Fig. 54). $P_{1.1}$ (7-27) and $P_{1.2}$ (5-28) contained the highest EC content, which resulted in greater height variation on sample surface after sintering due to decomposition of EC and the consequential formation of defects (MURAKAMI et al., 2014) (SEDLAČEK, PODGORNIK, VIŽINTIN, 2009). The mass loss on the surface of the screen printed layers after sintering can be observed as alterations in the topography in the images.

Figure 31 - Topography of sintered screen printed layers of synthesis pastes.

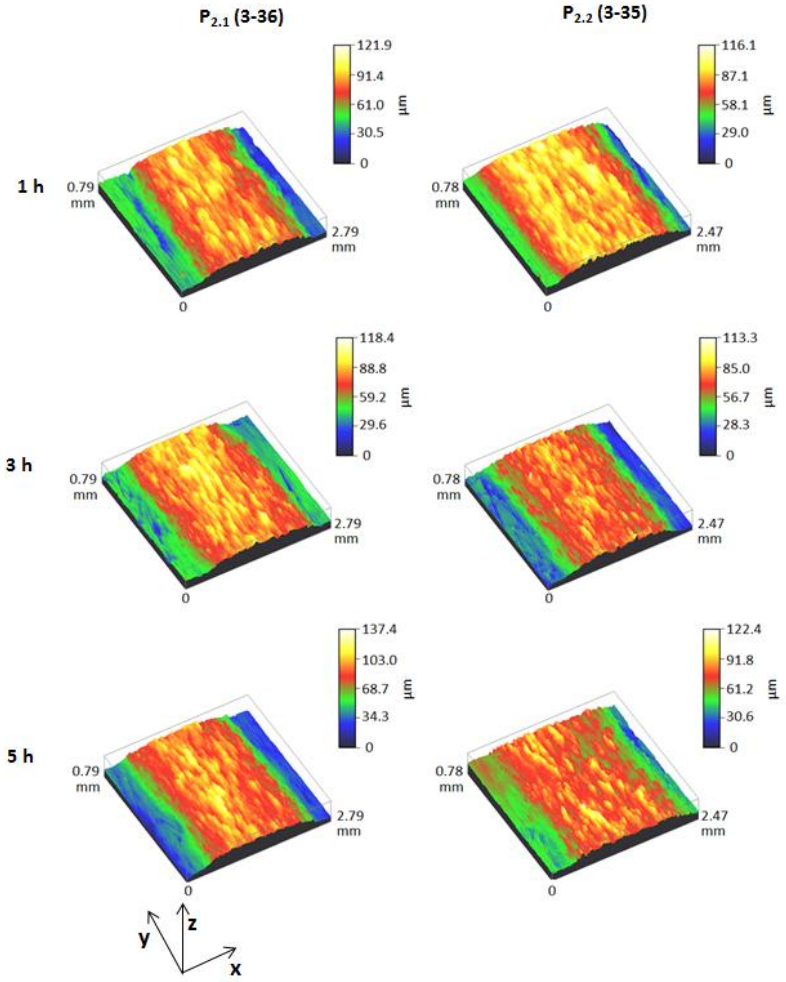

However, after sintering the influence of the powder composition on the surface roughness is evident. This is contrary to Ti_3SiC_2 pastes, where the R_a and R_q values increased after sintering. The thickness of all sample also increased. The line profiles for green and sintered screen printed layers of synthesis pastes are shown in appendix A.

Table 13 - Roughness value, R_a and R_q for sintered samples of synthesis pastes with different sintering times at 1400 °C.

Pastes	1 h Sintering		3 h Sintering		5 h Sintering	
	R_a (µm)	**R_q (µm)**	**R_a (µm)**	**R_q (µm)**	**R_a (µm)**	**R_q (µm)**
$P_{1.1}$ (7-27)	9.74 ± 1.07	12.91 ± 1.15	9.55 ± 2.74	13.22 ± 0.64	12.96 ± 1.78	16.41 ± 2.73
$P_{1.2}$ (5-28)	9.83 ± 0.96	11.99 ± 1.09	10.68 ± 1.33	13.36 ± 1.41	11.77 ± 1.58	15.33 ± 2.9
$P_{2.1}$ (3-36)	5.20 ± 0.40	6.54 ± 0.49	5.15 ± 0.79	6.43 ± 0.98	6.11 ± 0.99	7.68 ± 1.09
$P_{2.2}$ (3-35)	5.74 ± 0.65	7.22 ± 0.83	5.03 ± 0.65	6.21 ± 0.79	6.35 ± 0.50	8.15 ± 0.76

The increase of the thickness and surface roughness can be attributed to the reaction and products formed by sintering, which is discussed in 5.1.5.2.

5.1.5.2. Structural and microstructural analysis

Fig. 32 presents the X-ray diffraction pattern for the layers formed from synthesis pastes after different sintering times at 1400 °C. Ti_3SiC_2 was obtained for all pastes compositions in the time range of 1 h to 5 h of sintering. However, almost all layers showed the presence of secondary phases. Layers formed from pastes $P_{1.1}$ (7-27) and $P_{1.2}$ (5-28), which have no TiC in their initial composition showed $TiSi_2$, Ti_5Si_3 and Al_2O_3 as secondary phases. Layers formed from $P_{2.1}$ (3-36) and $P_{2.2}$ (3-35), which contained both TiC and excess Si, had SiC as an additional secondary phase. Furthermore, layers formed from pastes with TiC in their initial composition regardless of the stoichiometry, had only Ti_3SiC_2 without any other detectable phases after 3 and 5 h sintering, specifically layers formed from $P_{2.1}$ (3-36) after 3 and 5 h of sintering and paste $P_{2.2}$ (3-35) after 5 hour of sintering.

Figure 32 - X-ray diffraction pattern of layers formed from synthesis pastes sintered at 1400 °C for 1, 3 and 5 h.

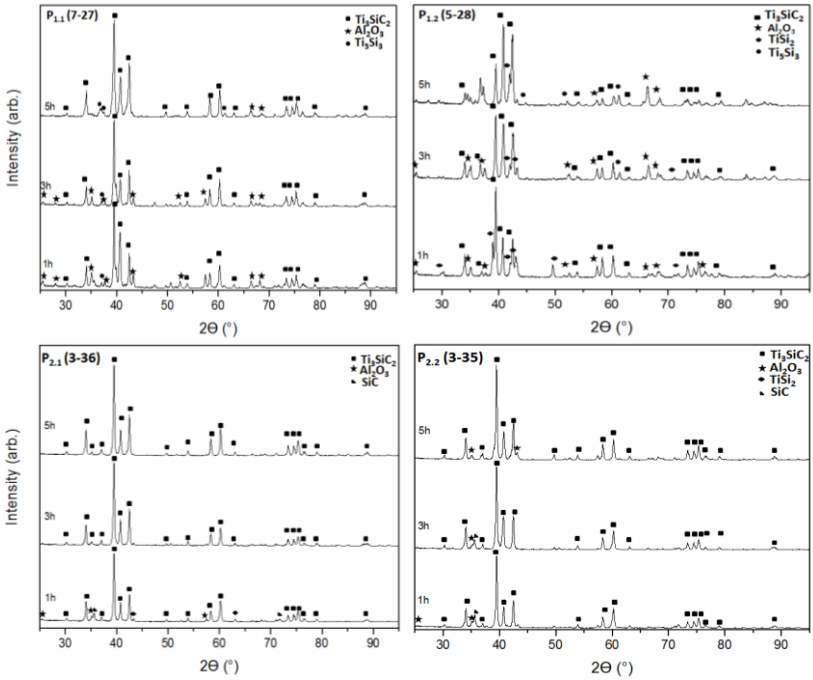

Fig. 33 shows the microstructure for the layers formed from synthesis pastes with after sintering at different times. A highly porous structure is observed from the layers formed from pastes $P_{1.1}$ (7-27) and $P_{1.2}$ (5-28) in comparison to those formed from pastes $P_{2.1}$ (3-36) and $P_{2.2}$ (3-35). The highly porous structure is a factor that can affect the adhesion between the substrate and screen printed layer. Furthermore, an increase in the density of the printed films is noticeable for films fabricated from pastes $P_{2.1}$ (3-36) and $P_{2.2}$ (3-35) with increasing sintering time.

Figure 33 - SEM micrographs of the microstructure of the sintered screen printed films formed from synthesis pastes at 1400 °C.

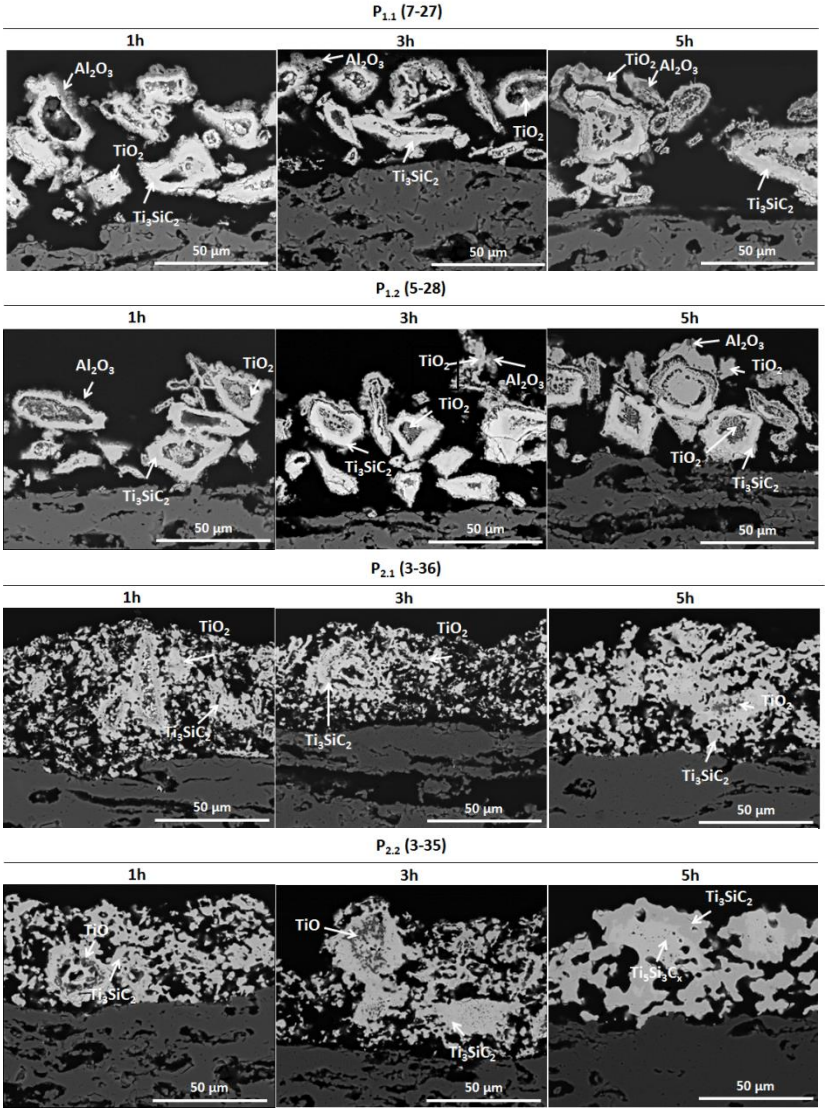

In agreement with XRD patterns, all samples contained Ti_3SiC_2 after sintering at different times. However, SEM images also showed the

presence of TiO_2 and Al_2O_3 as secondary phases. Although none of the samples presented a reaction zone in the interface between the substrate and the printed layers (Fig. 34), samples formed from pastes $P_{1.1}$ (7-27) and $P_{1.2}$ (5-28) had an Al_2O_3 outer layer and all samples contained domains within TiO_2 within their structures.

Figure 34 - SEM image of the interface between screens printed layers of synthesis pastes and Al_2O_3 substrate after 5 h sintering at 1400 °C.

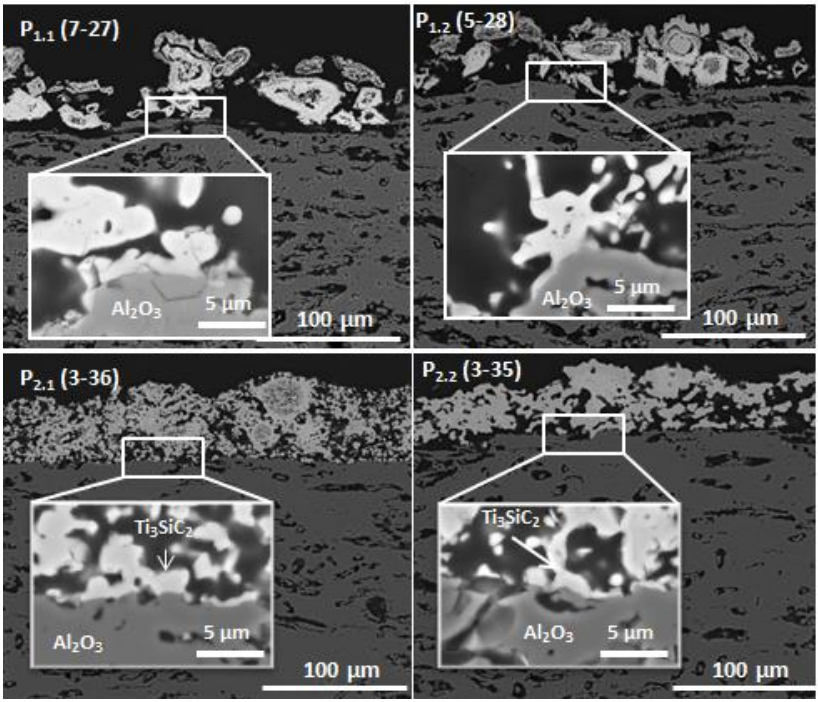

Due to the presence of Ti_3SiC_2 and TiO_2 after sintering, the occurrence of two simultaneous phenomena is suggested: (i) synthesis of Ti_3SiC_2 and (ii) the chemical reaction between Al_2O_3 and elementary Ti powder.

Further works have shown the formation of unwanted impurity phases, such as TiC and $TiSi_2$ during the synthesis of Ti_3SiC_2 (ARUNAJATESAN, CARIM, 1995; RACAULT, LANGLAIS, NASLAIN, 1994; SATO, LI, WATANABE, 2000; WU, KISI, RILEY, 2002; GAUTHIER et al., 2006; BARSOUM, EL-RAGHY, 1996; GAO, MIYAMOTO, ZHANG, 1999). Over the years, diverse attempts have

been proposed for the synthesis of Ti_3SiC_2 using different starting compositions, such as Ti/Si/C (GAUTHIER et al., 2006), Ti/SiC/C (WU et al., 2005; EL-RAGHY, BARSOUM, 1999; RILEY et al., 2002), Ti/Si/TiC (YANG, SUN, HASHIMOTO, 2004) and Ti/Si/C/SiC (KLEMM, TANIHATA, MIYAMOTO, 1993). Different reaction paths are obtained depending on the chosen starting reactants (ZHANG et al., 2006). In studies where Ti/Si/C were used as reactant powders, it was observed that the loss of Si was the most possible reason for the difficult of forming single phase Ti_3SiC_2 (PARK et al., 2001) and hence, the thermal stability can be increased by preventing Si removal from the surface (EMMERLICH et al., 2007). Lorenz *et al.* (2017) successfully synthesized paper-derived Ti_3SiC_2 by adjusting the starting stoichiometry to 3Ti/3TiC/3Si/C, in which both TiC and excess Si were contained (LORENZ et al., 2017). Therefore, for this work the starting composition Ti/Si/C and Ti/Si/TiC/C were chosen. Pastes with composition Ti/Si/C ($P_{1.1}$ and $P_{1.2}$) were produced with excess Si and variable C content, in order to avoid the formation of secondary phases and to investigate the influence of carbon. Pastes with the composition Ti/Si/TiC/C ($P_{2.1}$ and $P_{2.2}$) were also produced. In this case the influence of TiC and excess Si were investigated.

Gauthier and co-workers (2006) investigated the influence of the 3Ti/Si/2C powder mixture on the synthesis of bulk Ti_3SiC_2 via Self-Propagating High-Temperature process. The authors proposed that the synthesis mechanism is given heterogeneous nucleation of Ti_3SiC_2, where TiC_x reacts with Ti-Si liquid phase for formation of Ti_3SiC_2. Nevertheless, TiC_x was obtained as the major impurity and Ti-Si phases in small amount (GAUTHIER et al., 2006). Sato *et al.*, (2000) also showed the reactive synthesis of Ti/Si/C powder and related the increase in the amount of Ti_3SiC_2 with increasing sintering temperature. The reactions below show the possible mechanism for formation of Ti_3SiC_2 using Ti/Si/C as starting reactants, which is favored due to the high reactivity of Ti with carbon. (SATO, LI, WATANABE, 2000; GAUTHIER et al., 2006).

$$Ti + C \rightarrow TiC \qquad (1\text{-}1)$$

$$Ti + Si \rightarrow Ti\text{-}Si \qquad (1\text{-}2)$$

$$2TiC + Ti\text{-}Si_{(l)} \rightarrow Ti_3SiC_2 \qquad (1\text{-}3)$$

Zhang et al., (2007) proposed a similar reaction path to the mechanism presented by Sato et al., (2000) (ZHANG et al., 2007).

$$Ti + C \rightarrow TiC \quad (2\text{-}1)$$

$$Ti + 2Si \rightarrow Ti\text{-}Si_2 \quad (2\text{-}2)$$

$$TiSi_2 + 4TiC + Ti \rightarrow 2Ti_3SiC_2 \quad (2\text{-}3)$$

Zhang et al., (2007) synthesized Ti_3SiC_2 via spark plasma sintering at 1350 °C and proposed a reaction path similar to Sato et al., (2000) where they observed SiC and TiC as secondary phases (ZHANG et al., 2007). In contrast, Wu and Kisi (2001) used *in situ* neutron powder diffraction and proved that during the conventional synthesis using Ti/SiC/C powder, TiC_x and $Ti_5Si_3C_x$ are present as intermediary phases and through their consumption from 1200 °C Ti_3SiC_2 is formed without the presence of secondary phases (WU, KISI, 2001).

In this work, although sintered layers formed from pastes $P_{1.1}$ (7-27) and $P_{1.2}$ (5-28) did not show the presence of $TiSi_2$ and Ti_5Si_3 in the SEM images the amount of Ti_3SiC_2 in layers formed from pastes $P_{2.1}$ (3-36) and $P_{2.2}$ (3-35) was observed to be higher than those formed from $P_{1.1}$ (7-27) and $P_{1.2}$ (5-28). Furthermore, increasing the sintering time led to an increase in the amount of Ti_3SiC_2 formed from paste $P_{2.2}$ (3-35) and after 5 h sintering increased densification of the layers formed from both $P_{2.1}$ (3-36) and $P_{2.2}$ (3-35) occurred. The increased in the amount of Ti_3SiC_2 and densification is attributed to substitution of the carbon source to carbides in the starting reactants, which is known to minimize the amount of secondary phases formed (RADHAKRISHNAN, WILLIAMS, AKINC, 1999; PAMPUCH et al., 1989). The loss of Si is the most probable reason for the difficulty of forming single phase Ti_3SiC_2, loss of Si can be minimized by performing sintering experiments at lower temperatures (PARK et al., 2001).

Layers formed from sintering paste $P_{2.2}$ (3-35) for 5 h at 1400 °C resulted in the formation of Ti_3SiC_2 and $Ti_5Si_3C_x$ without the presence of TiO_2. This suggests that the elimination of TiO_2 phases can be achieved after 5 h of sintering at 1400 °C when pastes containing TiC and an excess of Si in the starting composition ($P_{2.2}$ = 3Ti/3TiC/4.5Si/C) are used. Analysis of SEM images of layers formed from sintering pastes $P_{2.2}$ (3-35) for 5 h sintering (Fig. 33) indicates that the nucleation and growth of Ti_3SiC_2 occurred within the $Ti_5Si_3C_x$ phases. XRD patterns corroborate the inference from SEM micrographs, as the main peaks of Ti_3SiC_2

overlap those of $Ti_5Si_3C_x$ (EL-RAGHY, BARSOUM, 1999). Similar results were observed by El-Raghy and Barsoum (1999). They demonstrated the reactive HIPing of Ti, SiC, and graphite powder to produce single-phase, fully dense, polycrystalline Ti_3SiC_2 samples. As intermediary phases they detected $Ti_5Si_3C_x$ and TiC_x and found that dense Ti_3SiC_2 samples could be produced in a wide range of temperature from, 1450 °C to 1700 °C with a sintering time of 1 to 8 h (EL-RAGHY, BARSOUM, 1999).

The Al_2O_3 substrates used are shown to have influence on the layers formed from the synthesis pastes after sintering. SEM images (Fig. 33) show the formation of Ti_3SiC_2 and the presence of a TiO_2 phase inside the screen printed layers and an Al_2O_3 outer layer on samples produced from pastes $P_{1.1}$ (7-27) and $P_{1.2}$ (5-28).

Previous work has investigated the interactions at the Ti/Al_2O_3 interface and the products formed (TRESSLER, MOORE, CRANE, 1973; LI et al., 1992; KANG, SELVERIAN, 1992; LU et al., 1995; KLIAUGA, FERRANTE, 2000). Lu and co-works (1995) revealed that when active metallic titanium was evaporated onto an Al_2O_3 surface at room-temperature the multiphase formation of titanium oxides, $(Ti, Al)_2O_3$ and metallic aluminum occurred. They suggested that the active oxygen anions on the surface of Al_2O_3 react and easily oxidize forming TiO_2 or titanium-rich oxides (TiO or Ti_2O_3) (LU et al., 1995). Kliauga *et al*. investigated the interfacial reaction products of Ti/Al_2O_3 joints formed by real diffusion bonding technology in a temperature range from 800 to 1000 °C and showed the formation of oxidized Ti and Ti_3Al phases (KLIAUGA, FERRANTE, 2000).

In this work, the presence of the Ti-O phase suggests that a reaction between the elementary powder Ti and the Al_2O_3 substrates has occurred yielding titanium oxide and metallic Al as products. Ti atoms can form chemical bonds with oxygens anions on the Al_2O_3 surface (LU et al., 1995). Moreover, due to the dissolution of Al_2O_3 at high temperatures the main mass transport that occurred into the pastes was of Ti (KLIAUGA, FERRANTE, 2000).

The EDS mapping of the interface between screen printed layers and substrate (Fig. 35) evidences that for layers formed from pastes $P_{1.1}$ (7-27), $P_{1.2}$ (5-28) and $P_{2.1}$ (3-36) after 5 hour sintering a small amount of diffusion of Al and O from the substrate into the screen printed layers had occurred. For layers formed from paste $P_{2.2}$ (3-35), there is no presence of Al on the screen printed layer and a TiO phase was not found after 5h sintering. Paste $P_{2.2}$ (3-35) has a higher amount of Si than $P_{2.1}$ (3-36), therefore formation of Ti_3SiC_2 is supported after 5 hour sintering and

hence, the formation of TiO_2 does not occur due to the small concentration of Ti atoms. Moreover, a non-homogeneous distribution of Si content in the screen printed layer can be seen in the EDS mapping analysis of layers formed from $P_{1.1}$ (7-27) and $P_{1.2}$ (5-28). This suggests that the initial amount of Si in the reactants was insufficient to guarantee synthesis of the Ti_3SiC_2 phase.

Figure 35 - EDS mapping of screen printed films of synthesis pastes after 5 h sintering at 1400 °C. The highlighted colored regions represent for different detected elements.

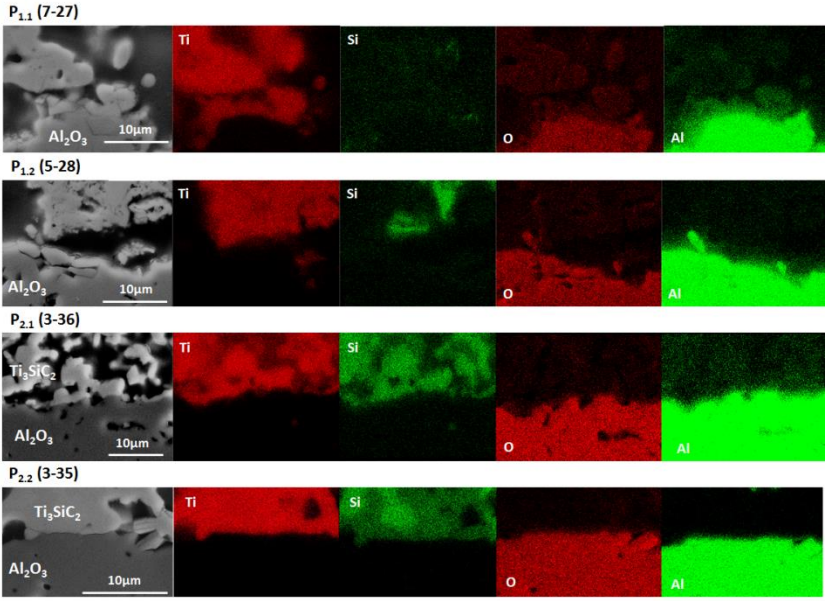

In addition, it should be noticed that EDS analysis also showed a small additional amount of Al and a small additional amount of Ti the Al_2O_3 outer layer.

5.1.5.3. Electrical properties

The layers formed from pastes $P_{2.1}$ (3-36) and $P_{2.2}$ (3-35) showed the best densification, adhesion and the highest amount of Ti_3SiC_2 phase of all tested pastes after 5 hours of sintering at 1400 °C. Therefore, the

electrical properties of these samples were analyzed. Fig. 36 presents the resistivity as function of temperature the layers formed from pastes $P_{2.1}$ (3-36) and $P_{2.2}$ (3-35) after 5 h sintering at 1400 °C.

Figure 36 – Electrical conductivity vs. temperature of layers formed from pastes $P_{2.1}$ (3-36) and $P_{2.2}$ (3-35) after 5 h sintering at 1400 °C.

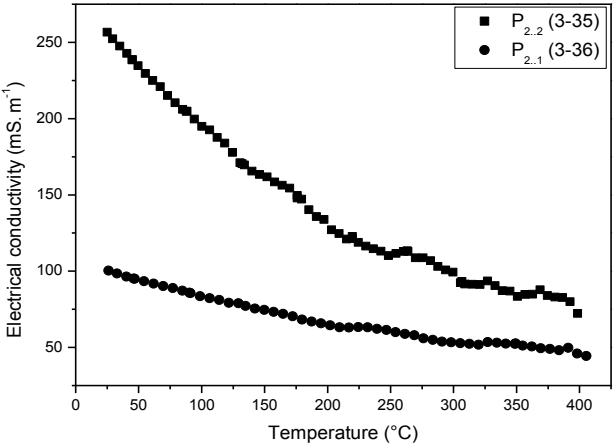

For both samples a metallic-like behavior is observed, where the resistivity increased with the increasing temperature. These results agree with Yoo et al., (2000) and Barsoum et al., (2000), who investigated the electrical properties of bulk Ti_3SiC_2 in the temperature range from 26 °C to 576 °C (BARSOUM et al., 2000; YOO, BARSOUM, EL-RAGHY, 2000). However, the electrical conductivity at 25 °C and 400°C of the screen printed films formed from pastes $P_{2.1}$ (3-36) and $P_{2.2}$ (3-35) after 5 h of sintering (Table 14) were two orders of magnitude lower than reported in literature.

Table 14 - Electrical conductivity at 25 °C and 400 °C of layers formed from pastes $P_{2.1}$ (3-36) and $P_{2.2}$ (3-35) after 5 h sintering at 1400 °C.

Samples	Electrical conductivity ($S.m^{-1}$)	
	25 °C	**400 °C**
$P_{2.1}$ (3-36)	9.99×10^4 ($\pm 6.90 \times 10^3$)	4.63×10^4 ($\pm 9.45 \times 10^3$)
$P_{2.2}$ (3-35)	2.57×10^5 ($\pm 1.85 \times 10^4$)	7.13×10^4 ($\pm 9.25 \times 10^4$)

Palmquist and co-workers (2004) performed a study involving the synthesis of different MAX phases in the Ti-Si-C systems by thin film fabrication via magnetron sputtering of Ti, Si and C targets. They observed that resistivity of $M_{n+1}AX_n$ phase films were noticeably low (Ti_3SiC_2 in a range of 0.5 to 0.3 μS.m) and TiC_x films returned values one order of magnitude lower. Importantly, the presence or addition of silicides in MAX phases are known to decrease conductance. For mixed phases of Ti_3SiC_2 with Ti_5Si_4 and Ti_5Si_3Cx the resistivity is more than doubles (0.4 to 0.8 μS.m) when compared to the single phase (PALMQUIST et al., 2004). Emmerlich and co-works (2004) produced Ti_3SiC_2/TiC_x thin films deposited via dc magnetron sputtering from three elemental targets of Ti, Si and C on MgO and Al_2O_3 with an electrical resistivity of 25 μS (EMMERLICH et al., 2004).

However, the electrical resistivity of a conductor is noted to be in the order of 10^{-9} S.m, this value can be influenced by a few factors, such as temperature, impurity alloying elements and plastic deformation (GUPTA, GUPTA, 2015b). As discussed above (section 5.1.4.3), the defects on the screen printed layer, such as cracks, porosity and high roughness, can influence the layers electrical properties. Therefore, it is worth noting that the Ti_3SiC_2 layers formed from pastes containing Ti_3SiC_2 has a lower roughness and more homogeneous composition after one hour sintering than those formed from the synthesis pastes regardless of the sintering time.

5.2. INK-JET PRINTING PROCESS

5.2.1. Ti_3SiC_2 powder

5.2.1.1. Particle size

With the aim of obtaining Ti_3SiC_2 particles with particle a size 100 times smaller than the piezoelectric print nozzle used for ink-jet printing the initial Ti_3SiC_2 powder with a D_{50} of 6.0 µm was milled. Fig. 37 and Table 15 show the particle size distribution and values of Ti_3SiC_2 powder after 0.5, 3, 4 and 5 h of milling, respectively.

Figure 37 - Particle size distribution of Ti_3SiC_2 powder as function of milling time.

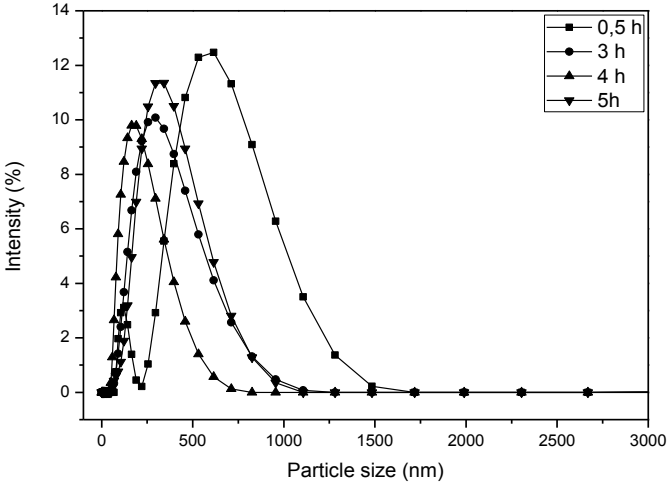

Table 15 – D_{50} of milled Ti_3SiC_2 powder as function of milling time.

Time (h)	D_{50} (µm)
0	0.60
0.5	0.50
3	0.26
4	0.16
5	0.29

The particle size distribution was seen to decrease with increased milling time up to 4 h and a narrowing of the particle size distribution also occurred. After 4 h milling, Ti_3SiC_2 with a D_{50} of 0.16 µm, which is more than 100 times smaller than the printer nozzle diameter, was obtained and thus, the requirement for failure-free printing was fulfilled (KUSCHER et al., 2012). The Ti_3SiC_2 powder milled for 5 h showed a D_{50} of 0.29 µm which is higher than the obtained value after 3h milling (0.26 µm). The milling for 5h resulted in the formation of agglomerates similar to that obtained by Kuscher et al. (2012) for TiO_2 particles (KUSCHER et al., 2012).

Fig. 38 shows representative SEM micrographs of the as-received Ti_3SiC_2 powder, with a D_{50} of 6 µm (Fig. 38 (a)) and the same powder after 4 h milling (Fig. 38 (b)) with a D_{50} of 0.16 µm. By energy milling processes a sufficiently small particle size, which can be used for ink formulation and further printing process, was successfully achieved.

Figure 38 - SEM images of Ti_3SiC_2 powder (a) before milling D_{50} = 6 µm and (b) after milling for 4h with D_{50} = 0.16 µm.

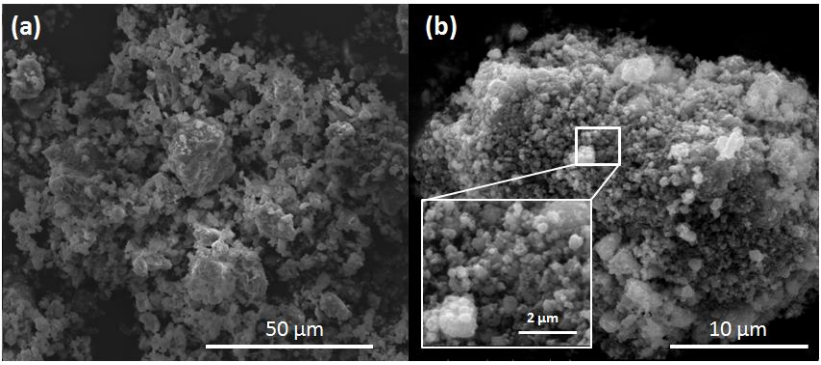

5.2.1.2. Phase determination

Fig. 39 presents the XRD pattern of the Ti_3SiC_2 powder with different particle sizes obtained by the milling process. The decrease in intensity of the peaks is attributed to the reduction of crystallite size which possibly occurs due to the delamination of the A layers characteristic in MAX Phases (BARSOUM, RADOVIC, 2011; SUN, 2011).

Figure 39 - XRD patterns of Ti_3SiC_2 powder with different particle sizes.

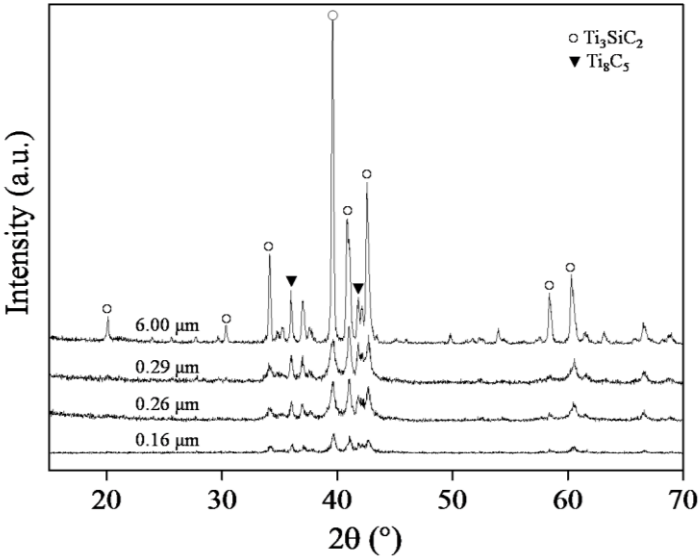

In the Ti_3SiC_2 structure, the delamination of the Si layer leads to a TiC structure. However, no TiC was detected by XRD, indicating that any TiC formed is probably in nanoscopic and any peaks formed may insignificantly intense. Table 16 details the crystallite size for the different particle sizes.

Table 16 - Crystallite size as function of particle size.

Particle size (μm)	Crystallite size (nm)
6.0	5.24
0.29	3.74
0.26	3.42
0.16	3.35

Changes in the Ti_3SiC_2 structures can be observed as changes in the vibration in the Raman spectra of the particles (Fig. 40). There are 2 types of vibrations, low and high energy. Low-shear mode (<300 cm^{-1}) involves atoms A and M (along direction a) and high energy modes correspond to the atoms X (along c axis). The corresponding peak positions show that

the M-A bonds are weaker bonds (low energy) compared to M-X bonds (BARSOUM, RADOVIC, 2011).

Figure 40 - Raman spectrum of Ti_3SiC_2 with D_{50} of 6 µm and 0.16 µm.

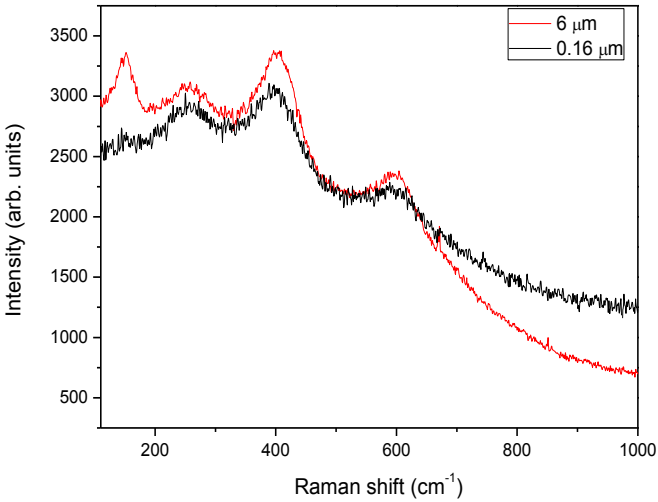

A soft mode at 150 cm^{-1} is characteristic of the shear mode between Ti and Si layers in Ti_3SiC_2 (Amer et al., 1998; Barsoum, 2000). The same peak is observed for Ti_3SiC_2 with a D_{50} of 6 µm. However, for Ti_3SiC_2 after 4 hours milling process this peak at 150 cm^{-1} was not as intense as for the Ti_3SiC_2 powder without milling. This may suggest that after high energy milling the delamination of Si layer has occurred.

5.2.2. Ti_3SiC_2 suspension preparation

With the aim of achieving a well dispersed suspension, a cationic dispersant (PEI) was used. Fig. 41 shows the ζ-potential of aqueous suspension containing Ti_3SiC_2 (D_{50} = 0.16 µm) and different PEI contents. The isoelectric point (IEP) for aqueous Ti_3SiC_2 suspensions without PEI addition is located at pH 4.6, and the particles are stable between pH 9 and 11. An addition of PEI between 1 and 2 wt% shifts the IEP to pH 9 and 10, respectively, and leads to a stability between pH 3 and 6 as well as 10 and 11, for 1 wt%, and between pH 3.5 and 9 for 2 wt%. These values agree with the results of Mishra et al. (2012), where Ti_3SiC_2 suspensions with water and ethanol as solvents were evaluated

for electrophoretic deposition. PEI is a highly branched macromolecule with $[–CH_2–CH_2–NH–]_n$ as monomers (MISHRA et al., 2012). The protonated amine groups of PEI adsorbed on the negatively charged surface of Ti_3SiC_2 particle and thus not only shifts the IEP to higher pH values, but also provides a good dispersion due to the electrostatic stabilization (TANG et al., 2006; MISHRA et al., 2012). A suspension is considered stable if its ζ-potential is greater or equal to |40| mV (BOTELLA, 2005).

Figure 41 - ζ-potential of aqueous Ti_3SiC_2 suspensions with different contents of PEI as function of pH.

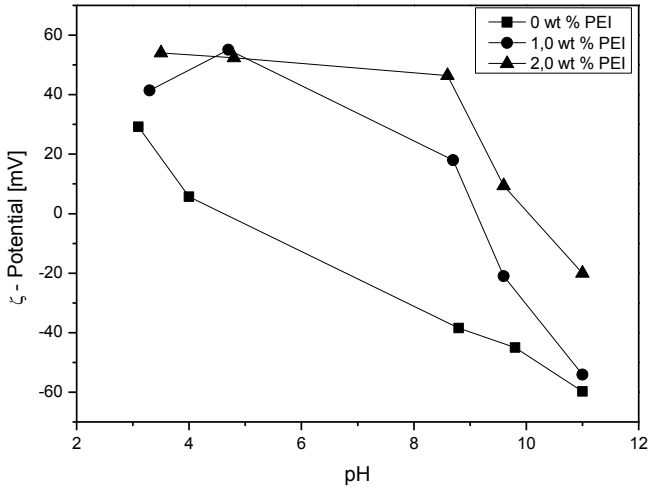

Rheological properties of the inks are also very important for the DCIJP process (MISHRA et al., 2012). Fig. 42 shows the effect of PEI content (from 1 to 3 wt%) on the viscosity of suspensions containing 5 vol% Ti_3SiC_2. It is observed that the viscosity decreases with increasing PEI content up to 2 wt% and, thus, provide flowability to the system (HU et al., 2011). An increase of the PEI content up to 3 wt% in the suspension results in an increase in viscosity due to excess of PEI. In this way, it is possible to conclude that 2 wt% of PEI is an adequate content of dispersant in the pH range between 3.5 and 9. These values are in good agreement with the results obtained by Hu et al. (2011) (HU et al., 2011). In their work, suspensions containing 10, 20 and 30 vol% of Ti_3SiC_2 and

PEI with content ranging from 0.5 to 2 wt% were analyzed. They found that the viscosity decreased when the PEI content was increased from 0.5 to 1.5 wt%. When the PEI content was increased again up to 2 wt% the viscosity increased. Despite observing viscosity increase with increasing solid content in their suspensions, they saw that the viscosity values remained lower for PEI contents of 0.5 to 1.5 wt%. A reasonable conclusion is that the viscosity increases with increasing solid content (HU et al., 2011; KUSCHER et al., 2012) and the optimum amount of dispersant to stabilize the suspension does not depend directly on the variation of the solid content.

Figure 42 – Viscosity vs. shear rate for aqueous Ti_3SiC_2 suspensions with different contents of PEI.

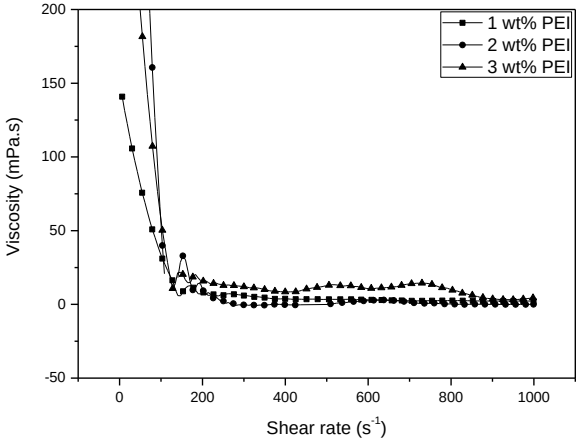

After optimizing the dispersant content, the aqueous suspensions containing 5, 1, 0.5 and 0.05 vol% of Ti_3SiC_2 with a D_{50} of 0.16 µm at pH 4.5 were prepared. All suspensions were filtrated in order to ensure that only particles with a size lower than 0.2 µm remained. Due to the small surface area of the filter, only the suspension with 0.05 vol% of Ti_3SiC_2 could be successfully obtained. Under these conditions aqueous suspensions containing 0.05 vol% Ti_3SiC_2 and 2 wt% PEI were chosen for further investigation.

As shown in Eq. 12, the Z value strongly increases with decreasing viscosity. For that reason, glycerol (viscosity of 1070 Pa at 20

°C) (KUSCHER et al., 2012) was used to increase the viscosity of the aqueous suspensions. Therefore, the influence of the glycerol amount on the viscosity, surface tension and Z values was investigated. Fig. 43 presents the relation between viscosity, printability and surface tension.

Figure 43- Viscosity and the calculated Z values of aqueous suspensions containing initially 0.05 vol% Ti_3SiC_2, 2 wt% PEI as function of glycerol content. The surface tension of each sample is represented by the arrow on the top of the graphic.

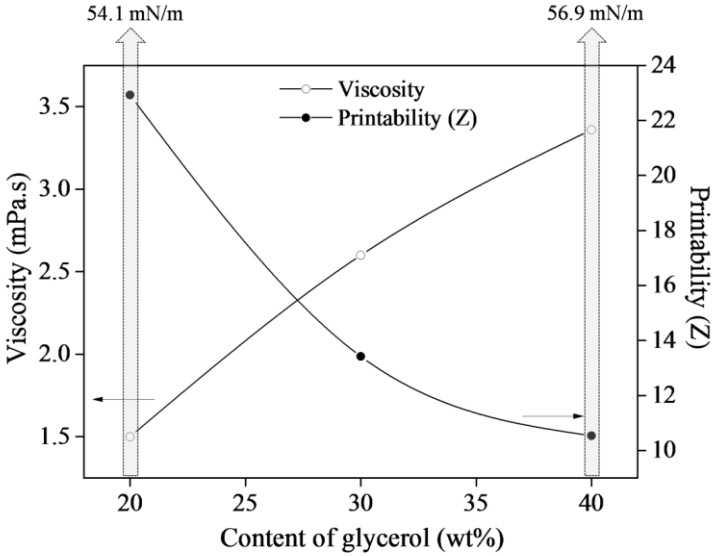

The viscosity of the printing suspension increases with increased glycerol content and the Z values decrease with the increased viscosity. Viscosity and printability are inversely proportional (Eq. 12). The highest value of Z is found for the suspension containing 20 wt% of glycerol with a value of approximately 22. This value is substantially higher when compared to the Z values predicted to be optimum in literature (Z values in the range from 4 to 14) (JANG, KIM, MOON, 2009; KUSCHER et al., 2012). For this reason, the suspension containing 20 wt% glycerol was not used for printing. The aqueous Ti_3SiC_2 suspension containing 40 wt% of glycerol has a Z value of approximately 11 which is in the printable range. Therefore, the aqueous suspension containing 0.05 vol% Ti_3SiC_2,

2 wt% PEI, and 40 wt% glycerol was chosen for evaluating the printability.

The surface tension of suspensions containing 20 and 40 wt% of glycerol were 54.1 and 56.9 mN/m, respectively. The surface tension value increases with the increasing glycerol content although it does not change significantly. This may occur due to the change of the Ti_3SiC_2 content. The suitability of the ink for ink-jet printing is characterized by passing it through the printer nozzle (KUSCHER et al., 2012). Fig. 44 shows the images taken from the camera attached to the printer nozzle. Despite the suspensions with 40 wt% glycerol having smallest Z value, it is important to mention the formation of satellites of the droplets occurs, which may decreases the accuracy of the printed structure (JANG, KIM, MOON, 2009; KUSCHER et al., 2012). Thus, among the obtained suspensions under given conditions, the aqueous suspension containing 0.05 vol% Ti_3SiC_2, 2 wt% PEI, and 40 wt% glycerol was selected for printing.

Jang et al. (2009) defined the optimum value of Z in a range from 4 to 14 by analyzing single droplet formation, minimum standoff distance, positional accuracy and maximum allowable jetting frequency. Fluids with a high Z value may cause destroy printing accuracy due to the formation of satellites to the droplets. Fluids with a low Z value provide structures with a low resolution due to the extended drop formation time and the formation of droplets with a long drop tail (JANG, KIM, MOON, 2009). The drying rate of the ink is also an important factor to achieve a good quality of the printed structure. A high drying rate may cause the clogging of the nozzle and cause the "coffee-ring effect" on substrates (KUSCHER et al., 2012).

Figure 44 - Snapshots of the drop ejection from aqueous 0.05 vol% Ti_3SiC_2, 2 wt% PEI, 40 wt% glycerol and Z equal 10: (a) 15 µs; (b) 22 µs and (c) 50 µs. The arrow indicates the formulation of the satellites.

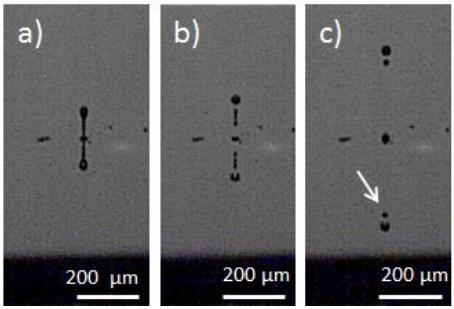

The acceptable formation of droplets indicates a good drying rate of the suspension which can be attributed to the added glycerol. An ink with a high drying rate can generate drops with improper shapes which after a certain period of time prevents jetting of the drops through the nozzle, as observed by Kuscher et al., (2012), for aqueous TiO_2 suspensions with Z value of 17 and a solid content of 15 vol%. The aqueous suspension containing 0.05 vol% Ti_3SiC_2, 2 wt% PEI, and 40 wt% glycerol was submitted to a piezoelectric printing voltage of 25 V (KUSCHER et al., 2012). However, with increasing voltage, there was a decrease in drop velocity leading to a longer time for drop formation and higher satellite formation. Therefore, the voltage of 24 V was chosen for printing.

5.2.3. Ink-jet printed structures

Fig. 45 shows the drop deposition of an aqueous suspension containing 0.05 vol% Ti_3SiC_2, 2 wt% PEI, and 40 wt% glycerol on the three different surfaces. The space dropping was set to 200 µm and the drop diameter was calculated by the average of 5 drops. The drops printed on glass, KOH and ITO had a diameter of 53 µm, 50 µm and 37 µm, respectively. The best dimensional stability was observed for the drops deposited onto the glass surface, which were the most spherical and symmetric drops (Fig. 46).

Figure 45 - Snapshot of deposited drops from an aqueous 0.05 vol% Ti_3SiC_2, 2 wt% PEI, 40 wt% glycerol suspension with and Z value of 11 onto glass, KOH and ITO surfaces.

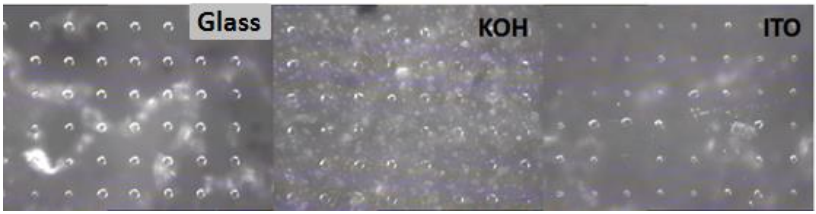

Despite the formation of satellites during the jetting process (Fig. 44), the accuracy of the printing was not affected, taking into account that the deflection of the drop was not significant. This suggests that the satellites were deposited in the same position as the drop.

Figure 46 - Snapshot of deposited drops of an aqueous ink containing 0.05 vol% Ti_3SiC_2, 2 wt% PEI, 40 wt% glycerol with a Z value of 11 onto glass substrates.

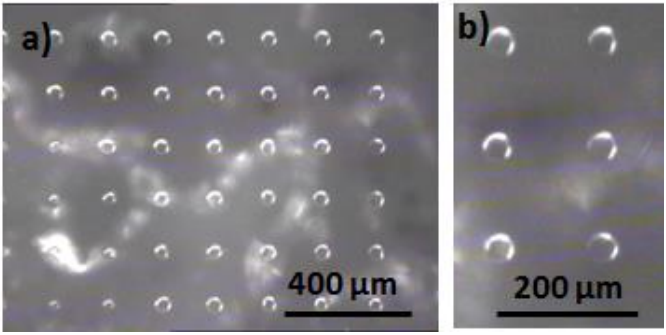

For the lines position, the droplet spacing was reduced to approximately half of the diameter previously found for each type of substrate. For glass and KOH substrates, an initial line spacing of 25 µm was used which did not allow for successful line formation in either case. Further testing with 23, 28 and 30 µm line spacing revealed that a line spacing of 30 µm gave the highest quality lines which are shown in Fig. 47. For the ITO substrates tests were performed with line spacing of 15 and 17 µm, however in both cases it was not possible to obtain a continuous line.

Figure 47 - Snapshot of deposited drops of an aqueous ink containing 0.05 vol% Ti_3SiC_2, 2 wt% PEI, 40 wt% glycerol with a Z value of 11 onto glass, KOH and ITO substrates.

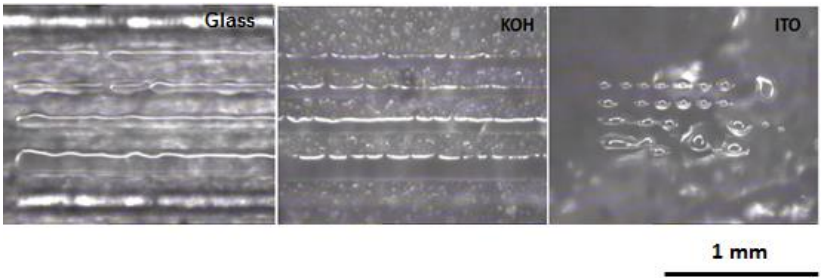

6. CONCLUSION

6.1. OVERALL

The formulation of a novel Ti_3SiC_2 inks for screen and ink-jet printing for subsequent use in electronic devices is presented. In addition, the *in situ* synthesis of Ti_3SiC_2 from elementary powders Ti, TiC, SiC via screen printing was also investigated and successfully performed. According to the presented results, for the screen printing process it is possible to conclude that:

- For all pastes, both the binder and the ceramic content were observed to have an influence on its rheological behavior;
- All samples were successfully screen printed, except pastes with 40 vol% Ti_3SiC_2 and 4 vol% EC and paste with 40 vol% Ti_3SiC_2 and 5 vol% EC which had the highest viscosities;
- Pastes with 30 vol% Ti_3SiC_2 regardless of EC content had the highest printing quality, smoothest surface and contained Ti_3SiC_2 after sintering for 1h at 1600 °C;
- Pastes containing 20 vol% and 40 vol% Ti_3SiC_2 mainly decomposed to TiC and gaseous Si during sintering for 1 h at 1600 °C in argon. The resulting films were rich in TiC phases and contained Ti_3SiC_2 as a secondary phase;
- It is postulated that there may exist a threshold value at which the content of both EC and Ti_3SiC_2 particles is optimal for screen printing.
- All screen printed layers showed the absence of cracks and good layer formation after sintering and pastes without the addition of EC seemed have the highest porosity, in addition to the largest pore sizes.
- The Ti_3SiC_2-based films deposited via screen printing, the electrical conductivity ranged from 1.25×10^5 $S.m^{-1}$ to 1.25×10^5 $S.m^{-1}$.

For the *in situ* synthesis of Ti_3SiC_2 via screen printing, pastes with Ti/Si/C and Ti/TiC/Si/C as reactants powders were prepared and observed that:

- Unlike the Ti_3SiC_2 pastes, in the synthesis pastes the EC content was observed to have the greatest influence on the viscosity and all green screen printed films presented a good printing quality.

- After sintering the screen printed films for 1, 3 and 5h at 1400 °C in argon Ti_3SiC_2 was obtained as the main phase with TiO_2, Ti_5SiC_x, $TiSi_X$ and Al_2O_3 as secondary phases. This suggests the occurrence of two simultaneous phenomenons: (i) synthesis of Ti_3SiC_2 and (ii) chemical reaction between Al_2O_3 and elementary Ti power.
- Pastes with Ti/TiC/Si/C in their initial composition showed lower roughness, a denser microstructure and higher adhesion in comparison to pastes without TiC content in their composition. Pastes containing Ti/TiC/Si/C and excess Si in their initial composition had Ti_3SiC_2 as the primary phase and Ti_5SiC_x as the secondary phase.
- Ti_3SiC_2-based films *in situ* synthesized via screen printing had an electrical conductivity in the range of 4.63×10^4 $S.m^{-1}$ to 2.57×10^5 $S.m^{-1}$.

For DCIJP process, a novel Ti_3SiC_2 ink was formulated and characterized. Parameters such as particle size, density, surface tension and viscosity were optimized with the aim of obtaining high quality printed structures. The presented results showed that:

- The suspension dispersion was improved by the addition of a cationic dispersant PEI. Through ζ-potential and rheological analysis the ideal amount of PEI was for ink formulation was found to be 2 wt%.
- The viscosity of the ink was seen to increase with increasing glycerol content. More specifically, ink containing 40 wt% of glycerol showed the best properties for the printing process.
- The jetting process exhibited good drop formation, which shows that the drying rate of the ink was low enough to avoid drying before drop ejection.
- The drop deposition on the glass, KOH and ITO surfaces showed drops with mean diameters of 53 µm, 50 µm and 37 µm, respectively.

The presented results are useful for the fabrication of aqueous Ti_3SiC_2 suspension for inks with fluid properties suitable for DCIJP, allowing the direct printing of ceramic parts. Additionally, the processing of Ti_3SiC_2 pastes via screen printing and the processing of pastes for the *in situ* synthesis of Ti_3SiC_2 via screen printing for subsequent use in electronic devices was achieved. The Ti_3SiC_2-based screen printed films offer a possible application in the field conductors and high temperature

materials, rendering the screen printing process as an alternative method for the manufacture of such components.

However, it is important to mention that despite the both processes allows the fabrication of Ti_3SiC_2-based structures, only using the screen printing process it was possible to produce structures with significant electrical conductivity.

6.2. SUGGESTIONS FOR FUTURE WORKS

- Optimization of the composition of Ti_3SiC_2 paste via screen printing;
- Optimization of the sintering temperature of Ti_3SiC_2 pastes, for instance 1400 °C and 1500 °C;
- Optimization of 3Ti/3TiC/4.5Si/C stoichiometry for *in situ* synthesis of Ti_3SiC_2 via screen printing;
- Optimization of an aqueous Ti_3SiC_2 ink with higher amount of ceramic content;
- DCIJP using an aqueous Ti_3SiC_2 ink onto paper-derived Al_2O_3 substrates and subsequent sintering;
- Evaluation of electrical properties of ink-jet printed Ti_3SiC_2/ Al_2O_3 after sintering;
- Production of paper-derived Al_2O_3 with higher density using calendaring process.

7. REFERENCES

ABU, M. J.; MOHAMED, J. J.; AHMAD, Z. A. Synthesis of high purity titanium silicon carbide from elemental powders using arc melting method. **International Journal of Refractory Metals and Hard Materials**, v. 47, p. 86–92, 2014.

AHUJA, R.; ERIKSSON, O.; WILLS, J. M.; JOHANSSON, B. Electronic structure of Ti_3SiC_2. **Applied Physics Letters**, v. 76, n. 16, p. 2226–2228, 2000.

ALKEMA, C. J.; Exploring Serigraphy. **Grand Valley Review**, v. 6, a. 12, 1990.

AMER, M.; BARSOUM, M. W.; EL-RAGHY, T.; WEISS, I.; LECLAIR, S.; LIPTAK, D. The Raman spectrum of Ti_3SiC_2. **Journal of Applied Physics**, v. 84, n. 10, p. 5817–5819, 1998.

ARUNAJATESAN, S.; CARIM, A. H. Synthesis of Titanium Silicon Carbide. **Journal of the American Ceramic Society**, v. 78, n. 3, p. 667–672, 1995.

BARSOUM M.W, El-Raghy T. Synthesis and Characterization of a Remarkable Ceramic: Ti3SiC2. **Journal of the American Ceramic Society**, 1996/79, n. 7, p. 1953–1956, 1996. Acesso em: 25 out. 2017.

BARSOUM, M. W. The Mn+1AxN Phases: A new Class of Solid: Thermodynamically Stable Nanolaminates. **Progress in Solid State Chemistry**, v. 28, 1-4, p. 201–281, 2000.

BARSOUM, M. W. The Topotactic Transformation of Ti_3SiC_2 into a Partially Ordered Cubic $Ti(C_{0.67}Si_{0.06})$ Phase by the Diffusion of Si into Molten Cryolite. **Journal of The Electrochemical Society**, v. 146, n. 10, p. 3919, 1999.

BARSOUM, M. W.; EL-RAGHY, T. Synthesis and Characterization of a Remarkable Ceramic: Ti_3SiC_2. **Journal of the American Ceramic Society**, v. 79, n. 7, p. 19953–19956, 1996.

BARSOUM, M. W.; RADOVIC, M. Elastic and Mechanical Properties of the MAX Phases. **Annual Review of Materials Research**, v. 41, n. 1, p. 195–227, 2011.

BARSOUM, M. W.; YOO, H.-I.; POLUSHINA, I. K.; RUD', V. Yu.; RUD', Yu. V.; EL-RAGHY, T. Electrical conductivity, thermopower, and Hall effect of Ti_3AlC_2,Ti_4AlN_3, and Ti_3SiC_2. **Physical Review B**, v. 62, n. 15, p. 10194–10198, 2000.

BOTELLA, R. M. **Reología de suspensiones cerámicas**. Madrid: Consejo Superior de Investigaciones Científicas, 2005. (Biblioteca de Ciencias).

BUDHANI, R. C.; TZENG, Sing-Mo H.; DOERR, H. J.; BUNSHAH, R. F. Synthesis of superconducting films of the Y-Ba-Cu-O system by a screen printing method. **Applied Physics Letters**, v. 51, n. 16, p. 1277–1279, 1987.

CARRIJO, M. M. M.; CARO, L. G.; LORENZ, H.; GREIL, P.; TRAVITZKY, N.; RAMBO, C. R. Ti_3SiC_2-based inks for direct ink-jet printing technology. **Ceramics International**, v. 43, n. 1, p. 820–824, 2017.

CARRIJO, M. M. M.; LORENZ, H.; FILBERT-DEMUT, I.; OLIVEIRA BARRA, G. M.; HOTZA, D.; YIN, X.; GREIL, P.; TRAVITZKY, N. Fabrication of Ti_3SiC_2-based composites via three-dimensional printing: Influence of processing on the final properties. **Ceramics International**, v. 42, n. 8, p. 9557–9564, 2016.

DAHLQVIST, M.; ALLING, B.; ROSÉN, J. Stability trends of MAX phases from first principles. **Physical Review B**, v. 81, n. 22, 220102(1)-220102(4), 2010.

DCOSTA, D. J.; SUN, W.; LIN, F.; EL-RAGHY, T. Freeform fabrication of Ti_3SiC_2 powder-based structures Part II: Characterization and microstructure evaluation. **Journal of Materials Processing Technology**, v. 127, p. 352–360, 2002.

DIMITROV, D.; SCHREVE, K.; BEER, N. Advanced in three dimensional printing: State of the art and future perspectives. **Rapid Prototyping Journal**, v. 12, n. 3, p. 136–147, 2006.

DIN 51105. **Hochleistungskeramik – Mechanische Eigenschaften monolithischer Keramik bei Raumtemperatur – Bestimmung der Doppelring-Biegefestigkeit**. Berlin: DIN Deutsches Institut für Normung e.V, 2010.

DIN EN 623-2. **Hochleistungskeramik -Monolithische Keramik Allgemeine und strukturelle Eigenschaften - Teil 2: Bestimmung von Dichte und Porosität**. Berlin: DIN Deutsches Institut für Normung e.V, 1993.

DIN EN 843-2. **Hochleistungskeramik – Hochleistungkermik - Mechanische Eigenschaften monolithischer Keramik bei Raumtemperatur - Teil 2: Bestimmung des Elastizitätsmoduls, Schubmoduls und der Poissonzahl**. Berlin: DIN Deutsches Institut für Normung e.V, 2007.

DIN EN ISO 4287. **Geometrische Produktspezifikation (GPS) – Oberflächenbeschaffenheit: Tastschnittverfahren – Benennungen, Definitionen und Kenngrößen der Oberflächenbeschaffenheit**. Berlin: DIN Deutsches Institut für Normung e.V, 2010.

DING, F.; GU, H.; LI, T. The fabrication of $YBa_2Cu_3O_{7-x}$ film by metal–organic deposition using terpineol-modified trifluoroacetates. **Superconductor Science and Technology**, v. 21, n. 9, p. 95004, 2008.

DING, X.; LI, Y.; WANG, D.; YIN, Q. Fabrication of BaTiO3 dielectric films by direct ink-jet printing. **Ceramics International**, v. 30, n. 7, p. 1885–1887, 2004.

DOLLEN, P. von; BARNETT, S. A Study of Screen Printed Yttria-Stabilized Zirconia Layers for Solid Oxide Fuel Cells. **Journal of the American Ceramic Society**, v. 88, n. 12, p. 3361–3368, 2005.

DONOVAN, E. P.; SPAEPEN, F.; TURNBULL, D.; POATE, J. M.; JACOBSON, D. C. Heat of crystallization and melting point of amorphous silicon. **Applied Physics Letters**, v. 42, n. 8, p. 698–700, 1983.

EBERT, J.; OZKOL, E.; ZEICHNER, A.; UIBEL, K.; WEISS, O.; KOOPS, U.; TELLE, R.; FISCHER, H. Direct inkjet printing of dental prostheses made of zirconia. **Journal of dental research**, v. 88, n. 7, p. 673–676, 2009.

EL-RAGHY, T.; BARSOUM, M. W. Diffusion kinetics of the carburization and silicidation of Ti_3SiC_2. **Journal of Applied Physics**, v. 83, n. 1, p. 112–119, 1998a.

EL-RAGHY, T.; BARSOUM, M. W. Processing and Mechanical Properties of Ti_3SiC_2: I, Reaction Path and Microstructure Evolution. **Journal of the American Ceramic Society**, v. 82, n. 10, p. 2849–2854, 1999.

EL-RAGHY, T.; ZAVALIANGOS, A.; BARSOUM, M. W.; KALIDINDI, S. R. Damage Mechanisms around Hardness Indentations in Ti_3SiC_2. **Journal of the American Ceramic Society**, v. 80, n. 2, p. 513–516, 1997.

EL-RAGHY, Tamer; BARSOUM, Michel W. Diffusion Kinetics of the carburization and silidation of Ti3SiC2. **Journal of Applied Physics**, v. 83, n. 1, p. 112–119, 1998b. doi:10.1063/1.366707.

EMMERLICH, J.; HÖGBERG, H.; SASVÁRI, S.; PERSSON, P. O. Å.; HULTMAN, L.; PALMQUIST, J. P.; JANSSON, U.; MOLINA-ALDAREGUIA, J. M.; CZIGÁNY, Z. Growth of Ti3SiC2 thin films by elemental target magnetron sputtering. **Journal of Applied Physics**, v. 96, n. 9, p. 4817–4826, 2004.

EMMERLICH, J.; MUSIC, D.; EKLUND, P.; WILHELMSSON, O.; JANSSON, U.; SCHNEIDER, J. M.; HÖGBERG, H.; HULTMAN, L. Thermal stability of Ti_3SiC_2 thin films. **Acta Materialia**, v. 55, n. 4, p. 1479–1488, 2007.

FADDOUL, R.; REVERDY-BRUAS, N.; BLAYO, A. Formulation and screen printing of water based conductive flake silver pastes onto green ceramic tapes for electronic applications. **Materials Science and Engineering: B**, v. 177, n. 13, p. 1053–1066, 2012.

FROMM, J. E. Numerical Calculation of the Fluid Dynamics of Drop-on-Demand Jets. **IBM Journal of Research and Development**, v. 28, n. 3, p. 322–333, 1984.

GAO, N.F; LI, J.T; ZHANG, D.; MIYAMOTO, Y. Rapid synthesis of dense Ti_3SiC_2 by spark plasma sintering. **Journal of the European Ceramic Society**, v. 22, n. 13, p. 2365–2370, 2002.

GAO, N.F; MIYAMOTO, Y.; ZHANG, D. Dense Ti_3SiC_2 prepared by reactive HIP. **Journal of Materials Science**, v. 34, n. 18, p. 4385, 1999.

GAUTHIER, V.; COCHEPIN, B.; DUBOIS, S.; VREL, D. Self-Propagating High-Temperature Synthesis of Ti_3SiC_2: Study of the Reaction Mechanisms by Time-Resolved X-Ray Diffraction and Infrared Thermography. **Journal of the American Ceramic Society**, v. 89, n. 9, p. 2899–2907, 2006.

GOLDBERG, H. D.; BROWN, R. B.; LIU, D. P.; MEYERHOFT, M. E. Screen printing: a technology for the batch fabrication of integrated chemical-sensor arrays. **Sensors and Actuators B**, v. 21, p. 171–183, 1994.

GOTO, T.; HIRAI, T. Chemically Vapor Deposited Ti_3SiC_2. **Materials Research Bulletin**, v. 22, p. 1195–1201, 1987.

GREIL, P. Biomorphous ceramics from lignocellulosics. **Journal of the European Ceramic Society**, v. 21, n. 2, p. 105–118, 2001.

GUPTA, K. M.; GUPTA, N. (Ed.). **Advanced Electrical and Electronics Materials:** Process and Applications. Hoboken, NJ: John Wiley & Sons, 2015a. 1 p. (Advanced Materials series).

GUPTA, K. M.; GUPTA, N. **Advanced electrical and electronics materials:** Processing and Applications. Hoboken, NJ: Wiley, Scriverner, 2015b. (Advanced Materials series).

HASEGAWA, S.; SHIRAKI, I.; TANIKAWA, T.; PETERSEN, C. L.; HANSEN, T. C.; BOGGILD, P.; GREY, F. Direct measurement of surface-state conductance by microscopic four-point probe method. **Journal of Physics: Condensed Matter**, v. 14, p. 8379–8392, 2002.

HÖGBERG, H.; HULTMAN, L.; EMMERLICH, J.; JOELSSON, T.; EKLUND, P.; MOLINA-ALDAREGUIA, J. M.; PALMQUIST, J.-P.; WILHELMSSON, O.; JANSSON, U. Growth and characterization of MAX-phase thin films. **Surface and Coatings Technology**, v. 193, 1-3, p. 6–10, 2005.

HU, C.; SAKKA, Y.; GRASSO, S.; SUZUKI, T.; TANAKA, H. Tailoring Ti_3SiC_2 Ceramic via a Strong Magnetic Field Alignment Method Followed by Spark Plasma Sintering. **Journal of the American Ceramic Society**, v. 94, n. 3, p. 742–748, 2011.

INUKAI, K.; TAKAHASHI, Y.; RI, K.; SHIN, W. Rheological analysis of ceramic pastes with ethyl cellulose for screen-printing. **Ceramics International**, v. 41, n. 4, p. 5959–5966, 2015.

JABBOUR, G.; RADSPINNER, R.; PERYGHAMBARIAN, N. Screen printing for the fabrication of organic light-emitting devices. **Journal of Selected Topics in Quantum Electronics**, v. 7, n. 5, p. 769–773, 2001.

JANG, D.; KIM, D.; MOON, J. Influence of fluid physical properties on ink-jet printability. **Langmuir : the ACS journal of surfaces and colloids**, v. 25, n. 5, p. 2629–2635, 2009.

JEE, H.J; SACHS, E. A visual simulation technique for 3D printing. **Advances in Engineering Software**, v. 31, n. 2, p. 97–106, 2000.

JEITSCHO, W.; NOWOTNY, H. Die Kristallstruktur von Ti_3SiC_2 – ein neuer Komplexcarbid-Typ. **Monatshefte für Chemie - Chemical Monthly**, v. 98, n. 2, p. 329–337, 1967.

JUNKES, J. A.; DERMEIK, B.; GUTBROD, B.; HOTZA, D.; GREIL, P.; TRAVITZKY, N. Influence of coatings on microstructure and mechanical properties of preceramic paper-derived porous alumina substrates. **Journal of Materials Processing Technology**, v. 213, n. 2, p. 308–313, 2013.

KANG, S.'; SELVERIAN, J. H. Interactions between Ti and alumina-based ceramics. **Journal of Materials Science**, v. 27, p. 4536–4544, 1992.

KLEMM, H.; TANIHATA, K.; MIYAMOTO, Y. Gas pressure combustion sintering and hot isostatic pressing in the Ti-Si-C system. **Journal of Materials Science**, v. 28, n. 6, p. 1557–1562, 1993.

KLIAUGA, A. M.; FERRANTE, M. Interface compounds formed during the diffusion bonding of Al_2O_3 to Ti. **Journal of Materials Science**, v. 35, p. 4243–4249, 2000.

KLUTHE, C.; DERMEIK, B.; KOLLENBERG, W.; GREIL, P.; TRAVITZKY, N. Processing, Microstructure and Properties of Paper-Derived Porous Al_2O_3 Substrates. **journal of Ceramic Science and Technology**, v. 3, p. 111–118, 2012.

KUSCHER, D.; STAVBER, G.; TREFALT, G.; KOSEC, M.; BRENNECKA, G. Formulation of an Aqueous Titania Suspension and its Patterning with Ink-Jet Printing Technology. **Journal of the American Ceramic Society**, v. 95, n. 2, p. 487–493, 2012.

LANGE, Christian; BARSOUM, Michel W.; SCHAAF, Peter. Towards the synthesis of MAX-phase functional coatings by pulsed laser deposition. **Applied Surface Science**, v. 254, n. 4, p. 1232–1235, 2007.

LEE, S.; PAIK, U.; YOON, S. M.; CHOI, J. Y. Dispersant-Ethyl Cellulose Binder Interactions at the Ni Particle-Dihydroterpineol Interface. **Journal of the American Ceramic Society**, v. 89, n. 10, p. 3050–3055, 2006.

LEWIS, J. A.; SMAY, J. E.; STUECKER, J.; CESARANO III, J. Direct Ink Writing of Three-Dimensional Ceramic Structures. **Journal of the American Ceramic Society**, v. 89, n. 12, p. 3599–3609, 2006.

LI, J. F.; SATO, F.; WATANABE, R. Synthesis of Ti_3SiC_2 polycrystals by hot-isostatic pressing of the elemental powders. **Journal of Materials Science Letters**, v. 18, p. 1595–1597, 1999.

LI, S. B.; ZHAI, H. X. Synthesis and Reaction Mechanism of Ti_3SiC_2 by Mechanical Alloying of Elemental Ti, Si, and C Powders. **Journal of the American Ceramic Society**, v. 88, n. 8, p. 2092–2098, 2005.

LI, X. L.; HILLEL, R.; TEYSSANDIER, S. K.; VAN LOO, F. J. J. Reactions and phase relations in the Ti-Al-O system. **Acta Matellurgica et Materialia**, v. 40, n. 11, p. 3149–3157, 1992.

LIN, H. W.; CHANG, C. P.; HWU, W. H.; GER, M. D. The rheological behavior of screen-printing pastes. **Journal of Materials Processing Technology**, v. 197, 1-3, p. 284–291, 2008.

LIS, J.; MIYAMOTO, Y.; PAMPUCH, R.; TANIHATA, K. Ti_3SiC_2-based materials prepared by HIP-SHS techniques. **Materials Letters**, v. 22, 3-4, p. 163–168, 1995.

LORENZ, H.; BONET, A.; AYRIKYAN, A.; GREIL, P.; TRAVITZKY, N. Paper-derived bioactive ceramics for complex shape bone implants. **Advanced Biomaterials and Devices in Medicine**, v. 2, p. 88–94, 2015.

LORENZ, H.; THÄTER, J.; CARRIJO, M. M. M.; RAMBO, C. R.; GREIL, P.; TRAVITZKY, N. In situ synthesis of paper-derived Ti_3SiC_2. **Journal of Materials Research**, v. 2, p. 1–6, 2017.

LU, H.; BAO, C. L.; SHEN, D. H.; ZHANG, X. J.; CUI, Y. D.; LIN, Z. D. Study on the Ti/Al_2O_3 interface. **Journal of Materials Science**, v. 30, p. 339–346, 1995.

MATSUO, Atsushi; GALLAGE, R.; FUJIWARA, T.; WATANABE, T.; YOSHIMURA, M. On-site fabrication of ceramics films from solution precursors by ink-jet and spray assisted processes. **Journal of Electroceramics**, v. 16, n. 4, p. 533–536, 2006.

MÉNDEZ-VILAS, A.; DÍAZ, J. (Ed.). **Modern Research and Educational Topics in Microscopy**. Badajoz, Spain: Formatex, 2007. (Microscopy series, 3).

MISHRA, M.; SAKKA, Y.; HU, C.; SUZUKI, T. S.; UCHIKOSHI, T.; BESRA, L.; ZHOU, Y. Electrophoretic Deposition of Ti_3SiC_2 and Texture Development in a Strong Magnetic Field. **Journal of the American Ceramic Society**, v. 95, n. 9, p. 2857–2862, 2012.

MORGIEL, J.; LIS, J.; PAMPUCH, R. Microstructure of Ti_3SiC_2-based Ceramics. **Materials Letters**, v. 27, p. 85–89, 1996.

MOTT, M.; EVANS, J.R.G. Zirconia/alumina functionally graded material made by ceramic ink jet printing. **Materials Science and Engineering: A**, v. 271, 1-2, p. 344–352, 1999.

MURAKAMI, S.; RI, K.; ITOH, T.; IZU, N.; SHIN, W.; INUKAI, K.; TAKAHASHI, Y.; ANDO, Y. Effects of ethyl cellulose polymers on rheological properties of $(La,Sr)(Ti,Fe)O_3$-terpineol pastes for screen printing. **Ceramics International**, v. 40, n. 1, p. 1661–1666, 2014.

NICKI, J. J.; SCHWEITZER, K. K.; LUXENBERG, P. Gasphasenabscheidung im system Ti-Si-C. **Journal of the Less-Common Metals**, v. 26, p. 335–353, 1972.

PALMQUIST, J.-P.; JANSSON, U.; SEPPÄNEN, T.; PERSSON, P. O. Å.; BIRCH, J.; HULTMAN, L.; ISBERG, P. Magnetron sputtered epitaxial single-phase Ti_3SiC_2 thin films. **Applied Physics Letters**, v. 81, n. 5, p. 835–837, 2002.

PALMQUIST, J.-P.; LI, S.; PERSSON, P. O. Å.; EMMERLICH, J.; WILHELMSSON, O.; HÖGBERG, H.; KATSNELSON, M. I.; JOHANSSON, B.; AHUJA, R.; ERIKSSON, O.; HULTMAN, L.; JANSSON, U. $M_{n+1}AX_n$ phases in the Ti−Si−C system studied by thin-film synthesis and ab initio calculations. **Physical Review B**, v. 70, n. 16, p. 329, 2004.

PAMPUCH, R.; LIS, J.; STOBIERSKI, L.; TYMKIEWICZ. Solid Combustion Synthesis of Ti_3SiC_2. **Journal of the European Ceramic Society**, v. 5, p. 283–287, 1989.

PAN, J.; TONKAY, G. L.; QUINTERO, A. Screen printing process design of experiments for fine printing of Thick Film Ceramic Substrates. **Journal of Electronics Manufacturing**, v. 09, n. 03, p. 203–213, 1999.

PARK, C. S.; ZHENG, F.; SALAMONE, S.; BORDIA, R. K. Processing of composites in the Ti-Si-C system. **Journal of Materials Science**, v. 36, 3313-3322, 2001.

PHAIR, J. W. Rheological Analysis of Concentrated Zirconia Pastes with Ethyl Cellulose for Screen Printing SOFC Electrolyte Films. **Journal of the American Ceramic Society**, v. 91, n. 7, p. 2130–2137, 2008.

PHAIR, J. W.; KAISER, A. F-J. Determination and Assessment of the Rheological Properties of Pastes for Screen Printing Ceramics. **Annual Transactions of the Nordic Rheology Society**, v. 17, 2009.

PHAIR, J. W.; LUNDBERG, M.; KAISER, A. Leveling and thixotropic characteristics of concentrated zirconia inks for screen-printing. **Rheologica Acta**, v. 48, n. 2, p. 121–133, 2009.

PRASAD, K. P.S.R.; REDDY, A. V.; RAJESH, P. K.; PONNAMBALAM, P.; PRAKASAN, K. Studies on rheology of ceramic inks and spread of ink droplets for direct ceramic ink jet printing. **Journal of Materials Processing Technology**, v. 176, 1-3, p. 222–229, 2006.

RACAULT, C.; LANGLAIS, R.; NASLAIN, R. Solid-state synthesis and characterization of the ternary phase Ti_3SiC_2. **Journal of Materials Science**, v. 29, p. 3384–3392, 1994.

RADHAKRISHNAN, R.; WILLIAMS, J. J.; AKINC, M. Synthesis and high-temperature stability of Ti_2SiC_3, v. 285, p. 85–88, 1999.

RADOVIC, M.; BARSOUM, M. W. MAX phases: Bridging the gap between metals and ceramics. **American Ceramic Societa Bulletin**, v. 92, n. 3, p. 20–27, 2013.

RAMAKRISHNAN, N.; RAJESH, P. K.; PONNAMBALAM, P.; PRAKASAN, K. Studies on preparation of ceramic inks and simulation of drop formation and spread in direct ceramic inkjet printing. **Journal of Materials Processing Technology**, v. 169, n. 3, p. 372–381, 2005.

RATAKONDA, D.; SINGH, R.; VEDULA, L.; NARAYANAN, S. Ohmic Contacts Formation of Silicon Schottky Diodes by Screen Printing and Rapid Isothermal Processing. **Journal of Electronic Materials**, v. 27, n. 5, p. 402–404, 1998.

RILEY, D. P.; KISI, E. H.; HANSEN, T. C.; HEWAT, A. W. Self-Propagating High-Temperature Synthesis of Ti3SiC2: I, Ultra-High-Speed Neutron Diffraction Study of the Reaction Mechanism. **Journal of the American Ceramic Society**, v. 85, n. 10, p. 2411–2424, 2002.

RYSHKEWITCH, E. Compression Strength of Porous Sintered Alumina and Zirconia. **Journal of the American Ceramic Society**, v. 36, n. 2, p. 65–68, 1953.

SAMBASIVAN, S.; PETUSKEY, T. Phase relationships in the Ti-Si-C system at high pressures. **Journal of Materials Research**, v. 7, n. 6, p. 1473–1479, 1992.

SATO, F.; LI, J. F.; WATANABE, R. Reaction synthesis of Ti_3SiC_2 from mixture of elemental powders. **Materials Transactions**, v. 41, n. 5, p. 605–608, 2000.

SAVAGE, J. Factors Affecting the Qualitity of Screen-Printed Conductors. **Thin Solid Films**, v. 4, n. 2, p. 137–148, 1969.

SCHLORDT, T.; DERMEIK, B.; BEIL, V.; FREIHART, M.; HOFENAUER, A.; TRAVITZKY, N.; GREIL, P. Influence of Calendering on the Properties of Paper-derived Alumina Ceramics. **Ceramics International**, v. 40, n. 3, p. 4917–4926, 2014.

SCHULTHEIß, J.; DERMEIK, B.; FILBERT-DEMUT, I.; HOCK, N.; YIN, X.; GREIL, P.; TRAVITZKY, N. Processing and characterization

of paper-derived Ti_3SiC_2 based ceramic. **Ceramics International**, v. 41, n. 10, p. 12595–12603, 2015. Acesso em: 3 abr. 2017.

SEDLAČEK, M.; PODGORNIK, B.; VIŽINTIN, J. Influence of surface preparation on roughness parameters, friction and wear. **Wear**, v. 266, 3-4, p. 482–487, 2009.

SHI, S.; ZHANG, L.; LI, J. Ti_3SiC_2 material: An application for electromagnetic interference shielding. **Applied Physics Letters**, v. 93, n. 17, p. 172903, 2008.

SILVA, R.; HARAGUCHI, S. K.; MUNIZ, E. C.; RUBIRA, A. F. Aplicações de fibras lignocelulósicas na química de polímeros e em compósitos. **Química Nova**, v. 32, n. 3, p. 661–671, 2009.

SLADE, C. E.; EVANS, J. R. G. Freeforming Ceramics Using a Thermal Jet Printer. **Journal of Materials Science Letters**, v. 17, p. 1669–1671, 1998.

SONG, J. H.; EDIRISINGHE, M. J.; EVANS, J. R. G. Formulation and Multilayer Jet Printing of Ceramics Inks. **Journal of the American Ceramic Society**, v. 82, n. 12, p. 3374–3380, 1999.

SUN, W.; DCOSTA, D. J.; LIN, F.; EL-RAGHY, T. Freeform fabrication of Ti3SiC2 powder-based structures Part I: Integrated fabrication process. **Journal of Materials Processing Technology**, v. 127, p. 343–351, 2002.

SUN, Z. M. Progress in research and development on MAX phases: A family of layered ternary compounds. **International Materials Reviews**, v. 56, n. 3, p. 143–166, 2011.

SUN, Z.; ZHOU, Y. Ab *initio* calculation of titanium silicon carbide. **Physical Review B**, v. 60, n. 3, p. 1441–1443, 1999.

TANG, F.; UCHIKOSHI, T.; OZAWA, K.; SAKKA, Y. Effect of polyethylenimine on the dispersion and electrophoretic deposition of nano-sized titania aqueous suspensions. **Journal of the European Ceramic Society**, v. 26, n. 9, p. 1555–1560, 2006.

TAY, B. Y.; EVANS, J. R. G.; EDIRISINGHE, M. J. Solid freeformfabrication of ceramics. **International Materials Reviews**, v. 48, n. 6, p. 341–370, 2013.

TONG, X.; OKANO, T.; ISEKI, T.; YANO, T. Synthesis and high temperature mechanical properties of Ti_3SiC_2/SiC composite. **Journal of Materials Science**, v. 30, n. 12, p. 3087–3090, 1995.

TRAVITZKY, N.; BONET, A.; DERMEIK, B.; FEY, T.; FILBERT-DEMUT, I.; SCHLIER, L.; SCHLORDT, T.; GREIL, P. Additive Manufacturing of Ceramic-Based Materials. **Advanced Engineering Materials**, v. 16, n. 6, p. 729–754, 2014.

TRAVITZKY, N.; WINDSHEIMER, H.; FEY, T.; GREIL, P. Preceramic Paper-Derived Ceramics. **Journal of the American Ceramic Society**, v. 91, n. 11, p. 3477–3492, 2008.

TRESSLER, R. E.; MOORE, T. L.; CRANE, R. L. Reactivity and interface characteristics of titanium-alumina composites. **Journal of Materials Science**, v. 8, n. 2, p. 151–161, 1973.

TSAI, T.; SCOTT, A. B. Bias Sputter Deposition of Dense Yttria-Stabilized Zirconia Films on Porous Substrates. **Journal of the Electrochemical Society**, v. 142, n. 9, p. 3084–3087, 1995.

TSENG, W. J.; LIN, S.-Y.; WANG, S.-R. Particulate dispersion and freeform fabrication of $BaTiO_3$ thick films via direct inkjet printing. **Journal of Electroceramics**, v. 16, n. 4, p. 537–540, 2006.

WAKELKAMP, W. J. J.; LOO, F. J. J.; METSELAAR, R. Phase relations in the Ti-Si-C system. **Journal of the European Ceramic Society**, v. 8, p. 135–139, 1991.

WU, E.; KISI, E. H. In Situ Neutron Powder Diffraction Study of Ti_3SiC_2 Synthesis. **Journal of the American Ceramic Society**, v. 84, n. 10, 2001.

WU, E.; KISI, E. H.; RILEY, D. P. Intermediate Phases in Ti_3SiC_2 Synthesis from Ti/SiC/C Mixtures Studied by Time-Resolved Neutron Diffraction. **Journal of the American Ceramic Society**, v. 82, n. 12, 2002.

WU, J.; ZHOU, Y.; WANG, J.; WANG, W.; YAN, C. Interfacial reaction between Cu and Ti_2SnC during processing of Cu-Ti_2SnC composite. **Zeitschrift für Metallkunde**, v. 96, n. 11, p. 1314–1320, 2005.

WU, R. F; PAN, W.; SHI, S. L.; HAN, R. B. Critical behaviors of the conductivity and dielectric constant of Ti_3SiC_2/Al_2O_3 hybrids. **Journal of Applied Physics**, v. 102, n. 5, p. 56104, 2007.

YANG, S.; SUN, Z. M.; HASHIMOTO, H. Reaction in Ti_3SiC_2 powder synthesis from a Ti–Si–TiC powder mixture. **Journal of Alloys and Compounds**, v. 368, 1-2, p. 312–317, 2004.

YOO, H.-I.; BARSOUM, M. W.; EL-RAGHY, T. Ti_3SiC_2 has negligible thermopower. **Nature**, v. 407, p. 581–582, 2000.

ZHANG, H. B.; ZHOU, Y. C.; BAO, Y. W.; LI, M. S.; WANG, J. Y. Intermediate phases in synthesis of Ti_3SiC_2 and $Ti_3Si(Al)C_2$ solid solutions from elemental powders. **Journal of the European Ceramic Society**, v. 26, n. 12, p. 2373–2380, 2006.

ZHANG, J. F.; WANG, L. J.; JIANG, W.; CHEN, L. D. Reaction Path and Microstructures of Ti_3SiC_2/SiC Composite by Spark Plasma Sintering. **Key Engineering Materials**, 336-338, p. 1368–1370, 2007.

ZHOU, Y.; SUN, Z. Electronic structure and bonding properties in layered ternary carbide Ti_3SiC_2. **Journal of Physics: Condensed Matter**, v. 12, L457-L462, 2000.

8. APPENDIX A - SCREEN PRINITING PROCESS

Figure 48 - Snapshot of pastes 20 vol% and 40 vol% Ti_3SiC_2 and different EC contents (a) green and (b) sintered.

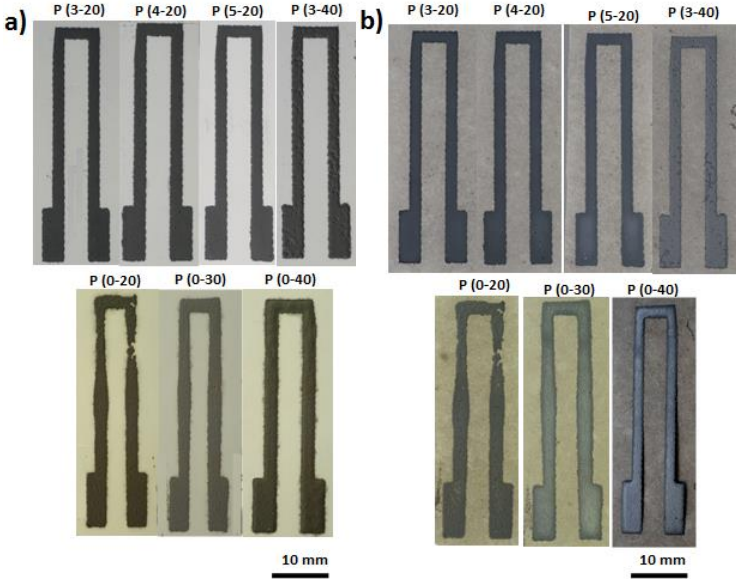

Figure 49 - Line profile for green screen printed films of Ti_3SiC_2 pastes.

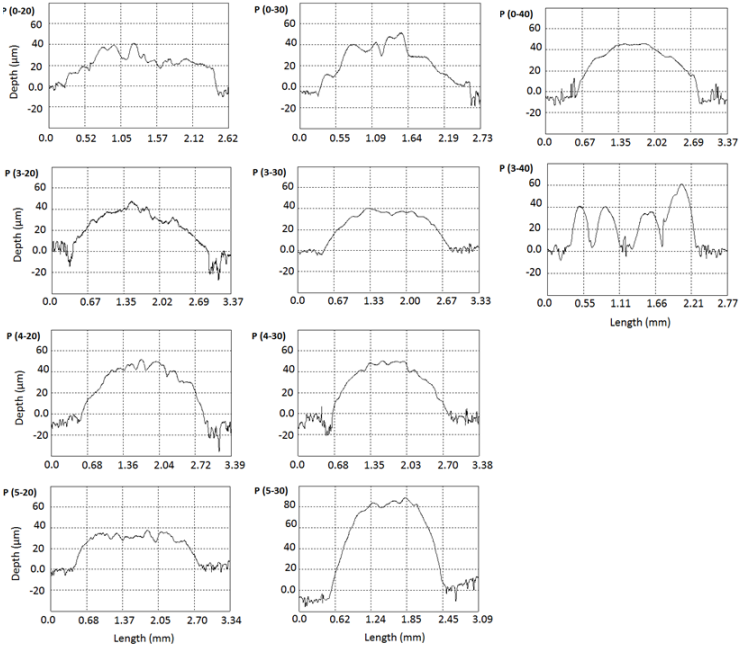

Figure 50 - Line profile for screen printed films of Ti_3SiC_2 pastes after sintering at 1600 °C for 1 h.

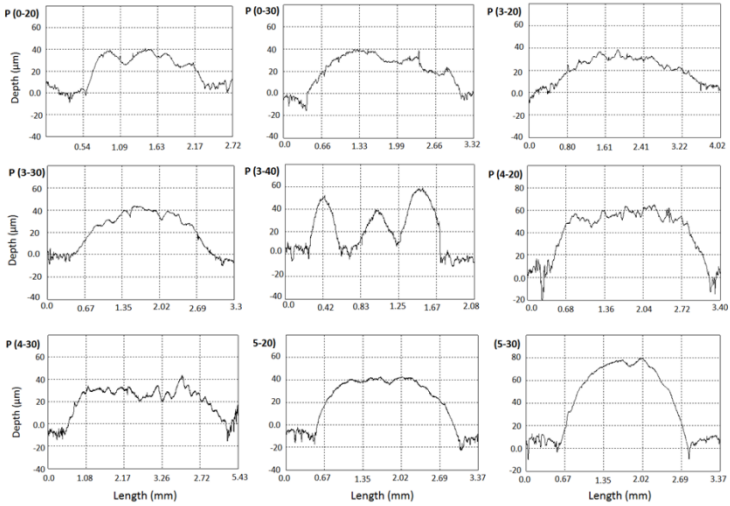

Figure 51 - TGA analysis of 3 vol% organic additives (EC+Terpineol) present in the pastes compositions.

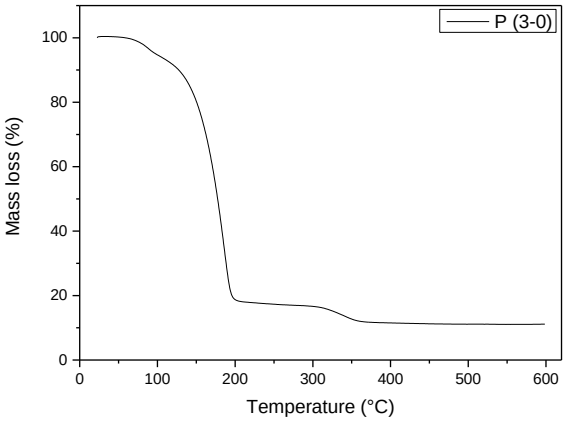

Figure 52 - Line profile for green screen printed films of synthesis pastes.

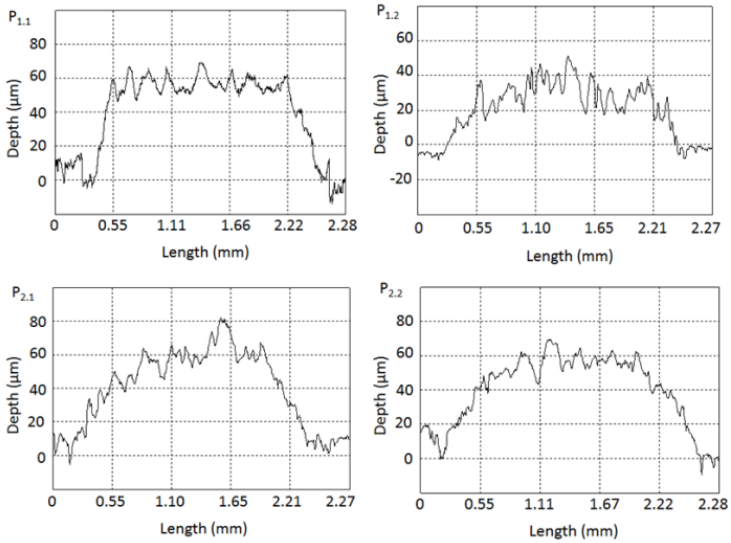

Figure 53 - Line profile for sintered screen printed films of synthesis pastes.

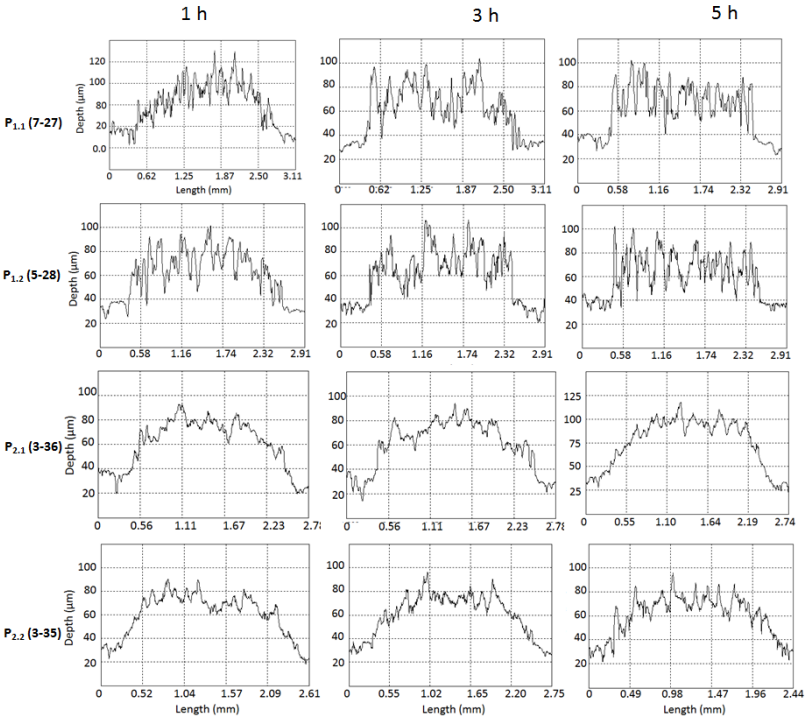

Figure 54 - Topography of sintered screen printed layers of synthesis pastes.

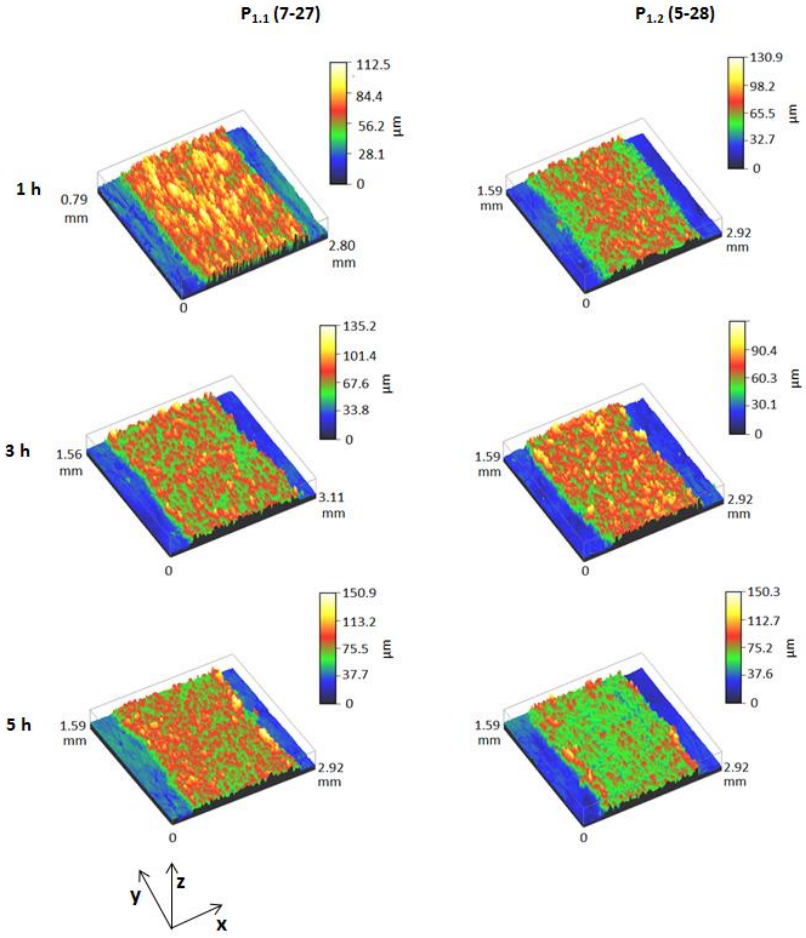

9. APPENDIX B - SCIENTIFIC PUBLICATIONS

CARRIJO, M. M. M.; CARO, L. G.; LORENZ, H.; GREIL, P.; TRAVITZKY, N.; RAMBO, C. R. Ti_3SiC_2-based inks for direct ink-jet printing technology. **Ceramics International**, v. 43, n. 1, p. 820–824, 2017.

CARRIJO, M. M. M.; LORENZ, H.; FILBERT-DEMUT, I.; OLIVEIRA BARRA, G. M.; HOTZA, D.; YIN, X.; GREIL, P.; TRAVITZKY, N. Fabrication of Ti_3SiC_2-based composites via three-dimensional printing: Influence of processing on the final properties. **Ceramics International**, v. 42, n. 8, p. 9557–9564, 2016.

CARRIJO, M. M. M.; LORENZ, H.; RAMBO, C.; GREIL, P.; TRAVITZKY, N. Fabrication of Ti_3SiC_2-based pastes for screen printing on paper-derived Al_2O_3 substrates. **Ceramics International**, in Press, 2018.

LORENZ, H.; THÄTER, J.; CARRIJO, M. M. M.; RAMBO, C. R.; GREIL, P.; TRAVITZKY, N. In situ synthesis of paper-derived Ti_3SiC_2. **Journal of Materials Research**, v. 2, p. 1–6, 2017.